The Scholar Journal for Sciences & Technology

ISSN
Print 2794 - 7629
Online 2794 - 4549

North Europe Academy
Journal published by the Danish Arab Center for Future Studies
Copenhagen - Denmark

The Scholar Journal for Sciences & Technology

The Scholar Journal for Sciences & Technology - NEA /Copenhagen - Denmark

VOL.2 NO.5

International Standard Serial Number
ISSN (Print) 2794 – 7629
ISSN (Online) 2794 - 4549

**The Scholar Journal for Sciences & Technology**
**International Standard Serial Number (ISSN)**

**ISSN (Print) 2794 – 7629**
**ISSN (Online) 2794 - 4549**

**Vol. 2** **NO. 5**

**Issue date: 29/01/2025**

## Chief Editor

**Prof.Dr.Harith Salman Hasaani**
**Professor General surgery**
**Consultant General Surgeon**
**General surgery**
**Al-kindy Teaching Hospital**
**MD PhD FACS**
**Ministry of health /Iraq**
**harith_salman@yahoo.co.uk**
**009647704587777**

## Deputy Editor-in-Chief

**Prof.Dr.Talib A. H. Mousa**
**College of Health & Medical Technology**
**Al-Ayen Iraqi University**
**Thi-Qar, 64001, Iraq**
**Talib.Abdulhussein@Alayen.edu.iq**
**009647801094939**

## Research Publications Officer

**Prof. Dr. Abbas Nagi AL Imami**
**Physiological Psychology & Chemistry Science**
**Director of the Danish Arab Center**
**CEO of Northern European Academy**
**Science and scientific research**
**abbas-45@hotmail.com**
**004571583979**

The Scholar Journal for Sciences & Technology

# Editorial board members

# Advisory Board

**The Scholar Journal for Sciences & Technology**
**International Standard Serial Number (ISSN)**
ISSN (Print) 2794 – 7629
ISSN (Online) 2794 - 4549

# Northern European Academy – Denmark

## About the Journal

1. The journal has a website on the Internet that can be accessed through the link:
**www.sst.journalnea.com**

It has been stated that the journal is a scientific refereed journal concerned with scientific research and studies that are committed to the terms and conditions of scientific publishing of papers not formerly published anywhere.

2. **NAME OF JOURNAL**:

(The Scholar Journal for Sciences & Technology)
This name is registered by the Danish Royal Library in Copenhagen.

3. **PEER REVIEW PROCESS**
All journal papers and materials are usually reviewed by domain experts and arbitrators prior to their submission for publication. This has been clearly declared on the Journal's website.

4. **OWNERSHIP AND MANAGEMENT:**
The journal is owned by the North European Academy for Sciences and Scientific Research and no publication of any content without the prior approval of the owner. Prof.Dr.Harith Salman Hasaani

5. **GOVERNING BODY:**
The journal has an editorial board consisting of a number of experts with the rank of Professor and Assistant Professor headed by the Editor-in-Chief / Prof. Dr. Harith Salman Hasaani and the Deputy Editor-in-Chief Prof. Dr./ Ihsan Edan Abdul - Kareem Al-Saimary, and the Research Publications Officer in it is Prof. Dr./ Abbas Nagi Al-Imami. A list of the names and addresses of the editorial board is shown on the site, and this list is published frequently in all its publications and it was confirmed on its website that the journal has an advisory board composed of a number of professors with scientific ranks and different specializations, and they work in well-known scientific and academic institutions and centers. On the above site, you will find a list of the names and addresses of the editorial board and the advisory board of arbitrators

## 6. **EDITORIAL TEAM / CONTACT INFORMATION**

The addresses of the editor-in-chief and his Deputy have been announced on the journal's website and in all issued numbers, including emails and phone numbers, to ensure ease and smooth communication.

## 7. **COPYRIGHT AND LICENSING:**

The publishing rights belong to the journal, and its contents may not be transferred or republished without the written consent of the journal's administration. An agreement has already been made with some parties to republish the Journal's contents in their repositories, such as (Dar Al Mandoumah), (EBSCO global databases) and (DOI Digital Object Identifier), Also, the journal has an International Classification (ISI) and has an Arab Impact Factor(AIP).

## 8. **PUBLICATION FEES**

An amount of $200 is paid for publishing research and studies that meet the conditions (After approval to publish the research), and this has been confirmed on the journal's website and in the terms of publication in the journal to make it easier for researchers to access before sending their research or studies for the purpose of publication.

## 9. **PROCESS FOR INDENTIFICATION OF AND DEALING With ALLEGATIONS OF RESEARCH MISCONDUCT**

All research and studies are subject to strict examination to ensure their safety and freedom from any bad research behavior, as follows:

. Examining the content to determine the percentage of plagiarism using the TURNITIN program. In the event that the plagiarism rate exceeds 15%, the research is rejected and not published.

- Require the researcher to sign a pledge not to publish the research or study in another journal, and that the research or study is his personal product and is not plagiarized from another source.

- The research is sent to two experts within the specialization and field of research and study to verify the integrity of the research scientifically, methodologically and linguistically, after concealing everything related to the researcher's contact 0information and place of work, and the experts' opinions are determined within the range of three options.
- 1. Approval of the publishing of research as it is.
- 2. Approval of publishing the research after making specific modifications.
- 3. Rejection of it.
- The research as it is not eligible for publication...
  In the event of approval of publication, a letter of initial approval is sent to publish the research, and the research takes precedence with other research for publication in the journal's issues. In the event that the two experts agree to publish the research after making modifications, the researcher is informed of the modifications that he should make, provided that the research is re-checked and examined after modifications have been made by the experts to verify that it fulfills the publishing conditions. Research which is not meeting the conditions of publication is, of course rejected.

10. **PUBLISHING SCHEDULE:**
The journal is published every six months.

11. **ACCESS:**
All readers can access the preparation of the electronic journal and view it through the journal's website.

12. **ARCHIVING:**
All published and unpublished research and studies are archived, in addition to keeping copies of the journal.

13. **REVENUE SOURCES:**
The journal's sources of income are as follows:

- Amounts of support provided by the Northern European Academy of Sciences and Scientific Research.
- Amounts collected from researchers for publishing their research and studies.
- The sums obtained from re-publishing the contents of the journal's editions in some repositories.

14. **ADVERTISING:**
The journal does not allow advertisements to be published on its website or on its printed pages.

15. DIRECT MARKETING
The journal does not have profitable marketing activities, except for what was mentioned in paragraph 13 in the case of a request for a hard copy.
Finally, all the previous information can be found on the journal's website in both Arabic and English.

**CONTACT US**

**WhatsApp: 0045 - 81946515**
**E-mail: Journal@neacademys.com**
**www.sst.journalnea.com**

All research and studies published in the journal are also published on the global database website EBSCO.
Dar Al-Mandumah website, Arabic databases, according to the cooperation agreement for scientific publishing

## Correspondence

**Address: Dybendal Allé 12, 1. Sal, nr. 18 / 2630-Taastrup,(Copenhagen) - DENMARK**
**Website: www.neacademys.com**
**E -Mail: Journal@neacademys.com**
**E – Mail: HR@neacademys.com**
**Tel: +45 7138 24 28**
**Tel : + 45 81 94 65 15**

## Annual subscription to the journal

You can subscribe annually to the electronic version of the journal for **$100** dollars, provided that it is sent to the person's email
**Academy account number – Denmark**
**Account.nr. 2600066970**
**Reg.nr. 9037**
**IBAN: DK 6090372600066970**
**SWIFT CODE: SPNODK 22**

## Journal publications schedule
## Semi-annual scientific journal published every six months according to the dates in below

**07/ 29 — 01/ 29**

**Published in this issue** **Index**

***Prof. Dr. Harith Salman Hasaani***

***Editor-in-chief of the Scholar Journal for Sciences & Technology***

## In the Name of Allah the Merciful

Praise be to Allah, Lord of the Worlds, and prayers and peace be upon the Seal of Messengers Muhammad Bin Abdullah and on his family and companions.

After here we meet with you in the first number of the Scholar Journal for Sciences & Technology, which we hope to be a lamp illuminating, For students of science everywhere, They receive the science and knowledge they need ،We are optimistic that we are on track to achieve the objectives of the Nordic Academy And its scientific journal, the dissemination of knowledge and the real information and provide it to anyone looking for it , and since it is difficult for any Journal to draw its features and determine its destination since the first issue, but we are trying to provide the basic indicators of ambition and direction in the way of culture long and difficult by careful to complete the requirements of scientific research sound in the published research and studies.

It is no exaggeration to say that the publication of a new scientific journal insisting and insisting on the availability of safety conditions and accuracy in its production of the first issue is to enter into a risk-free adventure at a time of explosion and decline in many of the concepts, visions and ethical values of scientific research , But the concern and emphasis on scientific values sound and correct despite the difficulty was and will remain the hope and goal of scientists and noble values at all times and places , And so it has been confirmed to achieve the conditions of publication specified in everything that is published, regardless of the reactions to maintain our balance of original researchers and students of science from the correct sources, it is not wise to collect a large number of writers and publishers, But the wisdom to attract diligent and diligent researchers, no matter how few they are, only a few who owe them credit in the antithesis of science and few owe them thanks to the enlightenment of humanity and guidance.

ISSN (Print) 2794-7629
ISSN (Online) 2794- 4549
Received 15/08/2024
Accepted 20/09/2024

**FULL PAPER**

# Combined White Laser and Slit Lamp for Human Eye Diagnostic

***Prepared by***

***Prof.Dr.Ziad Tarik Al-Dahan***
*Biomedical engineering Department*
*College of engineering*
*AlBayann University, Baghdad, Iraq*

***Ali Mahmoud issa***
*Biomedical engineering Department*
*College of engineering*
*AlBayann University, Baghdad, Iraq*

***Ammar Al-Jashaami***
*Consultant ophthalmologist*
*Ibn Al-Haitham eye Teaching Hospital,*
*Jenna ophthalmic center, Baghdad, Iraq*

**Abstract**

This study investigates the modification of the slit lamp, a crucial ophthalmic tool, by substituting a white laser for the conventional halogen light source. The purpose of this modification is to improve the slit lamp's efficiency and diagnostic capabilities. White laser technology enhances the visibility and differentiation of ocular tissues by providing better brightness, intensity, and color accuracy. White lasers also use less energy, produce a constant amount of light, and require less maintenance. The optical system will be adjusted, specific filters and lenses will be added, and appropriate heat management will be ensured as part of the redesign process. Image quality and diagnostic accuracy are further enhanced by the combination of a white laser light system with a high-resolution digital camera system. After outlining the advantages, potential difficulties, and implementation strategies, the study comes to the conclusion that using white Slit lamp lasers have the potential to greatly improve ocular diagnostics, which is advantageous to patients as well as ophthalmologists.

**Keyword:** Slit lamp, white laser, retinal eye, and image.

## 1. Introduction

In 2004, the World Health Organization (WHO) estimated that 285 million individuals worldwide were visually impaired, and 80 percent of those cases could be prevented or treated [1]. The yearly market for eyewear was valued at more than 20 billion euros in 2012. Furthermore, almost 57% of revenues were generated by eye care goods, diagnostic tools, and eye surgery. Because it has the potential to significantly enhance people's quality of life, research on human vision and eye optics therefore directly affects society [2]. Wave front deformations are the source of aberrations. Due to the order of the Zernike polynomials in which they are frequently reduced, they can be divided into low-order and high-order aberrations (HOA) [3] Fig. 1. About 90% of the total eye wave is caused by low-order aberrations.

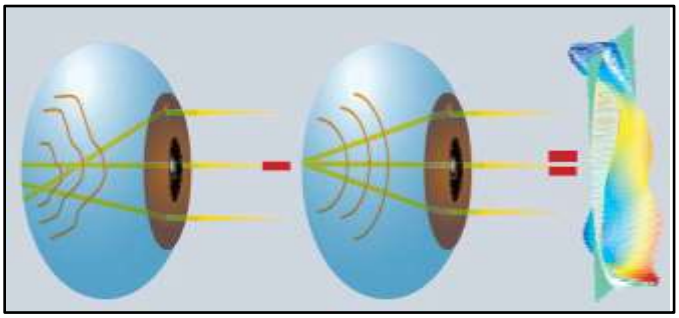

**Figure 1.** From left to right, aberrated wave front, spherical wave front and wave aberration map calculated as the difference between them [4].

One of the most common pieces of equipment in an ophthalmologist's office is the slit lamp biomicroscope, which is used to screen the outer structure and the anterior segment of the eye. As shown in Fig. 2, the device has three main components: stereomicroscope, slit lamp illumination unit, and the mechanics module.

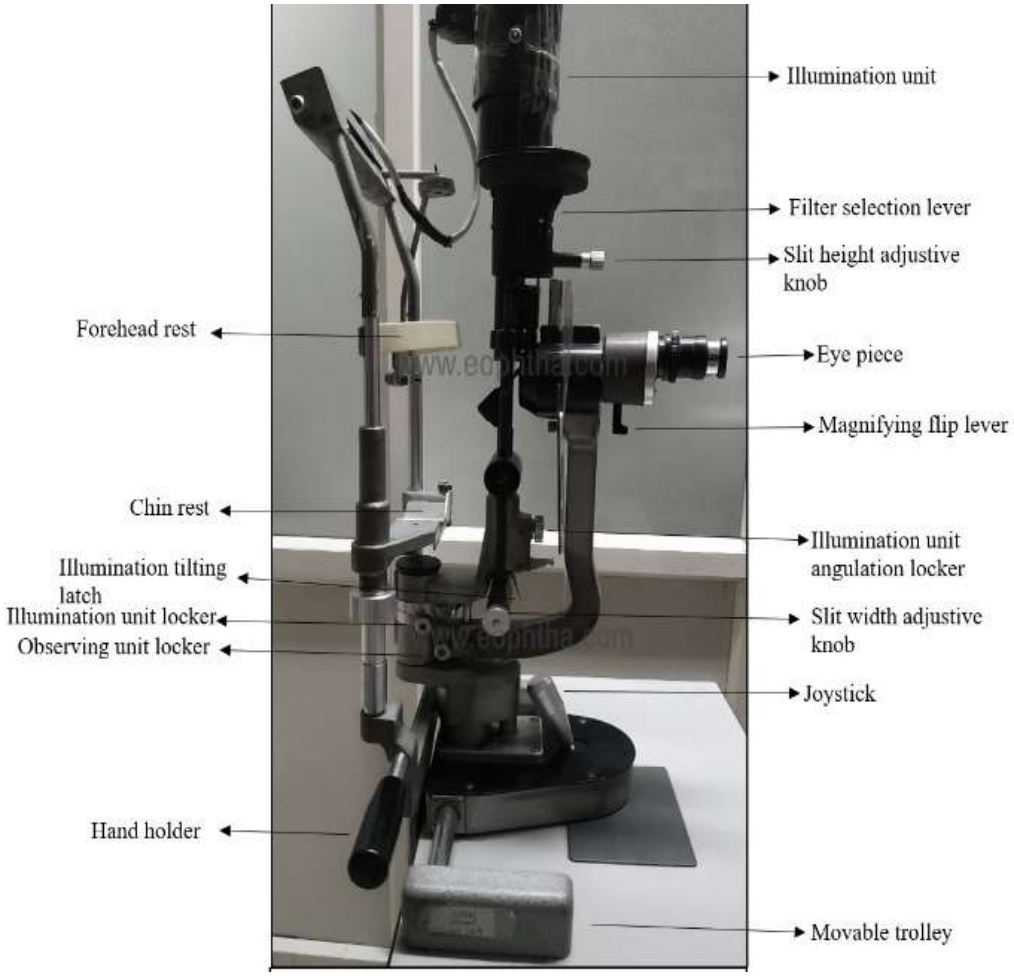


**Figure 2** : Slit lamp anatomy [5]

White Laser Light as an Alternative to Slit Lamp.herokuapp.com .

The slit lamp is one of the major and most commonly used instruments in ophthalmology, which is used to assess the anterior and posterior ocular tissues. Employment of slit light has been a traditional method, and these come with LED or halogen light for illuminating the eye. However, recent advancements in laser technology—particularly in the area of white lasers—offer a potent replacement.

## 2. Materials and methods

### 3.1. Redesigning the Slit Lamp with White Laser Illumination

Remodeling the slit lamp with a white laser light source, as depicted in Fig. 3, may improve its functionality and diagnostic capability. For those who provide eye care, this would also increase the lamp's effectiveness and usefulness. The benefits of white laser light over halogen light are shown in Table 1.

**Figure 3**: White laser source

**Table 1:** Benefits of white laser light

| Parameter | White Laser | Halogen Light |
|---|---|---|
| Brightness and Intensity | a highly intense and bright light, significantly improving the visibility of fine details in the eye structures | Less intense which may limit the ability to see minute details, especially in highly pigmented or densely packed tissues |
| Color Accuracy and Rendering: | Superior color rendering and accuracy, closely mimicking natural sunlight. This enhances the differentiation of various tissues and abnormalities in the eye. | broad spectrum of light but with lower color accuracy, which can make it harder to distinguish subtle differences in tissue coloration |
| Energy Efficiency | More energy-efficient, providing high brightness with lower power consumption, less heat generation and a longer operational lifespan | Consumes more power and generates more heat, which can necessitate additional cooling mechanisms and lead to shorter bulb life |
| Consistency and Stability | Offers stable and consistent light output over time, reducing the need for frequent adjustments and maintenance | Light output can degrade over time, leading to inconsistent illumination and the need for regular bulb replacements |

3.2.**Optical System Adjustments:**

- Beam Quality: Ensure the white laser produces a high-quality, uniform beam that can be finely adjusted in width, length, and angle, similar to traditional slit lamp beams.
- Filters and Lenses: Use specialized optical components designed to handle the intensity and specific properties of laser light. This includes UV and IR filtering to protect the eye and the user.

- **Light Source Replacement: Secure the installation of laser and remove the methods of attaching cooler systems.**
- **Optical Path Modifications: Add beam shaping optic filters lenses.**
- **Power Supply and Control: While using the device, they need to be able to control it either by an appropriate power source and buttons.**
- **Safety Features: The following organizational laser safety measures and Laser interlocks should be implemented.**
- **Implementation Steps**
- **Feasibility Study: Critique the potentials for gain, the challenges that may arise, and the costs.**
- **Prototyping: Functional testing in actual setting, and enhancements of the prototype.**
- **Iterative Design: Repeat the entire process based on the feedback received and results obtained.**
- **Manufacturing and Testing: Since they seek to provide customers with accurate information, the laws should be complied with to ensure that they do not present false information about the products. This paper shows that having white lasers extra to the slit lamps enhances better brightness, precision and time usage in the diagnosis process. Of all the potential redesigns, this particular one promises substantial benefits for the doctors and patients of the specialty. The individual parts and final system design are shown in Fig. 4.**

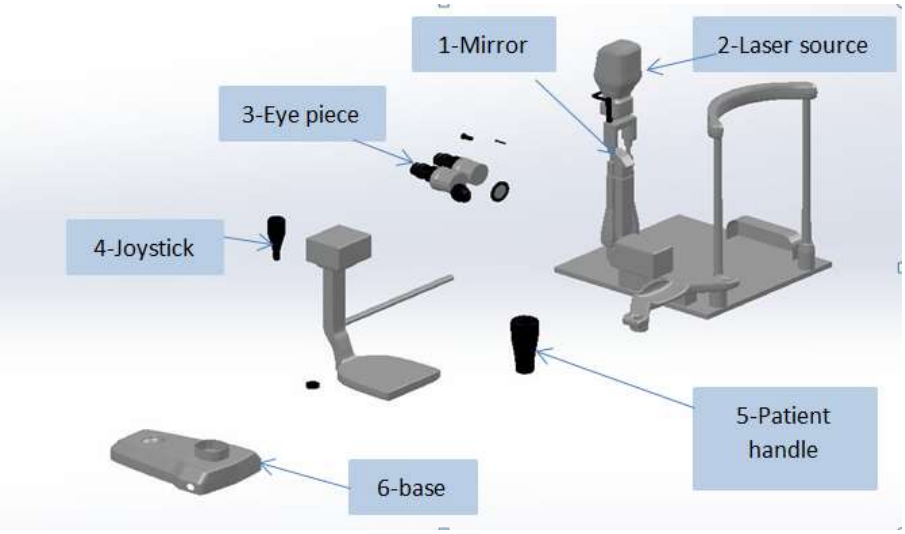


**Figure 4**: Individual parts and final system design

From figure 4, (1) represent the mirror used for reflection of laser beam, (2) white laser source, (3) Doctor eye piece, (4) user joystick, (5) patient handle, (6) base

### 3.3.**Thermal Management:**

- Cooling Mechanisms: Integrate fresher cooling systems to control the slight heat which the white Laser may produce for it to operate safely and for a long time.
- Materials: Ensure that the heat is well-coupled to reduce the temperature gradients using high thermal conductivity materials to retain the quality of the optical parts as shown in Fig. 5..

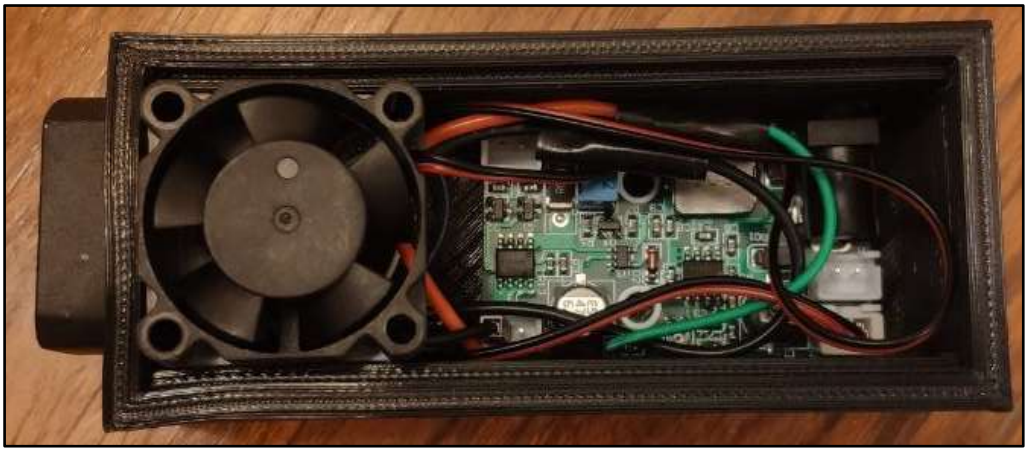

Figure 5: White laser with cooling fan

## 3. Results and discussions

A combination of a white laser in a slit lamp is also effective for the enhancement of its illumination, resolution, and power consumption. The following are some of the benefits that one is likely to benefit from whenever he opts for the white laser;

- Higher Intensity and Precision: Provided that light is improved or directed, one gets to see through or visions are enhanced or well-defined.
- Improved Image Quality: Improved performance in brightness and definition of image.
- Adjustable Wavelengths: Various niches to provide ultimate flexibility for changing the lighting for various diagnostics.
- Energy Efficiency: Some other advantages of smart retail include, lower power usage and less heat output from equipment.

Coordinate the white laser with high resolution digital camera system to obtain clearer photographs and videos helping in diagnostic system. Optimize the white laser illumination with an image processing methods that improve image resolution and contrast of captured images.

### 3.1.**Safety Enhancements:**

Laser Safety Standards: Manage laser visibility by strictly following the laser safety measures in order to reduce the risk of inflicting the patient or the operator in case something goes wrong.

Protective Measures: Install safety systems such as timers and safety switches to minimize instances where the laser beam is likely to fall on people around it.

### 3.2.**Interface and Control:**

- Control board: use board that regulate the power to the laser element different types of use boards are used in this are laser diode use board and lamp use board.
- Feedback Mechanisms: Develop features which are feedbacks that depict the state of the laser and the system at a glance- time based as shown in Fig. 6.

Figure 6: Laser control board

Figure 7: pictures by using white laser on the left and halogen light on the right

In figure (7) we can see the brightness of the white laser is more than the halogen light also the white light is more comfortable to the human eyes than the yellow light.

Figure 8: Eye pictures by using white laser light

In figure (8) we can see the eye pictures by using a white laser light in slit lamp.

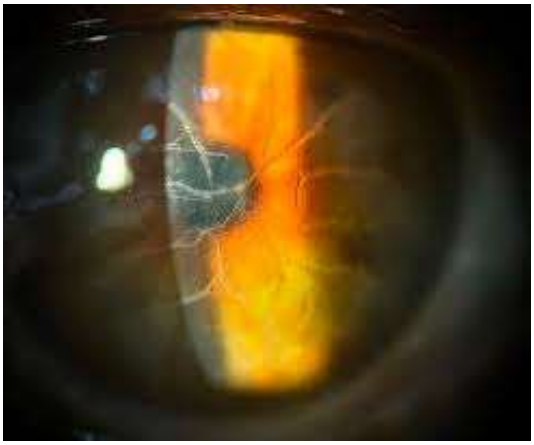

Figure 9: Eye pictures by using halogen light

In figure (9) we can see the eye pictures by using a halogen light in slit lamp.

From laser properties which is coherent that mean it have the ability to penetrate more than the halogen light also the brightness of the white laser is more than the halogen light and the white light is more comfortable to the human eyes than the yellow light therefore the picture enhanced and can be picturing the retina in case of thick glaucoma.

## 4. Conclusion

Adjusting the previous slit lamp design by integrating a white laser light has numerous advantages such as higher brightness, higher color rendering, saving of energy and higher and more stable output. However, there are certain difficulties which arise; nevertheless, the opportunities to improve diagnose and increase the effectiveness of work in ophthalmological practice are significant, so molecular optical imaging becomes one of the most successful modifications of ophthalmic equipment. Thus, with proper approaches as careful integration of the white laser technology, giving more attention to user safety, and extensive training of the practitioners, slit lamps that incorporates such improved white laser technology enhance eye care practice and impact patients positively.

***References***

[1] A. Pathipati and J. Tsai, "Eye Care Industry Analysis," Journal of Academic Ophthalmology, vol. 10, no. 01, Jan. 2018. doi:10.1055/s-0037-1620237

2] D. A. Atchison and G. Smith, "Retinal Image Quality," Optics of the Human Eye, pp. 349–376, Feb. 2023. doi:10.1201/9781003128601-22.

[3] T. Kuriakose, "The slit lamp examination," Clinical Insights and Examination Techniques in Ophthalmology, pp. 55–62, 2020. doi:10.1007/978-981-15-2890-3_6

[4] "Who releases new global estimates on visual impairment," World Health Organization, https://www.emro.who.int/control-and-preventions-of-blindness-and-deafness/announcements/global-estimates-on-visual-impairment.html

[5] Y. Ben-Menahem, Rethinking the Concept of Law of Nature: Natural Order in the Light of Contemporary Science. Cham: Springer, 2023.

ISSN (Print) 2794-7629
ISSN (Online) 2794- 4549
Received 18/08/2024
Accepted 10/09/2024

**FULL PAPER**

# Study of the Importance of Agricultural Extension Role in Agricultural Development from the Point of View of Workers in Agriculture Extension in Nineveh Governorate

***Prepared by***

***Prof. Dr. Ahmed Awad Talb Altalb***
*Dept. of Agricultural Extension & Technologies Transfer, College of Agriculture and Forestry, University of Mosul, Iraq*
*ahmed_altalb@uomosul.edu.iq*

***Hassan Hamed Sukar***
*Dept. of Agricultural Extension& Technologies Transfer, College of Agriculture and Forestry, University of Mosul, Iraq*
*h_info@uomosul.edu.iq*

***Dr. Sally Ibrahim Mahmoud Ibrahim***
*Ministry of agriculture and land Reclamation in New capital city, Egypt*
*sallyunes83ss@gmail.com*

**Abstract**

Aim of current research is to know role of agricultural extension on agricultural development from perspective of agricultural guides in Nineveh governorate in general, and on each item of research. To find correlation between role of agricultural guidance in realizing agricultural development from perspective of agricultural extension and the following independent variables (academic achievement, specialization). Research's society was (418) active agricultural guides in Nineveh governorate. Out of this society, a simple random sample of (168) personnel were chosen, representing (40%) and (30) were excluded after finding stability of research. Two parts survey was made to collect data: first part included independent variables of respondents. Second: (30) items scale of role of agricultural guidance on agricultural development from perspective of agricultural guides. Survey passed a panel of experts in agricultural guidance and rural development to verify its surface and content reliability. Stability was found using Alpha-Kronbach formula scoring (0.88).

Results showed that role of agricultural guidance from perspective of agricultural guides in Nineveh governorate is moderate tends to ascend. Results also showed positive moral correlation between role of agricultural guidance in agricultural development from perspective of agricultural guides and the following independent variables (academic achievement, specialization). However, no morally significant correlation was found between dependent variables and the following independent variables (age, years spent as an agricultural guide, participation in training course).

## Introduction and Problem of research

World seeks an integrated agricultural development by following numerous means and methods such as using modern agricultural methods and techniques, an important element in agricultural development focuses on perfect use of cultivated area to increase productivity (Samir 2018); (Al-Hashimi 2005). Agricultural development is an important way to preserve and expand cultivated Area , preserve water resources, develop and support agriculture academically and technically to achieve self-sufficiency (Baligh, 2004). Agricultural development aims at enhancing well-being of farmers in rural areas via increasing available cultivated (A-Akaf, 2014). Thus it's the duty of governments of developing countries in particular to fully support agricultural sector, solve relative problems due to obstacles of agricultural development on one hand and poor administrative, financial technical technological and information potentials of agricultural sector on the other hand (Ali, 2012). Agricultural development is the grale of guidance facilities, the outcome of activities of these bodies. The aim of these facilities is to qualify human element, raise its capacity and ensure participation in their guidance programs (Keshta, 2012).

Agricultural development is managing, preserving natural resources, steer technical foundation, change in a way guarantee meeting the needs of now and upcoming generations continually (Bashar ,2003).

For agricultural development to happen and realize its aims, all related parties (inhabitants and facilities) must participate in its plans and programs. One of these parties is agricultural guidance which provides agricultural activities and pedagogical services for farmers to make desired behavioural changes in their knowledge, skills and trends to enable farmers to participate in development processes. Agricultural guidance is a pedagogical process of a central job affecting all other aspects of rural society. Importance of agricultural guidance lies in developing rural life. It's starting line to solve rural problems. The most important aim of agricultural guidance is to increase agricultural production, improve quality, and raise well-being of rural families. Agricultural development can't happen without the link between agricultural research centers and farmers (Aziz, 2017). Thus one realizes role of agricultural guidance in enhancing agricultural development wheel. This agricultural guide transfers agricultural information and ideas to farmers and encourages farmers to apply them (Al-Karrot, 2019). Agricultural guidance is the link between farmers and agricultural researches centers, give farmers modern agricultural knowledge and take their problems to these centers to look for appropriate solutions (Al-Farkari, 2019); (Al-Zubaidi, 2018).

In Iraq in general and Nineveh governorate in particular , the reason behind weak agricultural development may be the result of obstacles facing plans of economical development in the past until nowadays, that caused production disorders from weak economical systems, vague agricultural policy , not to forget to mention external factors and its related challenges. Success of agricultural development processes depends on solving these problems (Nafi, 2015). Considering all the above mentioned, researchers decided to do this research to know agricultural development in Nineveh and the role played in success of agricultural development. Thus the researchers put the following questions:

- What is the role of agricultural guidance on agricultural development from the perspective of agricultural guides in Nineveh governorate in general?

- What is the correlation between role of agricultural guidance in agricultural development from perspective of agricultural guides with a number of personal, social, economical and communicative variables. The answer to these questions is what the current research is all about.

## Aims of Research

1- Know role of agricultural guidance in agricultural development from perspective of agricultural guides in Nineveh governorate in general.
2- Know role of agricultural guidance from perspective of agricultural extension measured through every item in research.
3- Know correlation between role of agricultural guidance in agricultural development from perspective of agricultural guides and independent variables (age, academic achievement, specialization, years spent in this job, participation in training courses).

## Materials and Methods

**1-Area:**

Research took place in Nineveh Governorate, one of most important governorates agriculturally with huge areas of cultivated lands with numerous agricultural branches and divisions with a lot of staff.

**2- Society and sample:**

Society was all (418) active agricultural guides. A random simple sample was chosen scoring (168) representing (40%) and excluded (30) persons participated in stability test.

## 3- Design tool (questionnaire):

A Two - parts survey was used to collect data. First part included all independent variables of researchers (age, academic achievement, specialization, years spent in this job, participation in training courses) second (30) items representing role of agricultural guidance in agricultural development from perspective of agricultural guides:

**4- Measuring variables:**

**A- Independent variables:**

- **Age**: Measured in years.

**- Academic achievement:** Measured via: agricultural secondary school graduate (1) agricultural institution graduate (2) university graduate (3) postgraduate (4).
**- Specialty:** Measured as follows: specialist (2), non-specialist (1).
**- Years spent in this job:** measured via period of working as an agricultural guide in years.
**- Participation in training courses:** measured: trained (2 points), untrained (1 point).
**- Participation in training courses:** Measured via: trained (2) untrained (1).

**B- Measuring dependent variable: Role of agricultural guidance in agricultural development:**

Measured through (30) items scale talks about role of agricultural guidance in agricultural development with (5) alternatives: imminently important (5), greatly important (4), moderately important (3) rarely important (2) unimportant (1). Sum of respondents answers represent role of agricultural guidance in agricultural development from perspective of agricultural guides.

**5- Reliability and stability:**
Research tool passed a panel of experts and specialists in agricultural guidance to verify surface and content reliability
**6- Collecting data:** The data was collected from the date (April until May, 2024).

## Results and discussion

### - Know role of agricultural extension in agricultural development from perspective of agricultural guides in Nineveh governorate in general:

Results showed that highest digit was (150) and the lowest was (30) with a means of (89) digital units. Respondents were categorized according to their answers into three types as shown in table (1).

Table (1): Categorizing sample according to importance of agricultural extension in agricultural development in genera:

| Categories | Number | Percentage% |
|---|---|---|
| Low (30-69) | 48 | 28,57 |
| Medium (70-109) | 65 | 38,69 |
| High (110-150) | 55 | 36,74 |
| Total | 168 | 100% |

Table (1) shows that medium category (70-109) scored highest (38,69) and low scored lowest (28,57). Meaning that most respondents think that role of agricultural guidance is moderate tends to ascend. This may be because respondents realize role of agricultural guidance in agricultural development.

### - Know role of agricultural guidance from perspective of agricultural guides measured through every item in research:

Research items were arranged according to average of respondent's answers as shown in table (2)

| No. | Items | Arithmetic Means |
|---|---|---|
| 1 | Extension saves soil from turning into desert | 4,70 |
| 2 | Guidance enhances productivity | 4,61 |
| 3 | Increases farmers realize role of using crops to fertilize soil | 4,50 |
| 4 | Guidance shows benefits of using machines | 4,44 |
| 5 | Helps in fully exploitation of rural natural resources | 4,32 |
| 6 | Deliver modern technologies and agricultural ideas into farmers | 4,25 |
| 7 | Spotify agricultural problems of farmers | 4,10 |
| 8 | Help farmers to use pesticides appropriately | 4,00 |
| 9 | Agricultural guidance preserves soil and warns against soil erosion | 3,98 |
| 10 | Encourage farmers adopt modern ways in cultivation | 3,90 |
| 11 | Increase farmers awareness of using improved seeds | 3,88 |

| | | |
|---|---|---|
| 12 | Engage farmers in agricultural guidance programs | 3,85 |
| 13 | Guidance celebrate field day to teach farmers about modern agricultural techniques | 3,80 |
| 14 | Make training courses for different agricultural techniques | 3,75 |
| 15 | Agricultural guidance increases farmers belief in results of agricultural centers | 3,66 |
| 16 | Agricultural guidance helps farmers to fully use available natural and human resources | 3,50 |
| 17 | Agricultural guidance increases farmers awareness of effective farm management | 3,44 |
| 18 | Agricultural guidance helps explain plow free cultivation | 3,33 |
| 19 | Find and support farm markets | 3,25 |
| 20 | Helps in setting goals of delivering appropriate agricultural technologies to farmers | 3,20 |
| 21 | Helps to magnify results of using this techniques | 3,18 |
| 22 | Activate role of cooperative societies in rural development | 3,10 |
| 23 | Shows importance of biological fertilizers in preserving soil | 2,90 |
| 24 | Encourage farmers to fight pests early | 2,80 |
| 25 | Apply modern methods to recycle domestic wastes in agriculture | 2,70 |
| 26 | Encourage farmers to use covered farming | 2,66 |
| 27 | Provide farmers by new production skills via practice | 2,50 |
| 28 | Organize training courses to utilize underground waters | 2,20 |
| 29 | Lowers costs of agricultural production | 2,10 |
| 30 | Chooses right spots to coordinate and imply guidance plans | 1,90 |

Table (2) shows that first three items (Extension prevents the soil change to desert, guidance enhances productivity, increases farmers realize role of using crops to fertilize soil). Scored high. Thiis may be because agricultural guides know role of agricultural guidance in preventing desert, enhance agricultural production and preserve soil fertility.

Last three items (Organize training courses to utilize underground waters , Lowers costs of agricultural production, chooses right spots to coordinate and imply guidance plans) meaning that respondents lack knowledge about roe of agricultural guidance in choosing spots to apply agricultural guidance plans, lowering costs and organize training courses for farmers.

**- Know correlation between role of agricultural guidance in agricultural development from perspective of agricultural guides and independent variables (age, academic achievement, specialization, years spent in this job, participation in training courses).**

**1- Age:**

Results showed that eldest respondents into the following three types shown in table (3).

Table (3): categorizing respondents according to their age and its relation to their perspective about role of agricultural guidance in agricultural development.

| Categories (years) | Number | Percentage% | Simple Pearson conjunction factor (r) | P-Value |
|---|---|---|---|---|

| | | | | |
|---|---|---|---|---|
| Low (27-36) | 43 | 25,57 | 0,037 | 0.541 |
| Medium (37-46) | 75 | 44.65 | | |
| High (47-56) | 50 | 29,78 | | |
| Total | 168 | 100 | | |

Table (3) shows that medium category (37-46) scored highest percentage (44.65) and low category scored (25.57). Results showed no correlation between role of agricultural guidance and age. Simple Pearson conjunction factor scored (0,037) it is not significant. Meaning that agricultural extension opinion is irrelevant to his age, rather it may be relevant to other factors like expertise.

**2- Academic achievement:**

Respondents were categorized according to their academic achievement into 3 types shown in table (4)

Table (4): categorizing researchers according to academic achievement and its relation to their opinion about role of agricultural guidance n agricultural development

| Categories (years) | Number | Percentage% | Spearman rank conjunction factor (rs) | P-Value |
|---|---|---|---|---|
| Graduate of agricultural secondary school | 37 | 22,02 | *0.190 | 0.04 |
| Graduate of agricultural institution | 48 | 28.57 | | |
| University graduate | 68 | 40,48 | | |
| Post graduate | 15 | 8,93 | | |
| total | 168 | 100 | | |

Table (4) shows that highest category was university graduates (40.48) and the lowest was postgraduates (8.93). Results showed positive moral relation between role of agricultural guidance in agricultural development and academic achievement. Spearman conjunction factor was (*0.190) significant at (0.05) level. Thus reject null hypothesis: no morally significant relation is found between role of agricultural guidance in agricultural development and academic achievement. Meaning that certificate of employee plays big effective role in knowing role of agricultural guidance in agricultural development.

**3- Specialization:**

Table (5): shows categorizing researchers according to specialization and its relation with role of agricultural guidance

| Categories | Number | Percentage% | Simple Pearson conjunction factor Spearman rank | P-Value |
|---|---|---|---|---|

| | | | conjunction factor (rs) | |
|---|---|---|---|---|
| Specialized | 50 | 29,16 | *0.360 | 0.02 |
| Non specialized | 118 | 70.25 | | |
| Total | 168 | 100 | | |

Table (5) shows that non-specialized scored high percentage (70.25%). Results show that there is positive morally significant relation between role of agricultural guidance in agricultural development and specialization. Pearson simple conjunction factor (*0.360) significant at the level (0.05). Thus reject null hypothesis: there is no correlation between role of agricultural guidance in agricultural development and specialization. Meaning that specialization of respondents plays big role in drawing his information of role of agricultural guidance in agricultural development.

**4- Years spent as agricultural guide:**

It was found that highest number of years spent as an agricultural guide was (50) and the least was (6) with an average of (28) years, respondents were categorized into the following three types shown in table (6).

Table (6): Categorizing researchers according to years spent as an agricultural guide

| Categories (years) | Number | Percentage% | Simple Pearson conjunction factor (r) | P- value |
|---|---|---|---|---|
| Low (7-21) | 30 | 17,86 | 0.087 | 0.8 |
| Medium (22-36) | 80 | 47.61 | | |
| High (37-59) | 58 | 34,53 | | |
| Total | 168 | 100 | | |

Table (6) shows that medium category scored highest percentage (47,61) while low category scored (17,86). Results showed that no morally significant relation between role of agricultural guidance in agricultural development and years spent as an agricultural guide. Simple Pearson conjunction factor was (r) (0.087) it is immoral. Meaning that years spent in this job is irrelevant to their opinion about role of agricultural guidance in agricultural development. Thus accept null hypothesis that there is no morally significant relation between role of agricultural guidance in agricultural development. Meaning that researchers' years as an agricultural guide have nothing to do with his opinion about role of agricultural guide in agricultural development.

**5- Participation in training courses:**

Researchers were categorized according to their participation in training courses into the following types shown in table (7).

Table (7): Categorizing researchers according to their participation in training courses and its relation to their point of view about role of agricultural guidance in agricultural development.

| Categories | Number | Percentage% | Spearman rank conjunction factor (rs) | P- Value |
|---|---|---|---|---|

| | | | | |
|---|---|---|---|---|
| Participated | 80 | 47,62 | 0.086 | 0.079 |
| Non-participant | 88 | 52.38 | | |
| Total | 168 | 100 | | |

Table (7) shows that non-participants scored highest percentage (52.38), Meaning that most researchers aren't trained on agricultural guidance and development. Results showed no correlation between role of agricultural guidance in agricultural development and participation in training courses. Spearman rank conjunction factor (0.086) immoral. Thus accept null hypothesis: there is no morally significant relation between role of agricultural guidance in agricultural development and participation in training courses. Meaning that participation in training courses doesn't affect researchers' opinion about role of agricultural guidance in agricultural development.

## Conclusions

1- It is concluded that respondents have full knowledge on role of agricultural guidance in agricultural development in general.

2- Item that scored high was (guidance saves soil from turning into desert) meaning that researchers are fully aware of role of agricultural guidance in preventing desert.

3-The following independent variables (academic achievement, specialization) is directly connected to respondents opinion of role of agricultural guidance in agricultural development in general.

## References

1. Ali, Mohammed Saleh Hamad (2012). The role of the state in solving the obstacles to agricultural development in Iraq after 2003, Journal of Accounting and Financial Studies, Volume 6, Issue 14, University of Baghdad / College of Education Ibn Al-Haytham.

2. Al-Akaf, Jadallah Ali Al-Mabrouk, Jibril Abdul Matlab Saleh Khalifa (2014). Obstacles to Agricultural Development in the Green Mountain Coast Style in Libya, The Agricultural Sector in the Green Mountain Coast Municipality, Published Research, Faculty of Arts and Sciences Al-Marg, University of Benghazi.

3. Al-Hashimi, Abdul Reda Matar (2015). Agricultural Development in the Afak District: A Study in the Components and Obstacles, Al-Qadisiyah Journal for Human Sciences, Volume 8, Issue 2-4, University of Al-Qadisiyah, Faculty of Arts.

4. Al-Zubaidi, Marwa Amjad Saeed (2018). The Role of Agricultural Employees in Managing the Process of Transferring Agricultural Technologies to Farmers in Nineveh Governorate, Master Thesis, University of Mosul, College of Agriculture and Forestry, Mosul, Iraq.

5. Al-Farkari, Afaf Shuaib Youssef (2019). Determinants of the work of research centers from the point of view of agricultural researchers working in them in the governorates of Nineveh and Salah Al-Din, Master Thesis, Faculty of Agriculture, Department of Agricultural Extension, University of Tikrit.

6. Al-Karrot, Abu Muslim Abu Zeid (2019). Lecture on Rural and Agricultural Development at the Agricultural Extension and Rural Development Research Unit in Ismailia, Egypt.

7. Aziz, Khaled Fadel Ahmed (2017). The impact of agricultural extension on rural agricultural development: A case study of Abu Zeid, West Kordofan State, supplementary research for obtaining a bachelor's degree with honors

8. Bashar, Fahmy, (2003). Towards Sustainable Agricultural Development in Iraq, FAO, Rome.

9. Baligh, Abdel Moneim (2004). Land, Man and Agricultural Development in the Arab World, 1st Edition, Egyptian Library, Alexandria.
10. Keshta Abdel Halim Abbas (2012). Agricultural Extension New Vision, Dar Al-Nada Printing, Faculty of Agriculture, Cairo University, Egypt.
11. Nafi, Dr. Faisal Abdel Fattah (2015), Agricultural Development Performance in Iraq and the Problem of Food Deficit, Al-Mustansiriya Journal for Graduate Studies, Issue 50.
12. Samir, Raafat Riad Abdel Wahab (2018).Obstacles to agricultural development from the point of view of agricultural employees in Salah al-Din Governorate, Master's thesis, University of Tikrit, Salah al-Din.

ISSN (Print) 2794-7629 Received 12/08/2024
ISSN (Online) 2794- 4549 Accepted 07/09/2024

**FULL PAPER**

# Iraqi Retinal Fundus Diabetic Retinopathy Dataset (IRFDRD)

***Prepared by***

***Prof.Dr.Ziad Tarik Al-dahan***
*Department of Biomedical Engineering*
*Al-Bayan University, Baghdad, Iraq.*
ziadrmt1959@yahoo.co.uk

***Noor Ali Sadek***
*Department of Biomedical Engineering*
*Al-Narain University, Baghdad, Iraq*
nooraliz810@gmail.com
ORCID: http://orcid.org/0009-0004-4013-0544

***Suzan Amana Rattan,***
*AlKindy College of Medicine,*
*University of Baghdad, Baghdad, Iraq.*
suzanamana@kmc.uobaghdad.edu.iq.

***Ahmed F.***
*Department of Artificial Intelligence*
*and Robotics Engineering*
*Al-Narain University*
ahmed.f.h.1976@gmail.com
ORCID: https://orcid.org/0000-0003-2483-0028

***Brendan Geraghty***
*Department of Musculoskeletal Biology*
*Institute of Ageing and Chronic Disease*
*University of Liverpool, L7 8TX, UK*
bren@liverpool.ac.uk
ORCID: https://orcid.org/0000-0003-0561-6667

***Ahmed Kazaili***
*Department of Biochemistry & Systems Biology*
*Institute of Systems, Molecular and*
*Integrative Biology, University of Liverpool*
*Liverpool, L69 3GH, UK.*
ahmed.kazaili@liverpool.ac.uk
ORCID: https://orcid.org/0000-0002-0400-7432

## Abstract

Diabetic Retinopathy (DR) is a leading cause of vision loss globally. Early diagnosis is crucial for preventing blindness. This research utilizes fundus camera images of the retina to analyze DR. The dataset is classified into five categories: healthy, mild, moderate, severe, and proliferative DR. Infrared fundus reflectance (IRFDR) images have shown promising outcomes when employed with deep learning algorithms

**Keywords:** DR, IRFDRD, deep learning, DR classification, DR detection.

Specification Table

| | |
|---|---|
| Subject area | Medicine and ophthalmology |
| More specific subject area | Retinal screening |
| Types of data | Images |
| Data format | JPEG |
| Experimental factors | All images are classified as healthy, mild, moderate, sever, and proliferative DR. |
| Experimental key finding | When fundus images are used for training of deep learning models, they show fast and accurate classification of DR. |
| Data source location | Al-Nahrain University/ College of Engineering/ Biomedical Engineering Department |
| Data accessibility | https://github.com/noor-aliz810/IRFDRD.git |

**Value of the Data**

- Fundus camera is mostly used in DR detection. Moreover, it is safe retinal imaging technique.
- IRFDRD can be used to train deep learning models that can classify early signs of DR.
- The data is comprehensive, containing DR severity stages (healthy, mild, moderate, severe, and proliferative DR).
- This dataset is- to our knowledge- the first Iraqi dataset publicly available.
- Researcher with interest in detection and classification of DR can use IRFDRD images, combine them with others' datasets, and resolve them for further perspectives.

**Background:** Diabetes Mellitus is an endocrine condition caused by elevated plasma glucose level due to abnormal insulin secretion. Diabetes Mellitus is a progressive disease that cause many complications such as retinopathy, nephropathy, neuropathy, and autonomic dysfunction (Reichel et al., 2015). Diabetic Retinopathy (DR) is one of the important complications, if it diagnosed earlier, severe loss of vision can be avoided. Therefore, it is essential that patient with diabetes undergo routine screenings for DR with a suitable diabetic eye screening tool. DR pathogenesis occurred from either microvascular occlusion or microvascular leakage affecting the retinal precapillary arterioles, capillaries, and venules. According to statistical research, DR affects 80% of people with diabetes who struggle with the disease for 15 to 20 years (Wilkinson, 2003). DR is the primary cause of blindness and visual impairment worldwide, and its rate is steadily rising as a result of an increase in the number of patients with Diabetes Mellitus (Daniel Shu Wei Ting et al., 2015 and Dolly Das et al., 2022). The diagnosis of DR involves an eye examination through a range of features that aim to detect microvascular damages in the retina such as; microaneurysms, haemorrhages, hard exudates, soft exudates (cotton wool spots), neovascularisation, and macular oedema, as shown in Figure (1). Diabetic retinopathy is classified into four stages according to its severity: mild, moderate, severe and proliferative Diabetic Retinopathy (Daniel Shu Wei Ting et al., 2015).

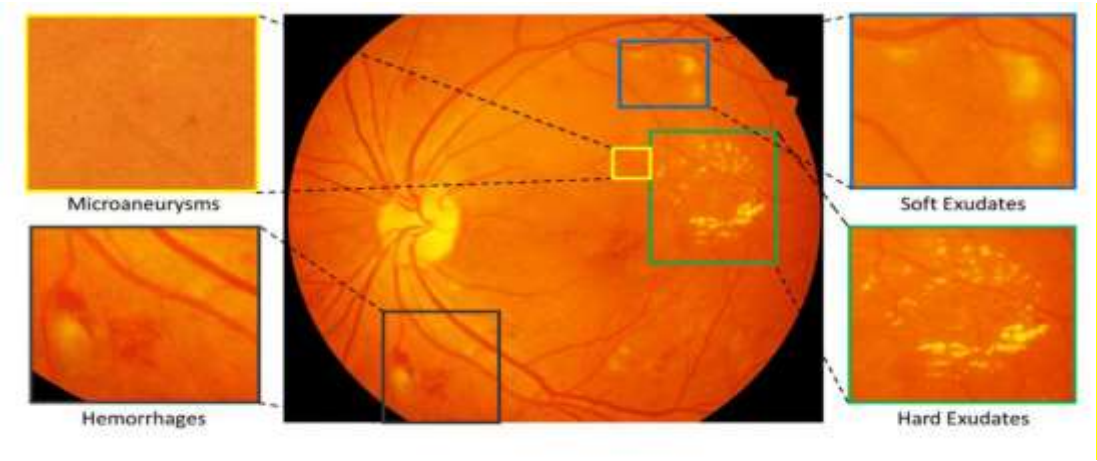


Figure (1) A color fundus image showing various retinal abnormalities linked to diabetic retinopathy. larger sections showing the presence of hard exudates, hemorrhages, soft exudates, and microaneurysms (Wilkinson, 2015).

## Dataset Description

The dataset in this study comprises fundus images of the retina collected from the main center of ophthalmology in Iraq. The IRFDRD is classified into five DR classes: healthy, mild, moderate, severe, and PDR, stored in JPEG format with a separate folder for each class. Each folder contained the fundus images, the total numbers of each group are shown in Table (2). These classes were very useful in facilitating the management of the data for training by deep learning algorithm.

## Method

This section consisted of retinal imaging system to observe the retinal disease for diagnostic operation at first. Then, a full description of the collected IRFDRD that have been used to evaluate the performance of the algorithms used for diagnosis or classification of eye diseases especially diabetic retinopathy.

## 1. Retinal imaging system:

Professional skill, a large cost, and a long time are required for the examination of the retina in conventional ways to detect DR, depending on the severity of the condition. In order to provide patients with appropriate treatment, ophthalmologists must examine each patient individually to assess their retinal health. A painless and non-invasive method of screening the retina is retinal fundus imaging. All Iraqi patients with suspected DR visit the major eye center in Iraq, where the fundus photos in the database were obtained. The Huvitz, shown in Figure (2), is an optical coherence tomography equipped with fundus camera that has become a key instrument for diagnosis of posterior eye segment diseases. The technology produces exceptional quality retinal images with enhanced color, resolution, and contrast, significantly aiding in clinical diagnosis and research.

**Figure (2)** Huvitz OCT.

Fast capture, small pupil mode, silent operation, low flash intensity and automated flicker detection, all contribute to the best images with specification of fundus camera shown in Table (1).

**Table (1)** Specification of Huvitz Fundus Camera.

| | | |
|---|---|---|
| Fundus camera | Type | Non-mydriatic fundus camera |
| | Resolution | 60line pair/mm or more (center) 40line pair/mm or more (middle) 25line pair/mm or more (periphery) |
| | Angle of view | 45° |
| | Camera | Built-in 12M pixel, color or built- in 20M pixel, color |
| | Minimum pupil diameter | 4 mm (normal mode), 3.3 mm (small pupil mode) |
| | Flash light | White light, 10 levels |
| | Pixel pitch at fundus | 3.69 um (20M pixel color), 4.63um (12M pixel color) |
| | Capture mode | Single, stereo, wide field panorama |

## 2. IRFDRD:

The IRFDRD was collected from the Iraqi patients at the main ophthalmology teaching center in Iraq. Patients with DR were admitted to the center from all Iraqi cities (https://github.com/noor-aliz810/IRFDRD.git, https://doi.org/10.5281/zenodo.12552326). The majority of the patients included in the dataset had experienced mydriasis before the photos were taken. One drop of tropicamide at a concentration of 0.5% was used to dilate the pupils in order to cause mydriasis. Figure (3) displays a sample image from the IRFDRD that shows the location of the optic disc, fovea center, OD (retinal image on the right), OS (retinal image on the left), and other necessary details.

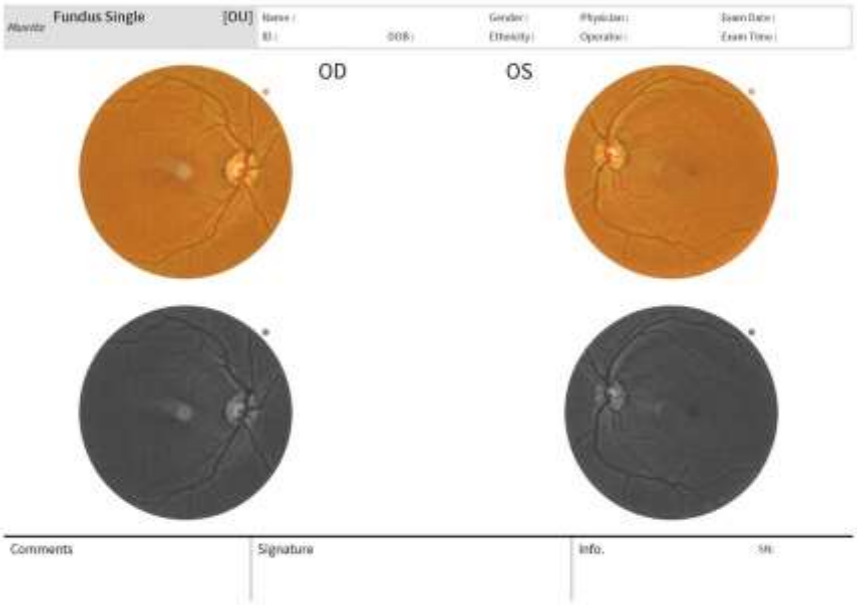


**Figure (3)** Sample image from the IRFDRD illustrating the OD (retinal image on the right), OS (retinal image on the left), optic disc and fovea center location.

This dataset consisted of 700 retinal fundus images that were collected from 350 subject. The mean age of the subjects was 45 years, with a standard deviation of 27 years and labeled under the supervision of specialized ophthalmologists in the college of medicine/ Baghdad University. Then, the data were classified according to (EDTRS) standards shown in Figure 4 in to five stages depending on the severity level of DR.

| **Types of DR in years** | 0<br>Normal eye | 3-5<br>Mild DR | 5-10<br>Moderate DR | 10-15<br>Sever DR | More than 15<br>PDR |
|---|---|---|---|---|---|
| **Severity level** | non- proliferative DR | | | | Proliferative DR |
| **Fundus changes** |  |  |  |  |  |
| **Retinal changes according to ETDRS severity levels** | No retinopathy | Few small microaneurysms only | Microaneurysms, exudates, venous beading. IRMA | More than 20 intraretinal hemorrhage each of 4Q, venous beading in 2Q, Irma in 1Q, no signs of PDR( 4:2:1 rule) | Neovasculization , vitreous/ preretinal hemorrhage |

**Figure (4)**: Diabetic retinopathy progression. This Figure describes the classification stages, time duration of each stage with the fundus and retinal changes according to the severity level of DR.

The first stage contained 153 fundas images diagnosed as healthy, the second stage included 59 images as mild, the third stage involved 304 images classed as moderate, the fourth stage consisted of 99 images as severe cases, and the last class was comprised of 85 images as PDR as shown in Table (2). The collected images were stored in the hospital server and could be used for teaching and research

purpose after obtaining ethical permission. The images captured with resolution of 3507 × 2480 pixels and were saved in jpeg format. 440 KB is the size of each image. These images were cropped using MATLAB program to obtain an individual left and right fundus image as shown in Figure (5). Therefore, the total number of the right side (OD) and left side (OS) retinal fundus images are 700 images (350 images for each side). Sample of the labelled dataset is shown in Figure (6)

**Table (2)** The five classes of DR and the number of images in each class.

| Cases | The quantity of images |
|---|---|
| Healthy (Normal) | 403 |
| Mild | 59 |
| Moderate | 304 |
| Sever | 99 |
| PDR | 85 |

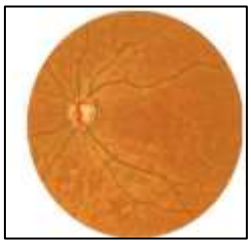

**Figure (5)** OS Cropped Retinal Fundus Image from IRFDRD.

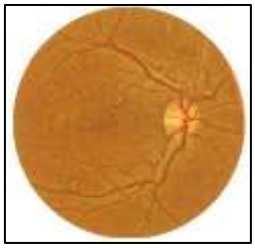

**Figure (6)** OD Cropped Retinal Fundus Image from IRFDRD.

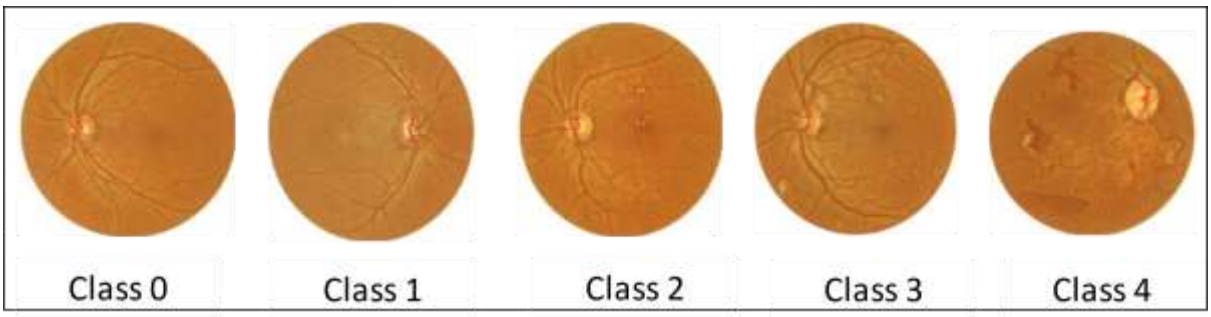


**Figure (7)**

Sample of the IRFDRD images with DR shows the main classification grades: 0 class represents the normal or healthy image; 1 class denotes the mild stage of DR; class2 represents the moderate stage; class3 shows the severe non proliferative DR and class 4 shows then last PDR stage.

## Ethical Consideration

This research adhered to ethical guidelines, including the 1964 Helsinki Declaration and our institution's research committee standards. The Ministry of Health granted ethical approval for the use of anonymized patient data from Iraqi sources.

## Acknowledgments

The authors would like to acknowledge all the technicians in Ibn Al-Haitham teaching hospital for ophthalmology for giving approval for the gathering and utilization of medical images in this research.

## Conflict of Interest

The authors confirm that no competing financial interests or personal relationships exist that could have been perceived to have influenced the research reported herein.

## References:

[1] C. P. Wilkinson, 2003. "*Proposed international clinical diabetic retinopathy and diabetic macular edema disease severity scales*," Ophthalmology, Sep., vol. 110, no. 9, pp. 1677–1682.

[2] Daniel Sh. W., Gemmy Ch., and Tien Y., 2015. *Diabetic retinopathy: global prevalence, major risk factors, screening practices and public health challenges: a review. Clinical & Experimental Ophthalmology*, 44(4):260–277.

[3] Dolly D.; Saroj Kr.; Sivaji B., 2022**.** *A critical review on diagnosis of diabetic retinopathy using machine learning and deep learning. Multimedia Tools and Applications*, vol:81, p.p:25613–25655. https://doi.org/10.1007/s11042-022-12642-4.

[4] Data available on: https://github.com/noor-aliz810/IRFDRD.git, https://doi.org/10.5281/zenodo.12552326.

[5] Reichel, E.; Salz, D., 2015 "*Diabetic retinopathy screening. In Managing Diabetic Eye Disease in Clinical Practice"*; *Springer: Berlin, Germany*; pp. 25–38. https://doi.org/10.3390/data3030025

ISSN (Print) 2794-7629 Received 15/08/2024
ISSN (Online) 2794- 4549 Accepted 12/09/2024

**FULL PAPER**

# Detecting Fake and True News by Applying Text Analysis and Deep Recurrent Neural Network

***Prepared by***

***A.Prof.Dr.Raid Rafi Omar Al-Nima***
*Technical College of Engineering for Computer and Artificial Intelligence / Mosul, Northern Technical University, Mosul, Iraq*
raidrafi1@gmail.com

***Karam Sameer Qasim Qassab***
*Technical Institute / Mosul, Northern Technical University, Mosul, Iraq*
*mti.lec14.karam@ntu.edu.iq*

***Imad Idan Abed Al-Khalaf***
*Technical College of Engineering for Computer and Artificial Intelligence Mosul, Northern Technical University, Mosul, Iraq*
amaadaydan27@ntu.edu.iq

**Abstract:**

Detecting fake news is a significant topic; it is valuable for warning people and protecting them from the consequences of such news. In this paper, a Deep Recurrent Neural Network (DRNN) is applied for detecting or recognizing fake and true news. Text data is first exploited and pre-processed. The pre-processing includes tokenizing, converting to lowercase, and erasing punctuation. Then, data is translated into sequences of values, which are utilized in the DRNN. The DRNN involves multiple layers: the sequence input layer, the word-embedding layer, the Long Short-Term Memory (LSTM) layer, the fully connected layer, the softmax layer, and the classification layer. A useful database from Kaggle named Fake News Detection (FND) is used; it has a huge amount of data. The obtained result achieved 99.77% accuracy, which is obviously very high.

***Keywords:*** *Deep Recurrent Neural Network, Fake News, True News, Text Analysis*

**المستخلص**

يعد الكشف عن الأخبار المزيفة موضوعًا مهمًا، فهو مفيد جدا لتحذير الناس وحمايتهم من عواقب هكذا أخبار. في هذا البحث، تم تطبيق الشبكة العصبية العميقة المتكررة (DRNN) للكشف أو التمييز بين الأخبار المزيفة والحقيقية. يتم أولاً الاستفادة من بيانات النصوص ومعالجتها معالجة مسبقة. تتضمن المعالجة المسبقة الترميز، والتحويل إلى أحرف صغيرة، ومحو علامات الترقيم. ثم يتم ترجمة البيانات إلى تسلسلات من القيم، والتي يتم استخدامها في الـ DRNN. تتضمن هذه الشبكة طبقات متعددة وهي: طبقة إدخال التسلسل، وطبقة تضمين الكلمات، وطبقة الذاكرة طويلة المدى (LSTM)، والطبقة المتصلة بالكامل، وطبقة سوفت ماكس، وطبقة التصنيف. استخدِمت قاعدة بيانات مفيدة من Kaggle تسمى بيانات كشف الأخبار المزيفة (FND)، وهي تحتوي على عدد كبير جدا من العينات. وقد وصلت النتيجة التي تم الحصول عليها إلى 99.72%، من الواضح أنها هذه النسبة هي لدقة عالية جدًا.

***كلمات مفتاحية:*** *الشبكة العصبية المتكررة العميقة، الأخبار المزيفة، الأخبار الحقيقية، تحليل النص*

## 1. INTRODUCTION

Detecting fake and true news is such an important issue. It is a part of pattern recognition. These patterns are represented by news. Many studies have focused on this subject, such as (Berrondo-Otermin & Sarasa-Cabezuelo, 2023; Dey et al., 2018; Mishra et al., 2022; Pranave et al., 2021; Zhang et al., 2023). This reflects the importance of this topic. Announcing fake news may cause big problems. Some of them may even lead to big consequences.

As mentioned, detecting fake and true news is part of pattern recognition, but their patterns can be texts, images, videos, etc. Recognizing or detecting fake and original patterns has also been considered in many works (Al-Hussein et al., 2022c, 2022a; Al-Nima et al., 2023; Al-Nima & Al-Hbeti, 2024; Ibrahim et al., 2021). Moreover, applying artificial intelligence to fake patterns, specifically deep learning, is a

recently obtained concentration (Agarwal, Farid, El-Gaaly, et al., 2020; Agarwal, Farid, Fried, et al., 2020; Chadha et al., 2021; Suganthi et al., 2022; Yang et al., 2019).

Various studies in the literature consider patterns of recognition of fakes and originals. In 2018, fake news recognition was concentrated by using linguistic analysis (Dey et al., 2018). In 2019, deep fakes were exposed by utilizing inconsistent head poses (Yang et al., 2019). In 2020, deep-fake videos were recognized based on behavior and appearance (Agarwal, Farid, El-Gaaly, et al., 2020). In 2021, fake and original fingerprint images were classified by a deep network (Ibrahim et al., 2021). In 2022, Deoxyribonucleic Acid (DNA) samples were recognized between clients and imposters (Al-Hussein et al., 2022b). In 2023, artificial intelligence applications were surveyed to detect fake news (Berrondo-Otermin & Sarasa-Cabezuelo, 2023). In 2024, fingerprints were clustered for fake and original by proposing unsupervised deep learning (Al-Nima & Al-Hbeti, 2024).

In this paper, the aim is to distinguish between fake and true news. Multiple processes are applied, including pre-processing texts, preparing data, and implementing a Deep Recurrent Neural Network (DRNN).

The paper's sections are arranged as follows: Section 1 provides the introduction; Section 2 explains the theoretical part; Section 3 illustrates the practical part; and Section 4 announces the conclusion.

## 2. THEORETICAL PART

As mentioned, the aim here is to detect fake and true news. The data in the news involves texts or strings, so they require pre-processing, preparation, and detecting classifiers. Figure 1 shows the detailed steps for analyzing the data. Honestly, all the applied processes are recorded with the help of Matlab (Matlab, 2020).

As can be seen from this figure, the process begins with news texts. In this case, valuable database named Fake News Detection (FND) (PATEL, 2021) was utilized. This database contains a large number of fake and true news texts; specifically, it includes 23488 fake news texts and 21417 true news texts (PATEL, 2021).

The employed texts require pre-processing. The applied pre-processing steps are tokenizing, converting to lowercase, and erasing punctuation. Tokenizing a text means considering the separated strings inside the text as tokens. Converting to lowercase obviously means changing all uppercase letters to lowercase letters. Erasing punctuation clearly means removing any existing punctuation.

To prepare the pre-processed text outputs for the detection classifier, they are translated into sequences of values. This process utilizes initialized token indices, where the same index is used for repeated tokens. Thus, sequences of values are represented by these indices. Subsequently, the Deep Recurrent Neural Network (DRNN) is employed, comprising multiple layers: the sequence input layer, word-embedding layer, Long Short-Term Memory (LSTM) layer, fully connected layer, softmax layer, and classification layer.

The sequence input layer accepts the translated sequences of values. The word-embedding layer maps indices to vectors (Matlab, 2020). The LSTM layer stores important information for a long time. This information can be deleted if more implementation is implemented. It actually learns which information to discard and which information to keep (A. Al-Obaidi et al., 2022; A. S. I. Al-Obaidi et al., 2022). A fully connected layer fully connects the output nodes of the previous layer to all determined nodes in this

layer. The Softmax layer provides the probability of relating a DRNN input to each output class. The classification layer outputs the recognition or detection decision.

The DRNN works in three phases: training, validation, and testing. In the training phase, it uses a set of data to learn how to distinguish between fake and true news. In the validation phase, it utilizes another set of data to check the validity of the train. In the testing phase, it exploits the remaining set of data to intelligently determine the fake and true news.

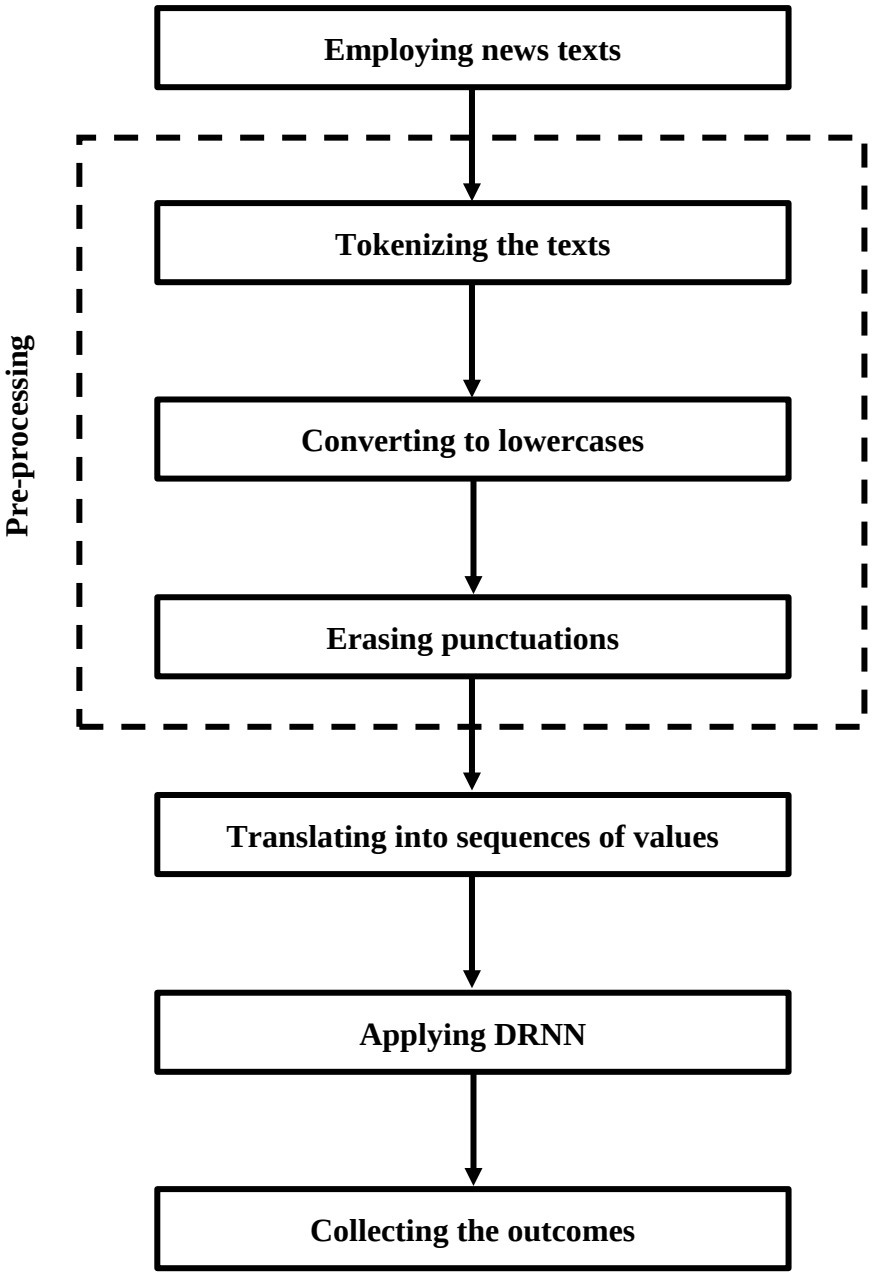


**Figure 1: Detailed steps of analyzing data of news texts**

## 3. PRACTICAL PART AND RESULTS

First of all, the FND (PATEL, 2021) is used, which is a useful database from Kaggle. It has a very large amount of fake and true news texts, as mentioned. In this work, the number of overall training data is 17960, the number of overall validation data is 4490, and the number of overall testing data is 22448. The fake and true class distribution of all utilized data is given in Figure 2.

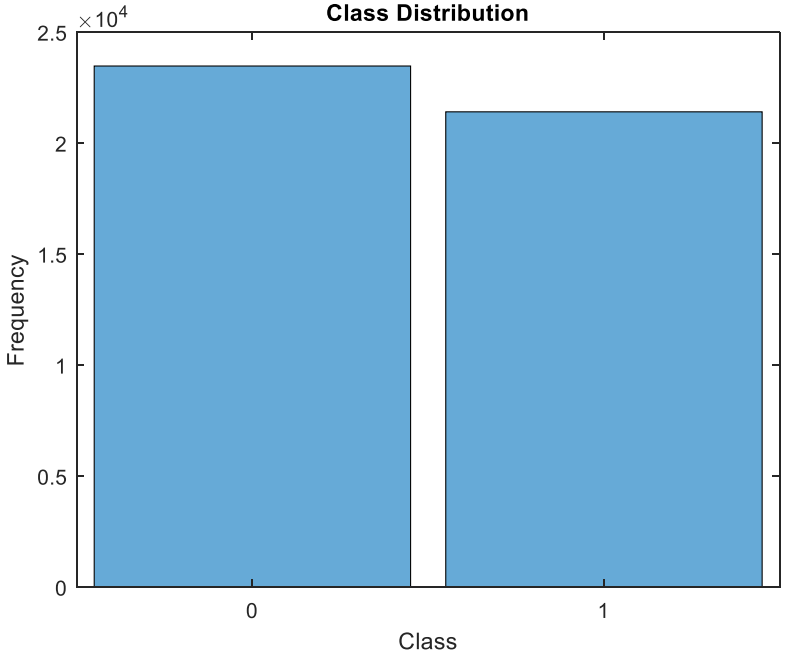


**Figure 2: Fake and true classes distribution of all utilized training, validation and testing data**

Figures 3 and 4 show Word cloud demonstrations for training and validation texts. These figures show that many news texts are considered, so this can provide advantages for the testing phase in evaluating any new text. Table 1 shows the DRNN architecture descriptions. Table 2 shows the DRNN training options and their values.


**Figure 3: Word cloud demonstrations for training texts**


**Figure 4: Word cloud demonstrations for validation texts**

**Table 1: DRNN architecture descriptions**

| DRNN Layers | Parameters and Values |
|---|---|
| Sequence input layer | Input size = 1 |
| Word embedding layer | Embedding dimension = 50,<br>Number of words = 100823 |
| LSTM layer | Number of hidden units = 80,<br>Output mode = last |
| Fully connected layer | Number of classes = 2 |
| Softmax layer | Number of classes = 2 |
| Classification layer | Number of classes = 2 |

**Table 2: DRNN training options and their values**

| Training Options | Values |
|---|---|
| Optimizer | Adam |
| Mini-batch size | 16 |
| Gradient threshold | 2 |
| Shuffle | Every-epoch |
| Verbose | False |

Figure 5 shows the DRNN training and validation curves. From this figure, it can be seen that a very high validation accuracy of 99.78% is benchmarked. In addition, both curves of accuracy and loss are adjusted toward the optimal values. These are strong evidences for DRNN training success.

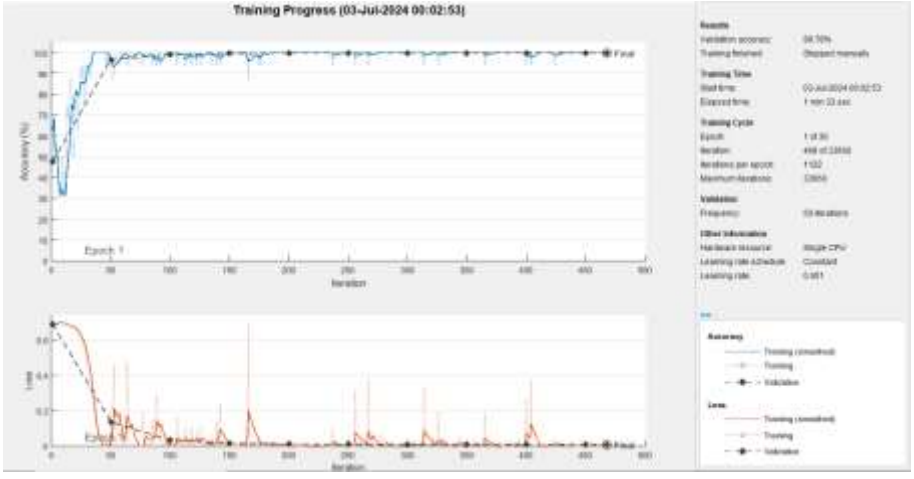


**Figure 5: DRNN training and validation curves**

In the testing phase, the DRNN accuracy attains 99.77%. Furthermore, the evaluation parameters of True Positives (TP), True Negatives (TN), False Positives (FP) and False Negatives (FN) obtained were 10671, 11725, 15, and 37, respectively. Hence, the sensitivity, specificity, precision, and f1-score achieve 99.65%, 99.87%, 99.86%, and 99.76%, respectively. Table 3 shows the reported testing results.

**Table 3: DRNN testing results**

| Evaluation Metrics | Testing Results |
|---|---|
| Accuracy | 99.77% |
| Sensitivity | 99.65% |
| Specificity | 99.87% |
| Precision | 99.86% |
| F1-score | 99.76% |

The obtained results reveal the high accuracy of detecting fake and true news. Therefore, this clearly indicates our detection study's success.

## 4. CONCLUSION

This paper concentrated on detecting fake and true news. Text analysis and DRNN were applied. The FND database was exploited; it has a huge amount of data for fake and true news texts. The employed data were first pre-processed. The pre-processing steps involved tokenizing, converting to lowercase, and erasing punctuation. Subsequently, the outcomes were translated into sequences of indices values in order to be used by the DRNN. So, the DRNN was utilized for detection or recognition.

Significant results have been attained. That is, the detection accuracy, sensitivity, specificity, precision, and f1-score have achieved 99.77%, 99.65%, 99.87%, 99.86%, and 99.76%, respectively. Clearly, such evaluations are outstanding and remarkable.

**References:**

Agarwal, S., et al. (2020). Detecting deep-fake videos from appearance and behavior. *2020 IEEE International Workshop on Information Forensics and Security (WIFS)*, 1–6.

Agarwal, S., et al. (2020). Detecting deep-fake videos from phoneme-viseme mismatches. *Proceedings of the IEEE/CVF Conference on Computer Vision and Pattern Recognition Workshops*, 660–661.

Al-Hussein, M. A. S., et al. (2022a). Applying the deoxyribonucleic acid (DNA) for people identification. *Journal of Harbin Institute of Technology*, *54*(8). https://doi.org/10.11720/JHIT.54082022.13

Al-Hussein, M. A. S., et al. (2022b). *Deoxyribonucleic Acid (DNA) for Individual Recognition*. Noor Publishing.

Al-Hussein, M. A. S., et al. (2022c). Employing deoxyribonucleic acid (DNA) for personal verification. *International Journal of Health Sciences*, *6*(S9).

Al-Nima, R. R. O., et al. (2023). An Artificial Intelligence Approach for Verifying Persons by Employing the Deoxyribonucleic Acid (DNA) Nucleotides. *Journal of Electrical and Computer Engineering*, *2023*.

Al-Nima, R. R. O., & Al-Hbeti, L. A. Y. (2024). Fingerprints clustering with unsupervised deep learning. *AIP Conference Proceedings*, *2944*(1).

Al-Obaidi, A., et al. (2022). *Interpreting the Sign Language of the Arabic Alphabet*. LAP Lambert Academic Publishing.

Al-Obaidi, A. S. I., et al. (2022). Interpreting Arabic sign alphabet by utilizing a glove with sensors. *International Journal of Health Sciences*, *6*(S6).

Berrondo-Otermin, M., & Sarasa-Cabezuelo, A. (2023). Application of artificial intelligence techniques to detect fake news: A review. *Electronics*, *12*(24), 5041.

Chadha, A., et al. (2021). Deepfake: an overview. *Proceedings of Second International Conference on Computing, Communications, and Cyber-Security: IC4S 2020*, 557–566.

Dey, A., et al. (2018). Fake news pattern recognition using linguistic analysis. *2018 Joint 7th International Conference on Informatics, Electronics & Vision (ICIEV) and 2018 2nd International Conference on Imaging, Vision & Pattern Recognition (IcIVPR)*, 305–309.

Ibrahim, A. M., et al. (2021). Deep fingerprint classification network. *TELKOMNIKA (Telecommunication Computing Electronics and Control)*, *19*(3), 893–901.

Matlab. (2020). *Classify Text Data Using Deep Learning* (2020a ed.). 1994-2020 The MathWorks, Inc.

Mishra, S., et al. (2022). Analyzing machine learning enabled fake news detection techniques for diversified datasets. *Wireless Communications and Mobile Computing*, *2022*(1), 1575365.

PATEL, S. (2021). *Fake News Detection*. (Version 3).

https://www.kaggle.com/code/therealsampat/fake-news-detection/

Pranave, S., et al. (2021). Frequent pattern mining approach for fake news detection. *International Conference on Deep Learning, Artificial Intelligence and Robotics*, 103–118.

Suganthi, S. T., et al. (2022). Deep learning model for deep fake face recognition and detection. *PeerJ Computer Science, 8*, e881.

Yang, X., et al. (2019). Exposing deep fakes using inconsistent head poses. *ICASSP 2019-2019 IEEE International Conference on Acoustics, Speech and Signal Processing (ICASSP)*, 8261–8265.

Zhang, Q., et al. (2023). A deep learning-based fast fake news detection model for cyber-physical social services. *Pattern Recognition Letters*, *168*, 31–38.

ISSN (Print) 2794-7629 Received 11/12/2024
ISSN (Online) 2794- 4549 Accepted 30/12/2024

**FULL PAPER**

# The Reality and Future of the Global Economy after (Covid 19) and the Russian-Ukrainian War

***Prepared by***

***A.prof.Dr.Ahmed Abbas Abdullah***
*College of Administration & Economics*
*University of Fallujah*
*ahmedabas67@uofallujah.edu.iq*

## Abstract

The topic of the global economy and the crises it has gone through has received the attention of many international institutions and writers alike due to the importance of this topic, especially what the aforementioned economy was exposed to during the year 2020, from a crisis known as Covid 19, which paralyzed the economy and the aforementioned / its impact on the Great Depression in 1929. The research aims to shed light on the reality of the global economy in light of the crises that the aforementioned economy was exposed to and to show the effects, especially the economic ones, that (Covid 19) left on the global economy, including a decline in economic growth. The research reached a number of conclusions, including that the (Covid 19) crisis, or what is called the Corona virus, contributed to a decline in the economic growth rate to below zero (-3%), while the research recommends the need to take measures, caution and caution and develop the necessary plans in order to confront such crises that may occur to the aforementioned economy in the future.

**Keywords**: Global Economy - (Covid - 19) - War Russia – Ukraine

## Introduction

The global economy witnessed during the year 2020, a super economic crisis resulting from the outbreak of the Corona pandemic or what is known as (Covid 19), which caused an economic, social and health crisis at the same time, bringing to mind what the global economy went through during the Great Depression in 1929. This crisis resulted in the complete halt of the wheel of life and caused waves of shocks that swept the global economy. This pandemic caused harm to the poor and most needy groups, in addition to that, it caused a clear decline in the wheel of global economic growth as a result of the cessation of trade exchange operations and other economic activities, travel and others. Despite everything that happened to the aforementioned economy, many experts expected that the global economy after the Corona pandemic would be a different world from the world we knew. During the aforementioned year, these experts stated that the global economy would witness a recovery in the economic growth rate to higher levels than it was during the (Covid 19) crisis, and the wheel of economic activity would return to turn again despite the ongoing conflict between Russia and Ukraine, which is a conflict that harmed the trade exchange process, especially for Ukraine, which is the exporter of a basket of food commodities To many countries of the world, including Iraq. Our research will address the topic of the reality and future of the global economy after (Covid 19), up to the Russian-Ukrainian war and the severe damage it caused to the aforementioned economy.

## Research problem:

The global economy has gone through many crises throughout its long history, and in every crisis it goes through, it comes out in the future with problems, effects and setbacks in varying proportions. However, what the aforementioned economy was exposed to during the (Covid-19) crisis in 2020, which became known as the Corona crisis and the resulting effects and major losses that cast their shadows on the reality and future of the aforementioned economy, as this crisis caused a slowdown in the growth of the global economy.

## Importance of the research:

The importance of the research comes from the topics that will be addressed related to the reality of the global economy before the crisis occurred and the great material and human losses it caused and the decline in the economic growth rate with a future vision of what the global economy will be like after the aforementioned crisis.

## Research Hypothesis:

The research is based on the hypothesis that (Covid-19 has created a clear rift and negatively affected the reality of the global economy, especially with regard to economic growth, which will continue for a long time until it regains its status again in the future).

## Research Objective:

The research aims to know the reality and future of the global economy in light of the successive crises that the aforementioned economy is going through, including (Covid-19), which left negative effects on the global economy, especially with regard to economic growth.

## Research Methodology:

The research relied on the descriptive-analytical method as one of the scientific research methods followed in writing scientific research, relying on some sources, publications, courses and books related to this topic.

## The concept of the global economy

## First: The concept of the global economy: Globalecon:

The concept of the global economy has witnessed a clear development during the stages that this economy has gone through during its long journey, which extends from the sixteenth century when trade flourished between the countries of the world, until today, after the need to organize international economic relations emerged, so what is known as the global (international) economy emerged.

The aforementioned economy was defined as an approach that seeks economic interactions between the different countries of the world, and analyzes the impact of international issues on global economic activity, in addition to studying political and economic issues related to international trade and finance, and then dealing with the economic activities of different countries and the results resulting from them (1).

The global economy was also defined as the comprehensive system that is concerned with studying and analyzing the processes of production, distribution, consumption, wealth and related concepts and activities such as the general level of prices, unemployment, inflation, and the movement of capital transfers, etc. (2)

In addition to the above concepts, the global economy was defined as the international exchange of goods and services expressed in monetary units of account or money (3)

While the researcher believes that the global economy is nothing but a means found for the exchange of goods and services and the transfer of capital between different countries of the world based on the need of those countries for this relationship in order to obtain the goods and other things they need as a result of the aforementioned exchange process.

## Second: The importance of the global economy:

The global economy plays an important role in the lives of different countries and peoples of the world, especially with regard to the problems facing society such as unemployment, inflation, poverty, and others. The economy can avoid these problems by finding appropriate solutions to them such as economic policies related to reducing unemployment, inflation, and others. Rather, the global economy is a field of science and knowledge that is employed in most areas of life and on both resources and individuals, as well as countries and organizations.

Its importance lies in its consideration as one of the basic pillars through which society can develop its work and life in order to meet its various needs, not to mention the solutions it provides to the problems facing the concerned society. The importance of the global economy is highlighted through the following:

1) The global economy is interested in taking into account competition in the global market for products, as it affects the state and its position among the different countries of the world.

2) The global economy is a criterion of the strength of the country in question because a strong country is the one that has the ability to control the production of the relevant goods and services (4).

3) The global economy is also interested in studying the aspects of economic activity that takes place between the different countries of the world, whether these transactions are based on bilateral trade transactions or multilateral trade transactions, whether directly or indirectly through international and regional institutions.

4) The economy helps predict different expectations, which in turn helps decision-makers know the expected results because it is a scientific field that is employed in various areas of life.

5) The economy also helps provide the necessary information and knowledge, which in turn helps in making the right decisions in daily life, by selecting profitable investment opportunities.

Accordingly, it can be said that this importance and others make the global economy a means through which the different countries of the world can achieve their goals in obtaining the goods, services, and others they need by carrying out the exchange process among themselves away from other influences.

## Third: Characteristics and components of the global economy:

The global economy is characterized by many characteristics and components that distinguish it from previous stages, although some of these characteristics have their roots in the past, as follows: (5)

1) Dynamism and unipolarity:

The global economy is characterized by rapid dynamism during the past twentieth century, with unipolarity dominating decision-making centers and economic powers in the world, as there are always many possibilities and scenarios that govern the arrangement and sequence of economic power centers in the world. The United States was the first superpower in the world to control the global economy several years ago, but what happened in the twenty-first century has proven otherwise, as Europe or the European

Union and China have been the only ones to top the global economy in the aforementioned century, followed by Japan in the global ranking.

2) Developments in transportation, communications and information technology:

The communications and information revolution is the material basis for the new global economic system in the current stage that the global economy is witnessing, and this characteristic has resulted in many influential results in the new global economy, namely:

A) The production revolution.

b) The marketing revolution and the growing growth in international trade.

c) In addition to the increasing trend towards more mutual economic investment.

3) The growing role of multinational companies:

The current twenty-first century has witnessed the growing role of multinational companies through:

a) The formation and composition of the new global economy is centrally dependent on multinational companies.

b) The revenues of these companies represent about (44%) of the global gross domestic product, in addition to representing about (40%) of the volume of global trade for the year (2021).

c) Their sales amounted to about (80%) of the world's sales for the year (2021).

d) The liquid assets of gold and cash reserves of the aforementioned companies exceeded about twice the global reserve.

e) The aforementioned companies play an important role in the global technological revolution, which is one of the pillars of the new global economy. (6)

4) The increase in economic blocs and new regional arrangements:

Economic blocs have witnessed a clear increase during the twenty-first century, and these blocs have taken the following forms:

A) There are about (45) types of economic bloc systems in the world in their various forms and stages.

B) These blocs include about (75%) of the world's countries and about (80%) of the world's population and control about (85%) of global trade in 2021.

5) The role of global economic institutions in managing the new economic system has increased:

The role of global economic institutions, especially the International Monetary Fund and the World Bank, has witnessed a clear increase through:

A) The role of economic institutions affiliated with this camp.

B) The management of the new global economic system has come to depend on three financial economic institutions, which are:

* The International Monetary Fund (IMF) is directly responsible for managing the international monetary system.

* The World Bank and its affiliated institutions are directly responsible for managing the financial system.

*The World Trade Organization (WTO) is responsible for managing the international trading system.

(6New structural features of the new global economic system:

Under the new global system, there is no longer a division between developed and developing countries, but rather the new structure of the new global economic system includes the following divisions and formations:

A) The group of the most developed countries such as the United States, Europe and Japan.

B) The group of developing countries or those seeking to achieve economic growth such as the countries of East Asia.

C) Economically backward countries or what are called the least developed and economically backward countries. (7)

Accordingly, it can be said that the new global economy is almost not free of contradictions that may occur in the world, like any large-scale global initiative. Despite this, it has contributed to creating new

patterns related to the division of labor process, in addition to forming new forms of economic relations between the countries of the world.

**The reality and future of the global economy in light of (Covid 19) First: The global economy before the (Covid 19) crisis**The global economy witnessed clear growth during the years preceding the emergence of the (Covid 19) virus, as the aforementioned economy two years ago, i.e. (2018-2019), was moving at a rapid growth rate in almost all regions of the world, and the global economy was expected to grow at a rate of (3.9%) during the years (2018-2019). After one year, the reality of the global economy changed, starting with the escalation of trade tensions between the United States and China, in addition to the overall economic pressures in Argentina and Turkey, not to mention the turmoil in the automotive industry in Germany, and the tightening of credit policies in China. All of these events clearly contributed to weakening the global expansion, especially during 2018, and this is due to what expectations indicate regarding the continuation of weakness until 2019, as the World Bank's World Economic Outlook report expected global growth to decline to (70%) for 2019, from the global economy, at a time when global growth reached its peak It reached (4%) during 2017, then decreased to (3.6%) in 2018, and it is expected to decrease according to economic experts to (33%) in 2019, despite the global expansion at that time (1), but it is still reasonable, and some expected the return of global economic growth to a rate of (3.6%) in 2020, and some also expected the global growth rate to reach (4.9%) in 2020, and Table (1) shows the growth rates of a number of countries in the world during 2019.

| % Growth rate | Countries of the World |
|---|---|
| 2.6 | The World |
| 1.7 | Developed Countries |
| 3.8 | Emerging Market Developing Countries |
| 5.8 | East Asia and the Pacific |
| 2.7 | Europe and Central Asia |
| 0.8 | Latin America and the Caribbean |
| 0.9 | Middle East and North Africa |
| 4.4 | South Asia |
| 2.5 | Sub-Saharan Africa |

**Source: World Bank Publications, World Economic Outlook 2022, available at https://www.imf.org.**

It is noted from Table (1) that the growth rate for the global economy was (2.6%) in 2019, while the East Asia and Pacific region recorded the highest growth, reaching (5.8%) in 2019, while the lowest growth rate recorded by Latin American and Caribbean countries and the countries of the East and North Africa was (0.8%) and (0.9%) respectively for the same year. Accordingly, it can be said that despite the difference in growth rates and percentages from one source to another, there is a general rule related to the economic growth rate, which is that the more the real growth equations increase, i.e. after removing the effect of rising prices (inflation) from (3%) or even (2.5%), this indicates that the economy of the country in question is moving towards prosperity and economic growth, and the less it falls below that limit towards (zero), i.e. (below zero), this indicates that contraction, elimination and decay have affected that economy.

**Second: The global economy in light of the (Covid-19) crisis:**

Two years ago, in 2020, the global economy went through a severe crisis that led to a complete paralysis in the aforementioned economy due to the spread of the (Covid-19) virus, recalling the global recession that occurred in (1929). The Corona pandemic caused the collapse of global economic activity despite the economic preparation measures taken by some countries and governments. Due to the depth of the crisis and the fact that it witnessed it, it is pushing emerging and developing economies towards contraction, although they enjoyed growth rates that were the highest in the world before the aforementioned crisis and

maintained them despite all circumstances, including the trade conflict between major economies, especially between the United States and China, in addition to the increasing debt problems and the decline in commodity prices during the years preceding the Corona crisis, (2) as the statistical figures issued by international institutions during the aforementioned crisis indicate that economic growth rates in most countries of the world fell below zero in 2020, meaning that the gross domestic product (GDP) of those countries shrank to the lowest level, as the average global economic growth reached less than (- 3%), that is (1-3%) specifically.

The distinguishing mark in this regard was China, which witnessed modest positive growth in its standards, as its economic growth rate reached (2.3%) according to the International Monetary Fund report (2.2) according to the World Bank report for the year 2020, because China is the largest economy in the world and according to the purchasing power parity (PPP). (3)

And the second largest economy in the world in the measure of the current exchange rate (yuan) against the US dollar. The World Bank report tables show striking statistics on economic growth rates directed at a number of countries that are smaller economies than China to varying degrees during the (Covid-19) crisis in 2020, and Table (2) shows the growth rates for a number of selected countries during the aforementioned crisis for the year 2020.

| % Economic growth rate | Countries |
|---|---|
| 6.1 | Ethiopia |
| 4.5 | Tajikistan |
| 3.6 | Egypt |
| 3.5 | Bangladesh |
| 3.4 | Iran |
| 3.2 | Myanmar |
| 1.8 | Türkiye |
| 1.7 | Uzbekistan |

**Source: World Bank Publications 2022.**

In addition, there are countries whose economies have been severely contracted and whose growth rate has become more than (-1.3%) in 2020, such as India, for example, which has brought its economy back to the forefront again after recovering from the aforementioned crisis that struck it, surpassing China during 2021. Table (3) shows the economic growth rates of the countries of the world after their economies were exposed to the (Covid-19) crisis during the years (2020-2021).

| Economic growth rates | | Countries of the World |
|---|---|---|
| 2021 | 2020 | |
| 5.5 | -3.4 | The World |
| 5.0 | -4.6 | Developed Countries |
| 6.3 | -1.7 | Emerging and Developing Market Countries |
| 7.1 | 1.2 | East Asia and the Pacific |
| 5.8 | -2.0 | Europe and Central Asia |
| 6.7 | -6.4 | Latin America and the Caribbean |
| 3.1 | -4.0 | Middle East and North Africa |
| 7.0 | -5.2 | South Asia |
| 3.5 | -2.2 | Sub-Saharan Africa |

**Source: World Bank Publications, Global Economic Prospects, available at albankaldawli.orpar/pul/2022.**

Despite the recovery of some global economies from the Corona pandemic, the global economy is still witnessing slow growth at a time when the pandemic is witnessing a new wave of infection and it seems that the cracks caused by (Covid-19) will continue for a longer period. It is expected that short-term divergence will leave permanent marks on medium-term performance, as the global economy is expected to achieve growth of (0.1%) in 2021, and (4.99%) in 2022, i.e. a decrease of (0.1%) in 2021, as some expected during the mentioned year. This decrease is balanced by a short-term improvement in some emerging or developing markets economies that export raw materials. What is striking is that after the viral pandemic (Covid-19), which left widespread effects on many countries during 2020, this impact even increased during 2021, as viral deaths exceeded, for example, (675,446) in the United States from the Spanish flu in 1918, which is the worst deaths associated with the pandemic in the United States in The previous pandemic disrupted life in all countries of the world and negatively affected global economic growth during 2020, as estimates indicate that the virus reduced global economic growth for 2020, to an annual growth rate of about (3.2%) with an expected recovery of (5.9%) in 2021, in addition to estimates indicating that global trade decreased by (5.3%) in 2020, but it is expected to grow by (8.0%) in 2020, which happened, albeit at a lower rate than mentioned, and Figure (1) shows the impact of (Covid-19) on the global economy

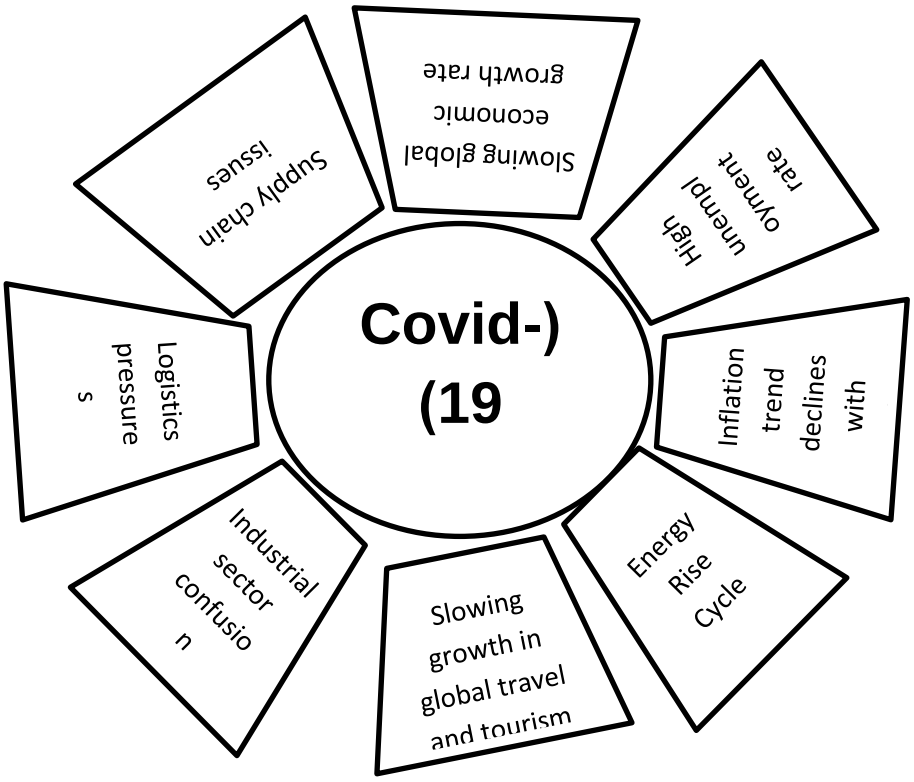


## Third: The reality and future of the global economy after the (Covid-19) crisis:

The global economy received the year 2022 in a weaker position than expected, which coincided with the spread of the new mutated strain or (microbe) of the (Covid-19) virus, which left a profound impact on

the countries of the world, including all economic, political, social, technological and other levels. This prompted some countries to impose restrictions on the movement of goods, people, and others, which led to an increase in the prices of crude oil and other commodities in global markets, in addition to a shortage of supplies of this material and other energy sources, which led to an increase in inflation, especially in the United States and a number of emerging and developing market economies, not to mention the limited growth in China due to the ongoing contraction in the real estate sector and the slow recovery of private consumption compared to expectations. On the other hand, some expect that global growth will record a clear decline from (5.9%) in 2021 to (4.4%) in 2022, a decrease of (0.5%) in 2022, while the International Monetary Fund expected in its 2022 report published on its official website that the global economic growth rate for 2022 will be lower than it was in 2021, as the International Monetary Fund estimates the economic growth rate for 2021 to be less than (6%), or (5.9%), considering that 2021 is the year of recovery from the Covid pandemic that hit the global economy with a severe crisis, which As a result, the global economy witnessed negative growth rates for most economies of the world, especially advanced, emerging and developing economies alike. (4) As for the economic rates in 2022, the International Monetary Fund and those concerned with global economic affairs also predicted that it would be less than (5%) by one degree, i.e. (4.9%), meaning that the growth rate for 2022 would be slightly less than what was expected for the previous year. In addition, the International Monetary Fund predicted that the global economic growth rate for 2023 would be less than (4%), i.e. (3.8%), which indicates that global economic growth is heading towards a gradual decline during these two years (2022, 2023), and Table (4) shows the growth rate for the countries of the world for the period (2022, 2024).

| 2024 | 2023 | 2022 | Countries of the World |
|---|---|---|---|
| 3.2 | 3.8 | 4.9 | The World |
| 1.5 | 2.3 | 3.8 | Developed Countries |
| 4.0 | 4.4 | 4.6 | Emerging and Developing Countries and Markets |
| 3.6 | 5.2 | 5.1 | East Asia and the Pacific |
| 3.0 | 2.9 | 3.0 | Europe and Central Asia |
| 1.9 | 2.7 | 2.6 | Latin America and the Caribbean |
| 2.7 | 3.4 | 4.4 | Middle East and North Africa |
| 5.6 | 6.0 | 7.6 | South Asia |
| 3.4 | 3.8 | 3.6 | Sub-Saharan Africa |

**Source: World Bank Publications, Global Economic Prospects 2024, available at https://www.alarabiya.net.2024.**

On the other hand, many economists believe that due to the ongoing war between Russia and Ukraine, and because the latter is the world's food basket and a major source of grains, oils, vegetables, etc., the agricultural sector contributes (14%) of Ukraine's gross domestic product, and the products of the aforementioned sector represent (45%) of total Ukrainian exports, as it exports approximately (50) million tons of grains annually, in addition to contributing (18.1%) of the world's wheat production and the fourth in the world in barley production, as it exports (18%) of the world's production, in addition to the fact that it ranks fifth in the world in yellow corn production, with a current (16%) of the world's production of this material. (5)

Accordingly, it can be said: The crisis that the global economy has gone through and is still going through as a result of the repercussions of Corona (Covid-19), in addition to the ongoing war between Russia and Ukraine, will put the global economy on the threshold of a new stage, as it pushes towards changing many of its laws and balances, and even forces many countries of the world to change the rules that have governed their economic relations system for more than seven decades. In this regard, expectations indicate that economic growth during the year 2024 will reach (3.2) and (3.3) in 2025, i.e. at the same pace as in 2023, and this indicates that global economic growth is heading towards decline in the future (6).

**The global economy in light of the Russian-Ukrainian war:**

Events and crises have followed one after the other on the global economy. As soon as the (Covid-19) crisis ended and its economic, social and health impacts on the countries of the world, another crisis emerged, but this time it was different from its predecessor, which is the (Russian-Ukrainian) war in 2022, and the events and destruction that accompanied it to the components that the economies of the two countries possess, especially for Ukraine, whose economy was expected to suffer a contraction in the national product by (0.2%) during the year of the aforementioned crisis. (7)

In addition, the two countries have a large share in the field of international trade exchange, and the effects of that war were represented in the lack of food security and the rise in energy prices (oil and natural gas), not to mention the rise in inflation rates that reached high levels.

The striking thing is that the aforementioned war cost the global economy an amount of (1.3) trillion dollars, as Europe was mainly affected by this war as a result of the disturbances in maritime and air navigation, especially in areas of economic activity.

The aforementioned war has caused negative effects on the global economy, which is represented by a slowdown in economic growth, as the two countries are among the largest producers of primary commodities. The cessation of supplying global markets with commodities produced by the two countries has led to a remarkable rise in global prices, especially as we mentioned with regard to energy prices.

As for Russia, which entered its third year of war against Ukraine, it was not significantly affected by this war as Ukraine was. Some sources stated that the Russian economy has a large reserve that enables it to grow, as evidenced by the fact that the gross domestic product (GDP) increased by (3.5%), industry grew by (6%), and investment by (10%), and it produced (11.1) million barrels of crude oil. (8) This indicates the extent of the Russian economy's ability to confront circumstances, challenges, crises, and others. In addition, commodity trade achieved a surplus of (308) billion dollars in 2024 according to Russian statistics and (292) billion dollars according to the World Trade Organization (WTO), making Russia second after China in the field of large surplus. () While inflation in the Russian economy reached (8%), the World Bank ranked the Russian economy fifth in the world in terms of purchasing power. As for Ukraine, some reports indicated that the Ukrainian Federation recorded a contraction of (35%) in 2022, as a result of The losses suffered by the Ukrainian economy as a result of the aforementioned war, which damaged production capacities, damaged agricultural lands, and decreased the supply of labor, as estimates indicate the displacement of (14) million Ukrainians and according to the World Bank report, which stated that the Ukrainian gross domestic product decreased by (35%) as we mentioned, while the economic damage was estimated at about (138) billion dollars, in addition to the losses incurred by the agricultural sector, which were estimated at about (34.1) billion dollars. The aforementioned estimate also stated that the needs for the reconstruction of the Ukrainian economy are estimated at (349) billion dollars at least, which is more than (5/1) times the size of the Ukrainian economy before the war in (2021). This indicates that the aforementioned war has clearly affected the Ukrainian economy, which has begun to receive American and European aid. Despite this, Ukrainian officials expected that the growth of the gross domestic product will reach (4.6%) in 2024, (6.8%) in 2025, and (6.6%) in 2026. Accordingly, it can be said This war has clearly affected the global economy, which depends on the contributions of these two countries, especially with regard to the export of food commodities and energy sources such as oil

and natural gas, as the two countries contribute 30% of global exports of wheat and 53% of the world's sunflower and seed crop.

**Conclusions**

1) Covid-19 has had a major impact on the global economy as a result of economic growth declining to less than (1%), i.e. (-3%), and completely disrupting the wheel of life, especially with regard to trade and tourism, which is consistent with the research hypothesis and proves its validity.

2) The economic recession that occurred due to the spread of Covid-19 brings to mind what happened in the world during the Great Depression in 1929, and even exceeded it in some economic activities.

3) The global economy is characterized by many characteristics that are characterized by dynamism and rapid change, in addition to creating new forms of economic blocs.

4) Economic growth before the Covid-19 crisis was normal growth, as the aforementioned growth rate reached (3.9%) during the years (2018-2019).

5) It is clear that the economic growth rate after the (Covid-19) crisis will be slow growth, as evidenced by the fact that it reached less than (5%) and perhaps less than this percentage in the future.

6) The Russian-Ukrainian war affected the global economy because the two mentioned countries contribute (30%) of global wheat exports and (53%) of the world's sunflower and seed crop.

**Recommendations**

1) The necessity of taking the necessary measures, precautions and precautions to confront any disaster that may occur in the world.

2) Unifying the efforts of all countries of the world and coordinating their positions, in addition to developing a future vision for the global economy.

3) The necessity of rearranging the status of the global economy to what it was before (Covid-19) and what it caused and the damages and losses it caused, especially with regard to the economic and social aspects.

4) The necessity of providing aid and assistance to countries that have been most affected by the spread of (Covid-19) based on the principle of cooperation between the countries of the world.

5) Forming joint committees from countries of the world with expertise and experience to provide advice and procedures related to dealing with crises in the event of their occurrence.

6) Intensifying efforts, efforts and direct interventions to stop the war between Russia and Ukraine due to the global economy's need for the goods and services produced by the economies of these two countries.

**Sources by Topics**
**Section One**
**First: The Concept:**
1) Definition of the Global Economy (2023). available at the link: https// www.borsaat.com.
2) Gregory Clark (2002). The Global Economy, Its Origins, Development and Future, Arab House of Sciences, p. 305.
3) Linda Sartawi, (2023). The Concept and Characteristics of the Global Economy , Available at the following link: https://www. Mawdoo3.com.
Second: (Importance):
4) Sarah Kafafi, (2023). The Importance of Economics in Contemporary Life.
Available at the following link: https://mawdoo3.COM
**Third: Characteristics and Components of the Global Economy:**
5) Tejvan Pettinger (2018). The importance.o of economics.
www.economics help,org. Retrieved. Available at the following link
6) Economics, (2023) Www.investopedian.com
7) Khaled Nashat Al-Jabri, (2022). International Economics in the Age of Globalization, First Edition, Dar Al-Fikr Al-Jami'i, Egypt, Cairo, p. 242.
**Section Two**
**First: Sources of the Global Economy Accepting the (Covid-19) Crisis:**
1) International Economics (2021). Everageed u. Retrieved.
Second: The Global Economy in Light of the (Covid-19) Crisis:
2) Muhammad Mahmoud Al-Sayyid, (2020). The Five Shocks to the Global Economy Due to Corona, Al-Mustaqbal Center.
3) Sakhra, Khaled Hussein Abu Saleh (2022). The Impact of the Corona Pandemic on the Economy in the World and the Middle East (AJSP) Issue 48. Available at: WEO, https://www.imf.org
4) International Monetary Fund (INE) indi … https://dota, albonk aidanti nou ding ge
5) Habib Al-Zaghbi (2020). The global economy after Corona, the repercussions of the crisis and investment opportunities.
6) inside in diana business, (2024).com.https://boatrading Economies.com.- httpsori
7) Sources with the consequences of the Russian-Ukrainian war.
8) The Russian-Ukrainian war and its impact on the global economy (2024)
•https://www.insideindianabusiness.com.
news. https//www.albankaldowli.org.

ISSN (Print) 2794-7629
ISSN (Online) 2794- 4549
Received 11/08/2024
Accepted 23/09/2024

**FULL PAPER**

# Individual Recognition Based on Multi-Spectrum Palm Images

***Prepared by***

***A.Prof.Dr.Raid Rafi Omar Al-Nima***
*Northern Technical University, Mosul, Iraq*
raidrafi1@gmail.com

***Marwan Khaleel Majeed ALali***
*Northern Technical University, Mosul, Iraq*
marwankh1970@ntu.edu.iq

***Saif Saadauldeen Ahmed***
*Al-Imam Al-Adham University College Nineveh, Iraq*
syfesaad@gmail.com

**Abstract:**

Individual recognition based on palm images is such an interesting subject. In this paper, multi-spectrums for full-palm images are considered. The spectra of 460nm and 940nm are employed. Each spectrum provides special features. That is, the spectrum of 460nm affords full-palm textures, and the spectrum of 940nm presents full-palm veins. These facilities are utilized here, where an Artificial Intelligence (AI) approach is suggested. The suggested approach consists of four Deep Learning (DL) networks. Each network is determined for a certain full-palm image, as there are four types of images: right hand full-palm textures, left hand full-palm textures, right-hand full-palm veins, and left-hand full-palm veins. Then, the outputs are fused to provide the final recognition decision. Two datasets are exploited; both are from the Chinese Academy of Sciences Institute of Automation's (CASIA) Multi-Spectral Palmprint Image Database (version. 1.0), where full-palm images of the two spectra 460nm and 940nm are obtained. High performances are achieved after applying the suggested approach.

***Keywords:*** *Deep Learning, Full-Palm Images, Multi-spectrums, Textures, Veins*

**المستخلص:**

يعد التعرف الفردي بناءً على صور راحة اليد موضوعًا مثيرًا للاهتمام. في هذه الدراسة، تم الأخذ بنظر الاعتبار أطياف متعددة لصور راحة اليد الكاملة. تم استخدام الأطياف 460 نانومتر و 940 نانومتر. يوفر كل طيف ميزات خاصة. أي أن طيف 460 نانومتر يُوفر نسيج راحة اليد الكاملة وطيف 940 نانومتر يُظهر أوردة راحة اليد الكاملة. تم استخدام هذه الخصائص هنا حيث تم اقتراح اسلوب للذكاء الاصطناعي (AI). يتكون الاسلوب المقترح من أربعة شبكات تعلم عميق (DL). تم تحديد كل شبكة لصورة راحة يد كاملة معينة حيث توجد أربعة أنواع من الصور لـ: نسيج راحة اليد الكاملة لليد اليمنى، نسيج راحة اليد الكاملة لليد اليسرى، أوردة راحة اليد الكاملة لليد اليمنى وأوردة راحة اليد الكاملة لليد اليسرى. بعد ذلك، تم دمج المخرجات معًا من أجل الحصول على قرار التمييز النهائي. تم استغلال مجموعتين للبيانات، كلاهما من قاعدة بيانات صور بصمات راحة اليد متعددة الأطياف التابعة لمعهد الأتمتة للأكاديمية الصينية للعلوم (CASIA) (الإصدار 1.0)، حيث تم الحصول على صور راحة اليد الكاملة للطيفين 460 نانومتر و940 نانومتر. تم تحقيق نتائج عالية بعد تنفيذ الاسلوب المقترح.

***كلمات مفتاحية:*** *التعلم العميق، صور لراحة الكف الكاملة، أطياف متعددة، أنسجة، أوردة*

## 1. INTRODUCTION

The palm is a significant part of the human hand; it is located in the opposite direction of the hand dorsal. It has rich characteristics that each can be used as a valuable biometric. The full palm refers to the inner surface of a hand, including the inner surfaces of five fingers.

The whole inner surface area of a hand, the full palm, has useful characteristics that can be considered for recognition. There are two main characteristics: textures and veins. Such characteristics

can be obtained by using determined spectra (lights) (Hao et al., 2007, 2008). For example, the spectrum of 460nm reveals the textures, and the spectrum of 940nm provides the veins (Al-Kaltakchi et al., 2018; Al-Nima, 2017). Figures 1 and 2 show demonstrations for these two characteristics in images from the CASIA Multi-spectral Palmprint Image (CMPI) database (Version 1.0).

In the literature, multiple studies were presented for individual recognition based on the inner surface of palm and finger images. In 2019, a texture recognition study by contactless finger and palmprint was provided. A combination approach of deep learning was proposed. Convolutional Neural Networks (CNN) were utilized to perform the combination between the inner finger texture and palmprint for one hand (Genovese et al., 2019). In the same year, palm images of multispectral were exploited. Face images were reproduced. Multi-fusion methods were utilized (Al-Nima et al., 2019). In 2020, a review for recognizing palm veins was presented. It included a wide survey of prior researches for palm veins in the case of recognition. It also involved basic information, acquiring data, a common dataset, processing, feature collection, and classification. Additionally, there was concentrating on related fusion too (Wu et al., 2020). In 2021, images of palm textures were used for verification. A special deep learning network was proposed. The deep learning network was confirmed after many experiments (Albak et al., 2021). In 2022, the latest advancements were illustrated for

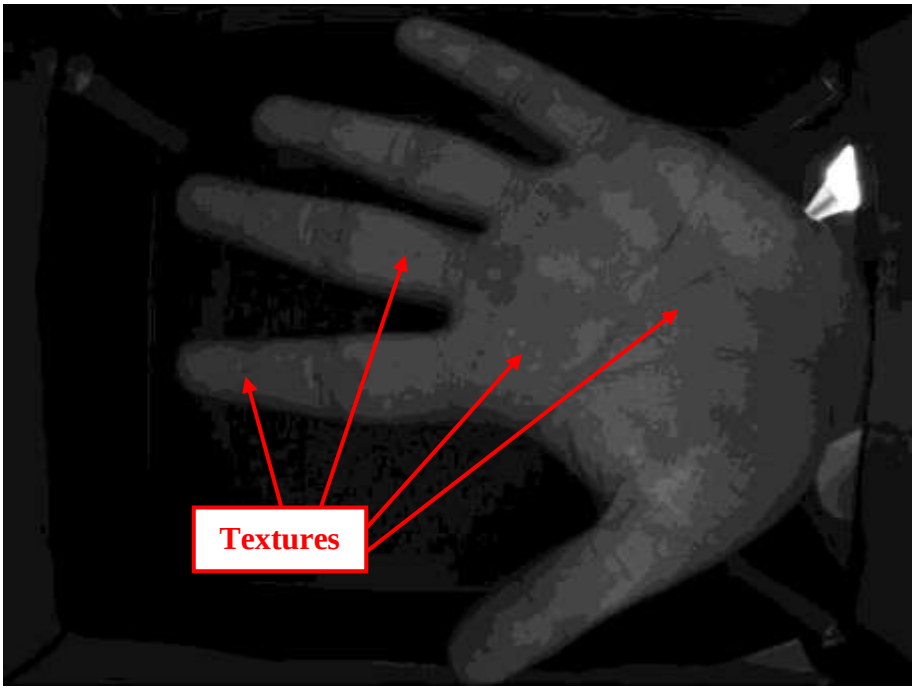


**Figures 1: Demonstrations for full-palm textures from the database of CMPI (*CASIA-MS-PalmprintV1.*, n.d.)**

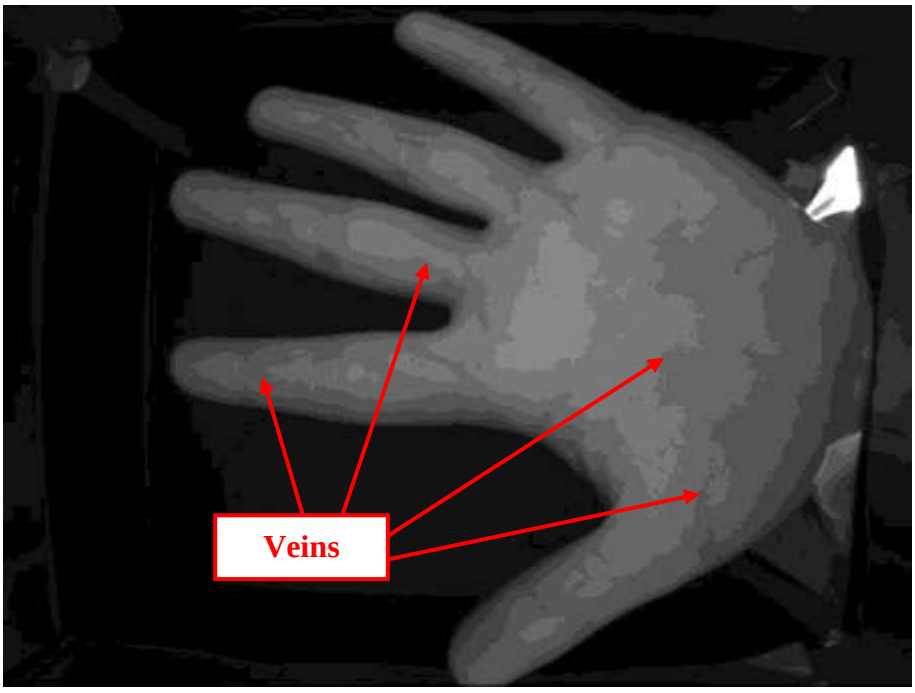


**Figures 2: Demonstrations for full-palm veins from the database of CMPI (*CASIA-MS-PalmprintV1.*, n.d.)**

finger veins. The case of recognition was considered. Chances, difficulties, and methodology were discussed (Shaheed et al., 2022). In 2024, lightweight CNN was utilized. Palm veins were used for the recognition purpose. Multispectral and contactless existences were taken into account (Teotia & Bansal, 2024).

This paper considers full-palm images for individual recognition. It also introduces an Artificial Intelligence (AI) approach that fuses palm images acquired under multi-spectrums. It exploits two full-palm characteristics: textures and veins.

The paper's sections are as follows: Section 1 introduces general information. Section 2 reveals the suggested approach method. Section 3 demonstrates practical results. and Section 4 summarizes the paper.

## 2. SUGGESTED APPROACH

In this paper, we propose a comprehensive approach. Individual recognition uses four types of full-palm images as follows:

- Full-palm textures image of a left hand for the acquisition wavelength of 460nm.
- Full-palm texture image of a right hand for the acquisition wavelength of 460nm.
- Full-palm vein image of a left hand for the acquisition wavelength of 940nm.
- Full-palm vein image of a right hand for the acquisition wavelength of 940nm.

Each one of such images is preprocessed and analyzed by a Deep Learning (DL) network. Then, the outcomes of all networks are combined for obtaining the recognition output. Figure 3 shows a demonstration of the suggested approach.

This figure shows that there are multiple stages in the proposed approach. The first stage is for inputting four full-palm images of a single individual, where both hands (right and left) are used and two acquisition wavelengths (460 nm and 940 nm) are employed. The second stage involves preprocessing. That is, each inputted full-palm image is preprocessed by using advised augmentation and resizing operations. Table 1 exposes the advised augmentation operations.

This table illustrates the number of augmentation operations advised to use. These are the color processing, random reflection, random rotation, and random translation. The table shows that every operation has a determined parameter or parameters. Consequently, the resizing operation is considered, where any augmented image is resized to 128×128 pixels. Such operation is useful in further size reduction of employed images, which helps in speeding up the next stage analysis work.

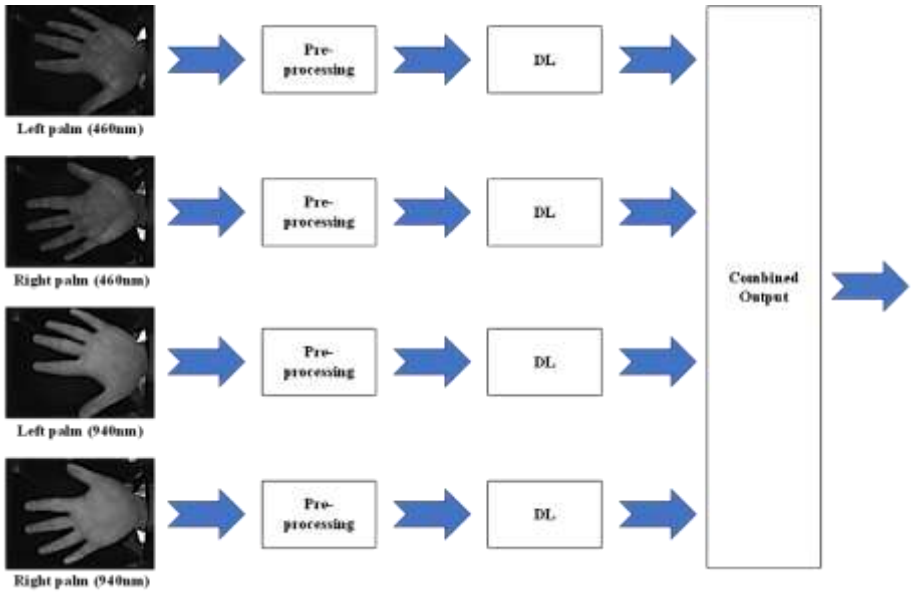


**Figure 3: Demonstration of the suggested approach**

**Table 1: Pre-processing of the advised augmentation operations**

| Augmenta-tion's No. | Augmentation's Name | Parameter(s) |
|---|---|---|
| 1 | Color processing | Converting from grayscale to RGB (if needed) |
| 2 | Random reflection | Probability = 50% |

| | | |
|---|---|---|
| 3 | Random rotation | Rotation range = [-20°, 20°] |
| 4 | Random translation | Horizontal translation range = [-5, 5] and vertical translation range = [-5, 5] |

The third stage is for DLs analysis. This stage involves 4 DL networks. All of them have the same advised structure. The name of each network is known as the Convolutional Neural Network (CNN). CNN is a famous DL technique that has been used in many fields such as medical (Arena et al., 2003; Kayalibay et al., 2017), engineering (Sharma et al., 2023; Zhong, 2024), physics (Pistellato et al., 2021; Wei & Chen, 2019), chemistry (Hirohara et al., 2018; Meyer et al., 2019), and industry (Y. Hu et al., 2019; Medus et al., 2021). Here, the advised CNN structure is detailed in Table 2.

**Table 2: Details of the advised CNN structure**

| Layer's No. | Layer's Name | Parameter(s) |
|---|---|---|
| 1 | Image Input | Image size = 128×128 pixels |
| 2 | Convolution | Filter size = 3×3 pixels, no. of filters = 32 filters, stride size = 1×1 pixel and padding mode = same as input |
| 3 | Rectified Linear Unit (ReLU) | ReLU activation function |
| 4 | Pooling | Pooling type = maximum, pooling size = 2×2 pixels and stride size = 2×2 pixels |
| 5 | Convolution | Filter size = 3×3 pixels, no. of filters = 64 filters, stride size = 1×1 pixel and padding mode = same as input |
| 6 | ReLU | ReLU activation function |
| 7 | Pooling | Pooling type = maximum, pooling size = 2×2 pixels and stride size = 2×2 pixels |
| 8 | Convolution | Filter size = 3×3 pixels, no. of filters = 128 filters, stride size = 1×1 pixel and padding mode = same as |

| | | input |
|---|---|---|
| 9 | ReLU | ReLU activation function |
| 10 | Pooling | Pooling type = maximum, pooling size = 2×2 pixels and stride size = 2×2 pixels |
| 11 | Fully connected | No. of nodes = 256neurons |
| 12 | ReLU | ReLU activation function |
| 13 | Fully connected | No. of nodes = 100 neurons |
| 14 | Softmax | Softmax activation function and No. of nodes = 100 neurons |
| 15 | Classification | No. of nodes = 100 neurons |

So, it consists of 1 image input layer, 3 convolution layers, 4 ReLU layers, 3 pooling layers, 2 fully connected layers, 1 softmax layer, and 1 classification layer. Table 2 provides the parameters of these layers and their sequences. Essentially, any CNN works in one of two phases: learning and evaluation. In the learning phase, the network recognizes samples of images. In the evaluation phase, the network uses what it learns to evaluate other images (G. Hu et al., 2015).

The fourth stage involves the combinations between the outcomes of DLs. There are multiple types of combinations based on the applied rules (Al-Kaltakchi et al., 2018). In this work, the OR rule combination type is considered as the rule that proves its effectiveness (Al-Nima et al., 2020). Subsequently, the recognition output is collected after applying the combination.

## 3. PRACTICAL RESULTS

First of all, and as mentioned, the CMPI database (Version 1.0) (*CASIA-MS-PalmprintV1.*, n.d.) is exploited. This database consists of multi-spectral full-palm images where six spectra are used in the acquisitions. These are the white, 850nm, 940nm, 630nm, 700nm, and 460nm illuminations. They provide two types of characteristics: textures and veins. A total of 100 individuals participated; each individual allowed capturing six full-palm images for each hand and acquisition illumination (*CASIA-MS-PalmprintV1.*, n.d.).

This study uses only the 460 nm and 940 nm spectra. The 460nm reveals textures, while, the 940nm exposes veins (Al-Nima, 2017). The overall number of images that have been used here is 2400 images of full palms, 1200 images for both spectrums and 1200 images for both hands.

Each set of images for determined illumination and hand is partitioned into 75% for the learning phase and 25% for the evaluation phase. Moreover, the same parameters of the provided training options are assigned to any utilized DL as given in Table 3.

Learning performances show successful achievements. Figures 4, 5, 6, and 7 reveal the performances of learning curves for all 4 DLs, where 1st DL is for left full-palms with the 460nm, 2nd DL is for right full-palms with the 460nm, 3rd DL is for left full-palms with the 940nm, and 4th DL is for right full-palms with the 940nm.

There are two types of learning curves, as seen in these figures. The upper curves expose the relations between the accuracy and iterations. The lower curves expose the relations between the losses and iterations. Each curve approves the learning accomplishment either by increasing accuracy or decreasing loss.

**Table 3: Provided training options and parameters that are assigned to any DL**

| Index | Training options | Parameter(s) |
|---|---|---|
| 1 | Optimizer | Optimizer type = Stochastic Gradient Descent with Momentum (SGDM) |
| 2 | No. of epochs | Maximum epochs = 20 |
| 3 | Initial learning rate | $1\times10^{-3}$ |
| 4 | Mini batch size | Mini batch size = 64 |
| 5 | Shuffle | Every epoch |
| 6 | Verbose | False |


**Figure 4: 1st DL learning curves for left full-palms with 460nm acquisition**


**Figure 5: 2nd DL learning curves for right full-palms with 460nm acquisition**


**Figure 6: 3rd DL learning curves for left full-palms with 940nm acquisition**

**Figure 7: 4thDL learning curves for right full-palms with 940nm acquisition**

For evaluation, the achievements of each DL and overall combination (the suggested approach) are comprehensively considered. That is, multiple evaluation metrics are taken into account, namely: accuracy, sensitivity, specificity, precision, and f1-score. Table 4 shows comparison of evaluations for each DL and suggested approach.

This table shows that there are multiple achievements to be discussed. 1st DL attains 99.12%, 56.00%, 99.56%, 56.00%, and 56.00% for the accuracy, sensitivity, specificity, precision, and f1-score, respectively. 2nd DL obtains 99.04%, 52.00%, 99.52%, 52.00%, and 52.00% for the same metrics of accuracy, sensitivity, specificity, precision, and f1-score, respectively. 3rd DL achieves 99.02%, 51.00%, 99.51%, 51.00%, and 51.00% also for the same metrics of accuracy, sensitivity, specificity,

**Table 4: Comparison of evaluations for each DL and suggested approach**

| Method | Metrics | | | | |
|---|---|---|---|---|---|
| | Accuracy(%) | Sensitivity(%) | Specificity(%) | Precision(%) | F1-score(%) |
| 1st DL (for left full-palms with 460nm) | 99.12 | 56.00 | 99.56 | 56.00 | 56.00 |
| 2nd DL (for right full-palms with 460nm) | 99.04 | 52.00 | 99.52 | 52.00 | 52.00 |
| 3rd DL (for left full-palms with 940nm) | 99.02 | 51.00 | 99.51 | 51.00 | 51.00 |
| 4th DL (for right full-palms with 940nm) | 98.96 | 48.00 | 99.47 | 48.00 | 48.00 |
| Suggested approach (for DLs combination) | 99.87 | 87.00 | 100 | 100 | 93.05 |

precision, and f1-score, respectively. 4th DL yields 98.96%, 48.00%, 99.47%, 48.00%, and 48.00% again for the same metrics of accuracy, sensitivity, specificity, precision, and f1-score, respectively.

Clearly, our suggested approach benchmarks the highest evaluations of 99.87%, 87.00%, 100%, 100%, and 93.05% for the accuracy, sensitivity, specificity, precision, and f1-score, respectively. It overcomes other DLs in their separate work. It especially has further enhanced the evaluations of sensitivity, precision and f1-score. So, it has recorded significant achievements.

## 4. CONCLUSION

To conclude, this paper considered individual recognition using multi-spectrum full-palm images. It contributed with a suggested approach. This approach consisted of four stages. The 1st stage was determined for the input full-palm images, where for a single person, both hands of right and left were utilized and two acquisition wavelengths of 460nm and 940nm were exploited. The 2nd stage was assigned for using pre-processing operations of advised augmentation and resizing operations. The 3rd stage was determined for applying an advised DL network with its provided training options four times, where 4 DLs were employed. The 4th stage was assigned for implementing a combination between all outcomes of DLs. The recognition outputs were obtained from the last stage.

The results showed such attractive performances. Learning curves yield acceptable accomplishment. Evaluation values for multiple metrics reveal interesting achievements. The suggested approach attained the highest results of 99.87%, 87.00%, 100%, 100% and 93.05% for the accuracy, sensitivity, specificity, precision, and f1-score, respectively. It significantly further improved the values of sensitivity, precision, and f1-score.

**Acknowledgment:**

" *Portions of the research in this paper use the CASIA-MS-PalmprintV1 collected by the Chinese Academy of Sciences' Institute of Automation (CASIA)* ".

**References:**

Al-Kaltakchi, M. T., Omar, R. R., Abdullah, H. N., Han, T., & Chambers, J. A. (2018). Finger texture verification systems based on multiple spectrum lighting sensors with four fusion levels. *Iraqi Journal of Information and Communication Technology*, *1*(3), 1–16.

Al-Nima, R. R. O. (2017). *Signal Processing and Machine Learning Techniques for Human Verification Based on Finger Textures*. Newcastle University.

Al-Nima, R. R. O., Al-Ridha, M. Y., & Abdulraheem, F. H. (2019). Regenerating face images from multi-spectral palm images using multiple fusion methods. *Telkomnika (Telecommunication Computing Electronics and Control)*, *17*(6). https://doi.org/10.12928/TELKOMNIKA.v17i6.12857

Al-Nima, R. R. O., Hasan, S. Q., & Esmail, S. (2020). Exploiting the deep learning with fingerphotos to recognize people. *International Journal of Advance Science and Technology*, *29*(7), 13035–13046.

Albak, L. H., Al-Nima, R. R. O., & Salih, A. H. (2021). Palm print verification based deep learning. *TELKOMNIKA (Telecommunication Computing Electronics and Control)*, *19*(3), 851–857.

Arena, P., Basile, A., Bucolo, M., & Fortuna, L. (2003). Image processing for medical diagnosis using CNN. *Nuclear Instruments and Methods in Physics Research Section A: Accelerators, Spectrometers, Detectors and Associated Equipment*, *497*(1), 174–178.

*CASIA-MS-PalmprintV1*. (n.d.). http://Biometrics.Idealtest. Org/.

Genovese, A., Piuri, V., Scotti, F., & Vishwakarma, S. (2019). Touchless palmprint and finger texture recognition: A deep learning fusion approach. *2019 IEEE International Conference on Computational Intelligence and Virtual Environments for Measurement Systems and Applications (CIVEMSA)*, 1–6.

Hao, Y., Sun, Z., & Tan, T. (2007). Comparative studies on multispectral palm image fusion for biometrics. *Asian Conference on Computer Vision*, 12–21.

Hao, Y., Sun, Z., Tan, T., & Ren, C. (2008). Multispectral palm image fusion for accurate contact-free palmprint recognition. *2008 15th IEEE International Conference on Image Processing*, 281–284.

Hirohara, M., Saito, Y., Koda, Y., Sato, K., & Sakakibara, Y. (2018). Convolutional neural network based on SMILES representation of compounds for detecting chemical motif. *BMC Bioinformatics*, *19*, 83–94.

Hu, G., Yang, Y., Yi, D., Kittler, J., Christmas, W., Li, S. Z., & Hospedales, T. (2015). When face recognition meets with deep learning: an evaluation of convolutional neural networks for face recognition. *Proceedings of the IEEE International Conference on Computer Vision Workshops*, 142–150.

Hu, Y., Zhang, D., Cao, G., & Pan, Q. (2019). Network data analysis and anomaly detection using CNN technique for industrial control systems security. *2019 IEEE International Conference on Systems, Man and Cybernetics (SMC)*, 593–597.

Kayalibay, B., Jensen, G., & van der Smagt, P. (2017). CNN-based segmentation of medical imaging data. *ArXiv Preprint ArXiv:1701.03056*.

Medus, L. D., Saban, M., Francés-Víllora, J. V, Bataller-Mompeán, M., & Rosado-Muñoz, A. (2021). Hyperspectral image classification using CNN: Application to industrial food packaging. *Food Control*, *125*, 107962.

Meyer, J. G., Liu, S., Miller, I. J., Coon, J. J., & Gitter, A. (2019). Learning drug functions from chemical structures with convolutional neural networks and random forests. *Journal of Chemical Information and Modeling*, *59*(10), 4438–4449.

Pistellato, M., Bergamasco, F., Torsello, A., Barbariol, F., Yoo, J., Jeong, J.-Y., & Benetazzo, A. (2021). A physics-driven CNN model for real-time sea waves 3D reconstruction. *Remote Sensing*, *13*(18), 3780.

Shaheed, K., Mao, A., Qureshi, I., Kumar, M., Hussain, S., & Zhang, X. (2022). Recent advancements in finger vein recognition technology: methodology, challenges and opportunities. *Information Fusion*, *79*, 84–109.

Sharma, S. P., Singh, L., & Tiwari, R. (2023). Design of an efficient integrated feature engineering based deep learning model using CNN for customer's review helpfulness prediction. *Wireless Personal Communications*, *133*(4), 2125–2161.

Teotia, K., & Bansal, M. (2024). Using a Lightweight Convolutional Neural Network for Contactless Multispectral Palm-Vein Recognition. *Revista Electronica de Veterinaria*, *25*(1S), 60–75.

Wei, Z., & Chen, X. (2019). Physics-inspired convolutional neural network for solving full-wave inverse scattering problems. *IEEE Transactions on Antennas and Propagation*, *67*(9), 6138–6148.

Wu, W., Elliott, S. J., Lin, S., Sun, S., & Tang, Y. (2020). Review of palm vein recognition. *IET Biometrics*, *9*(1), 1–10.

Zhong, M. (2024). Risk early warning model of tunnel engineering based on computer vision and CNN. *Journal of Physics: Conference Series*, *2816*(1), 12026.

ISSN (Print) 2794-7629
ISSN (Online) 2794- 4549
Received 02/11/2024
Accepted 01/12/2024

**FULL PAPER**

# Toeplitz Operators on Finite Dimension Spaces with Truncated Values

***Prepared by***

***Dr. Manal Yagoub Ahmed Juma***
*Department of mathematic*
*College of Science*
*Qassim University*
*Buraidah Saudi Arabia*
M.juma@qu.edu.sa

**Abstract**

This work discusses matrix representations of Toeplitz operators' compressing to finite dimensional model spaces $H^2 \ominus BH^2$, where the Blaschke product $B$ is finite. We use the matrix representation to determine if a linear transformation on $H^2 \ominus BH^2$compresses the Toeplitz operator, and if so, what are the sufficient and necessary conditions for this to happen? This result validates a related observation made by Sarason (D. Sarason 1994, D. Sarason2007).

**Key words :**
Clark operators, representations, model spaces, matrix and Toeplitz operators

## 1. Introduction

If $L^2 = L^2(\partial\mathbb{D}, d\theta/2\pi)$ is projected orthogonally onto $H^2$ by $P$, where $H^2$ is an open unit disk, $\mathbb{D} := \{|z| < 1\}$ , is standard Hardy space, refer to (P. L. Duren 1970). for the fundamental definitions), $T_\varphi$ is the Toeplitz operator defined on $H^2$, for $\varphi \in L^\infty$ using the following formula: $T_\varphi f = P(\varphi f)$. A recent investigation into truncated Toeplitz operators was started by Sarason (N. A. Sedlock. (2011). On the model spaces $K_\vartheta := H^2 \cap (\vartheta H^2)^\perp$, these operators $A_\varphi$are defined, where $A_\varphi f := P_\vartheta(\varphi f)$, where $\vartheta$ is an inner function. In this case, $L^2$ is orthogonally projected onto $K_\vartheta$ by $P_\vartheta$. Written otherwise, $A_\varphi$ represents the compression of $T_\varphi$ to $K_\vartheta$. The set in (N. A. Sedlock. 2011).:

$$\mathcal{T}_\vartheta := \{A_\varphi : \varphi \in L^2 \ , A_\varphi \text{ is limited}\}$$

is described as follows: When functions $g_1, g_2 \in K_\vartheta$exist, then a bounded operator $A$ on $K_\vartheta$ belongs to$\mathcal{T}_\vartheta$

$$A = A_z^* A A_z + g_1 \otimes k + k \otimes g_2, \quad (1)$$

Where $k(z) := \frac{\vartheta(z)-\vartheta(0)}{z}$,and the rank-one operator is shown by

$$h_1 \otimes h_2 . h_1 \otimes h_2(f) = \langle f, h_2 \rangle h_1 .$$

The condition in (1) is difficult to develop because it relies on the presence of the functions $g_1, g_2 \in K_\vartheta$, which establish which bounded operators on $K_\vartheta \in \mathcal{T}_\vartheta$. In the case where $K_\vartheta$ is finite dimensional, we will

define a more explicit condition. A limitless n-dimensional model space is defined as $K_B$, where B is a finite Blaschke product with zeros $\{a_1, \dots, a_n\}$.It's generally knowledge that all functions with the type $K_B$are are constructed of

$$f(z) = \frac{p(z)}{\prod_{j=1}^{n}(1-\overline{a_j}z)} \qquad (2)$$

where $p$ can be any polynomial with a maximum degree of $n-1$. Additionally,

$$k_\lambda(z) := \frac{1-\overline{B(\lambda)}B(z)}{1-\overline{\lambda}z} \qquad (3)$$

is the $K_B$ resembling kernel such that $k_\lambda \in K_B$,for each $\lambda \in \mathbb{D}$

$$f(\lambda) = \langle f, k_\lambda \rangle \quad \forall f \in K_B.$$

The formula above uses $L^2$ inner product. $\langle f, g\rangle = \int_{\mathbb{T}} f(\zeta)\overline{g(\zeta)}\frac{|d\zeta|}{2\pi}$, where $T := \partial\mathbb{D}$. Using (2) and interpolating, we can easily demonstrate that the set $\{k_{\lambda_1}, \dots, k_{\lambda_n}\}$ serves as a basis for $K_B$ for multiple points $\lambda_1, \dots, \lambda_n \in \mathbb{D}$. If the zeros $a_1, \dots, a_n$ of $B$ are distinct, $\{k_{a_1}, \dots, k_{a_n}\}$ forms a non-orthonormal basis for $K_B$. $k_{a_j}(z) = \frac{1}{1-\overline{a_j}z}$.

Dimensional $n^2$ defines the complex vector field of all linear transformations on $K_B$, given in fundamental linear algebra. The dimension of $\mathcal{T}_B$ is $2n-1$,by Sarason (P. L. Duren 1970). Naturally, this raises the question of which linear transformations on $K_B \in \mathcal{T}_B$. This is the first theorem that we have.

**Remark (1.1)**

(1) The principal horizontal values and first row form a matrix representing a truncated Toeplitz operator according to Theorem (1.8). Observe that since $\mathcal{T}_B$ has size $2n-1$, similar matrices should also have dimension $2n-1$.

(2) The first row is not particularly noteworthy. An analogous outcome, for instance, can be achieved if the first column and entries along the major diagonal define the representation matrix.

(3) The demonstration of this theorem additionally includes an algorithm for generating the symbol $\varphi$ from matrix elements.

(4) When $n = 2$, the distribution matrix $\begin{pmatrix} r_{1,1} & r_{1,2} \\ r_{2,1} & r_{2,2} \end{pmatrix}$ represents the truncated Toeplitz operator in terms of the basis $\{k_{a_1}, k_{a_2}\}$ if and only if $\overline{B'(a_1)}r_{1,2} = r_{2,1}\overline{B'(a_2)}$. $\{k_{a_1}, k_{a_2}\}$ is a valid basis for $K_B$, although it is not orthonormal. The Clark basis $\{v_{\zeta_1}, \dots, v_{\zeta_n}\}$, is an essential orthonormal basis for $K_B$. It consists of normalizing vectors that correspond to the eigenvalues $\zeta_j \in \mathbb{T}$ for the Clark unitary operator $U_\alpha$ where $\alpha \in \mathbb{T}$. This takes the following shape: Because $B$ is an open area of $\mathbb{D}^-$with a finite Blaschke product, the kernel function $k_\zeta$ gives the analytical function on $\mathbb{D}$ for any $\zeta \in \mathbb{T}$. Typically, it is shown that $k_\zeta \in K_B$B and:

$$f(\zeta) = \langle f, k_\zeta \rangle \quad \forall f \in K_B. \qquad (4)$$

Using the assumption that $B'$ never disappears on $\mathbb{T}$, a routine exercise will demonstrate that for any $\alpha \in \mathbb{T}$, there are precisely $n$ different locations $\zeta_1, \dots, \zeta_n \in \mathbb{T}$ for which:

$$B(\zeta_j) = \frac{\alpha + B(0)}{1+\overline{B(0)}\alpha}, \quad j = 1, \dots, n.$$

One more standard workout will demonstrate that $\left\|k_{\zeta_s}\right\|^2 = |B'(\zeta_s)|$, hence, the normalized kernel functions are formed.

$$v_{\zeta_s} := \frac{k_{\zeta_s}}{\sqrt{|B'(\zeta_s)|}}. \tag{5}$$

It shows out that the eigenvalues of the Clark unitary operator are the points $\zeta_1, \dots, \zeta_n$.

$$U_\alpha := A_z + \frac{B(0)+\alpha}{1-|B(0)|^2}\ \left(k_0 \otimes \tilde{k}_0\right) \tag{6}$$

$v_{\zeta_1}, \dots, v_{\zeta_n}$, the appropriate eigenvectors.

$$\tilde{k}_\lambda(z) := \frac{B(z)-B(\lambda)}{z-\lambda}. \tag{7}$$

It is observable (P. L. Duren1970). that for any $\tilde{k}_\lambda \in K_B$for all $\lambda \in \mathbb{D}$. Therefore, $K_B$. has an orthonormal basis of $\{v_{\zeta_1}, \dots, v_{\zeta_n}\}$. In-depth research and generalization have been done on the operators $U_\alpha$, which Clark (N. A. Sedlock. 2011). Initially examined (D. Sarason, John 1994 and Bu, Q., Chen, Y. & Zhu, S. 2021). The matrix shows $U_\alpha$ with regard to this basis is diag $(\zeta_1, \dots, \zeta_n)$, as determined by the spectral theorem. Our subsequent theorem substitutes the kernel functions' basis $\{k_{a_1}, \dots, k_{a_n}\}$ with the Clark basis $\{v_{\zeta_1}, \dots, v_{\zeta_n}\}$.

**Theorem (1.2):** Take $B$ be the finite Blaschke product of degree $n$ having $\alpha \in \mathbb{T}$. A can be used to denote any transform that is linear in the space with $n$ -dimensions $K_B$.

A is only a part of $A \in \mathcal{T}_B$ if and only if $M_A = (r_{i,j})$ ,the multidimensional representation of $A$ in relation to the Clark basis $\{v_{\zeta_1}, \dots, v_{\zeta_n}\}$ corresponding to $\alpha$.

$$r_{i,j} = \frac{\sqrt{|B'(\zeta_1)|}}{\zeta_j - \zeta_i}\left(\frac{\zeta_j}{\zeta_i}\frac{1}{\sqrt{|B'(\zeta_j)|}}(\zeta_1-\zeta_i)r_{1,i} + \frac{1}{\sqrt{|B'(\zeta_i)|}}(\zeta_j-\zeta_1)r_{1,j}\right) \tag{8}$$

all $1 \le i, j \le n$, and $i \ne j$.

**Remark (1.3)**: As in the previous theorem, the elements along the main diagonal and the first row determine the matrix representation of a truncated Toeplitz operator.

(1) An algorithm for obtaining the symbol $\varphi$ from the matrix entries will also result from the proving of this theorem.

(2) If $n$ is 2, the matrix $\begin{pmatrix} r_{1,1} & r_{1,2} \\ r_{2,1} & r_{2,2} \end{pmatrix}$ is the truncated Toeplitz operator's matrix representation with regard to basis $\{v_{\zeta_1}, v_{\zeta_2}\}$ if and only if

$$\zeta_1 r_{1,2} = \zeta_2 r_{2,1}.$$

If we alter the basis $\{v_{\zeta_1}, \dots, v_{\zeta_n}\}$ slightly, we get even more. Indeed, let

$$\beta_\alpha := \frac{\alpha + B(0)}{1+\overline{B(0)}\alpha},\quad w_s := e^{-\frac{i}{2}(\arg(s)-\arg(\beta_\alpha))},\quad e_{\zeta_s} := \frac{1}{\sqrt{|B'(\zeta_s)|}} w_s k_{\zeta_s}. \tag{9}$$

$\{e_{\zeta_1}, \dots, e_{\zeta_n}\}$ is an orthonormal basis that, has the additional characteristic that, in addition to diagonalizing the Clark operator $U_\alpha$, the matrix representation of any truncated Toeplitz operator with respect to this basis is complex symmetric, as shown by Garcia and Putinar in (Bu, Q., Chen, Y. & Zhu, S. 2021). If a matrix $M = M^t$, where $t$ is the transpose, then $M$ is complex symmetric. The Clark basis $\{v_{\zeta_1}, \dots, v_{\zeta_n}\}$ is replaced with the new basis $\{\{e_{\zeta_1}, \dots, e_{\zeta_n}\}$ by the theorem that follows.

**Theorem (1.4): Assume** that $B$ is a finite Blaschke product with $\alpha \in \mathbb{T}$,and degree $n$.

$A$ can be used to represent any linear transformation on the n-dimensional space $K_B$.

$A \in \mathcal{T}_B$ if and only if $M_A$ is complex symmetric and $M_A = (r_{i,j})$ represents $A$ as a matrix with respect to the basis $\{e_{\zeta_1}, \dots, e_{\zeta_n}\}$that corresponds to $\alpha$ .

$$r_{i,j} = \frac{\sqrt{|B'(\zeta_1)|}}{\overline{w_1}} \frac{1}{\zeta_j - \zeta_i} \left( \frac{\overline{w_j}}{\sqrt{|B'(\zeta_j)|}} (\zeta_1 - \zeta_i) + \frac{\overline{w_i}}{\sqrt{|B'(\zeta_i)|}} (\zeta_j - \zeta_1) r_{1,j} \right) \qquad (10)$$

for all $1 \le i, j \le n$, $i \ne j$.

**Proof:** we prove theorem (1.2) and theorem (1.4) together:

Assume $\alpha_1 \ne \alpha_2$ and fix $\alpha_1, \alpha_2 \in \mathbb{T}$. Let the points of $\mathbb{T}$ that $\{\zeta_j, \eta_j : j = 1, \dots, n\}$are those that $B(\zeta_j) = \beta_{\alpha_1}$, $B(\eta_j) = \beta_{\alpha_2}$, $j = 1, \dots, n$. Remark (1.11) informs us that any member of $\mathcal{T}_B$ adopts the form $\sum_{j=1}^n c_j k_{\zeta_j} \otimes k_{\zeta_j} + \sum_{j=1}^n d_j k_{\eta_j} \otimes k_{\eta_j}$, regarding a few complex constants, $c_j, d_j$. Assume that $e_{\zeta_s} = w_s v_{\zeta_s}$, where:

$$w_s = e^{-\frac{i}{2}(\arg(\zeta_s) - \arg(\beta_{\alpha_1}))}. \qquad (11)$$

Theorem (1.4) can be established by using

$\langle \left( \sum_{j=1}^n c_j k_{\zeta_j} \otimes k_{\zeta_j} + \sum_{j=1}^n d_j k_{\eta_j} \otimes k_{\eta_j} \right) e_{\zeta_p}, e_{\zeta_s} \rangle$,the operator's matrix representation with regard to the basis $\{e_{\zeta_1}, \dots, e_{\zeta_n}\}$, Since $\{e_{\zeta_1}, \dots, e_{\zeta_n}\}$ is an orthonormal basis for $K_B$, the `Fourier' expansion is available for every $f \in K_B$.

$$f(z) = \sum_{s=1}^n \langle f, e_{\zeta_s} \rangle e_{\zeta_s}(z) = \sum_{s=1}^n \frac{\overline{w_s}}{\sqrt{|B'(\zeta_s)|}} f(\zeta_s) e_{\zeta_s}(z)$$

and so

$$\langle f, g \rangle = \sum_{s=1}^n \frac{f(\zeta_s)\overline{g(\zeta_s)}}{\sqrt{|B'(\zeta_s)|}}, \quad f, g \in K_B. \qquad (12)$$

First notice that

$$e_{\zeta_s}(\zeta_q) = \frac{w_s}{\sqrt{|B'(\zeta_s)|}} k_{\zeta_s}(\zeta_q) = \begin{cases} w_s \sqrt{|B'(\zeta_s)|}, & \text{if } s = q; \\ 0, & \text{if } s \ne q \end{cases}.$$

Using the inner product formula given before in (12), we get

$$\langle\left(k_{\zeta_j}\otimes k_{\zeta_j}\right)e_{\zeta_p},e_{\zeta_s}\rangle=\sum_{q=1}^{n}\frac{\left(\left(k_{\zeta_j}\otimes k_{\zeta_j}\right)e_{\zeta_p}\right)(\zeta_q)\overline{e_{\zeta_s}(\zeta_q)}}{\sqrt{|B'(\zeta_q)|}}=\left(\left(k_{\zeta_j}\otimes k_{\zeta_j}\right)e_{\zeta_p}\right)(\zeta_s)\frac{\overline{w_s}}{\sqrt{|B'(\zeta_s)|}}$$

$$=\frac{\overline{w_s}}{\sqrt{|B'(\zeta_s)|}}\langle e_{\zeta_p},k_{\zeta_j}\rangle\,k_{\zeta_j}(\zeta_s)$$

$$=\frac{\overline{w_s}}{\sqrt{|B'(\zeta_s)|}}\frac{w_p}{\sqrt{|B'(\zeta_p)|}}k_{\zeta_p}(\zeta_j)k_j(\zeta_j)=\begin{cases}|B'(\zeta_s)|, & \text{if } s=p=j;\\ 0, & \text{otherwise.}\end{cases}$$

In a similar way,

$$\langle\left(k_{\eta_j}\otimes k_{\eta_j}\right)e_{\zeta_p},e_{\zeta_s}\rangle=\frac{\overline{w_s}}{\sqrt{|B'(\zeta_s)|}}\frac{w_p}{\sqrt{|B'(\zeta_p)|}}k_{\zeta_p}(\eta_j)k_{\eta_j}(\zeta_s)$$

$$=\frac{\overline{w_s}}{\sqrt{|B'(\zeta_s)|}}\frac{w_p}{\sqrt{|B'(\zeta_p)|}}\frac{1-\overline{B(\zeta_p)}B(\eta_j)}{1-\overline{\zeta_p}\eta_j}\frac{1-\overline{B(\eta_j)}B(\zeta_s)}{1-\overline{\eta_j}\zeta_s}$$

$$=\frac{\overline{w_s}}{\sqrt{|B'(\zeta_s)|}}\frac{w_p}{\sqrt{|B'(\zeta_p)|}}\frac{1-\overline{\beta_{\alpha_1}}\beta_{\alpha_2}}{1-\overline{\zeta_p}\eta_j}\frac{1-\overline{\beta_{\alpha_2}}\beta_{\alpha_1}}{1-\overline{\eta_j}\zeta_s}$$

$$=\left|1-\overline{\beta_{\alpha_2}}\beta_{\alpha_1}\right|^2\frac{\overline{w_s}}{\sqrt{|B'(\zeta_s)|}}\frac{w_p}{\sqrt{|B'(\zeta_p)|}}\frac{1}{1-\overline{\zeta_p}\eta_j}\frac{1}{1-\overline{\eta_j}\zeta_s}$$

$$=\left|1-\overline{\beta_{\alpha_2}}\beta_{\alpha_1}\right|^2\frac{\overline{w_s}}{\sqrt{|B'(\zeta_s)|}}\frac{w_p}{\sqrt{|B'(\zeta_p)|}}\frac{1}{1-\overline{\zeta_p}\eta_j}\frac{1}{1-\overline{\eta_j}\zeta_s}\frac{(-\eta_j)\zeta_p}{(-\eta_j)\zeta_p}$$

$$=-\eta_j\left|1-\overline{\beta_{\alpha_2}}\beta_{\alpha_1}\right|^2\frac{\overline{w_s}}{\sqrt{|B'(\zeta_s)|}}\frac{w_p\zeta_p}{\sqrt{|B'(\zeta_p)|}}\frac{1}{\eta_j-\zeta_s}\frac{1}{\eta_j-\zeta_p}$$

Using (11) is notion of $w_p$, the true nature,$\zeta_p=\beta_{\alpha_1}\overline{w}_p^2$. Apply this characteristic to change the previous expression's final line in order to

$$-\beta_{\alpha_1}\eta_j\left|1-\overline{\beta_{\alpha_2}}\beta_{\alpha_1}\right|^2\frac{\overline{w_s}}{\sqrt{|B'(\zeta_s)|}}\frac{\overline{w_p}}{\sqrt{|B'(\zeta_p)|}}\frac{1}{\eta_j-\zeta_s}\frac{1}{\eta_j-\zeta_p}.$$

Putting this all together, we get

$$\left\langle \left( \sum_{j=1}^{n} c_j k_{\zeta_j} \otimes k_{\zeta_j} + \sum_{j=1}^{n} d_j k_{\eta_j} \otimes k_{\eta_j} \right) e_{\zeta_p}, e_{\zeta_s} \right\rangle$$

$$= c_p \left| B'(\zeta_p) \right| \delta_{s,p} - \beta_{\alpha_1} \left| 1 - \overline{\beta_{\alpha_2}} \beta_{\alpha_1} \right|^2 \sum_{j=1}^{n} \eta_j d_j \frac{\overline{w_s}}{\sqrt{|B'(\zeta_s)|}} \frac{\overline{w_p}}{\sqrt{|B'(\zeta_p)|}} \frac{1}{\eta_j - \zeta_s} \frac{1}{\eta_j - \zeta_p}.$$

Partial fraction decomposition is used.

$$\frac{1}{\eta_j - \zeta_s} \frac{1}{\eta_j - \zeta_p} = \frac{1}{\zeta_s - \zeta_p} \left( \frac{1}{\eta_j - \zeta_s} - \frac{1}{\eta_j - \zeta_p} \right),$$

The identities in can be confirmed in (10). The requirements in (10), are then satisfied by any truncated Toeplitz operator's matrix representation with respect to the basis $\{e_{\zeta_1}, \dots, e_{\zeta_n}\}$. The inverse proof is almost identical to the converse proof in Theorem (1.8). By employing comparable computations to the Theorem (1.4) proof, it is demonstrated that

$$\left\langle \left( \sum_{j=1}^{n} c_j k_{\zeta_j} \otimes k_{\zeta_j} + \sum_{j=1}^{n} d_j k_{\eta_j} \otimes k_{\eta_j} \right) v_{\zeta_p}, v_{\zeta_s} \right\rangle =$$

$$c_p \left| B'(\zeta_p) \right| \delta_{s,p} - \beta_{\alpha_1} \left| 1 - \overline{\beta_{\alpha_2}} \beta_{\alpha_1} \right|^2 \sum_{j=1}^{n} \eta_j d_j \frac{1}{\sqrt{|B'(\zeta_s)|}} \frac{\zeta_p}{\sqrt{|B'(\zeta_p)|}} \frac{1}{\eta_j - \zeta_s} \frac{1}{\eta_j - \zeta_p}.\text{S}$$

Proceed with the remaining steps in Theorem (1.4) proof to establish Theorem (1.2).

**Remark (1.5):** Any complex symmetric 2×2 matrix represents a truncated Toeplitz operator with regard to the basis $\{e_{\zeta_1}, e_{\zeta_2}\}$, according to the theorem for $n = 2$. Sarason had noted this before (R.Garcia and M.Putinar, August 2007 & Balayan, L., Garcia, S.R., 2010).
Sarason started talking about how the truncated Toeplitz operators are generated by the Clark unitary operators in some way in Remark (1.10) below, (N. A. Sedlock. 2011). In finite dimensions, the outcome is as follows.

**Theorem (1.6):** Assume that $\alpha_1, \alpha_2 \in \mathbb{T}$, where $\alpha_1 \neq \alpha_2$, and that a Blaschke product of degree $n$ is represented by $B$. Next, for any $\varphi \in L^2$, there exist polynomials $p; q$ with a maximum degree of $n$, such that

$$A_\varphi = p(U_{\alpha_1}) + q(U_{\alpha_2}). \qquad (13)$$

**Proof:** One can obtain the ensuing lemma from (P. L. Duren (1970). Here we provide evidence.

**Remark (1.7):**

(1) Sarason (P. L. Duren 1970). establishes that for any polynomial $p$ and each $\alpha \in \mathbb{T}$, $p(U_\alpha) \in \mathcal{T}_B$. In reality, the spectral theorem for unitary operators and Theorem (1.6) may be extracted from the proof in (N. A. Sedlock. 2011).
(2) Remark (1.9) will demonstrate that the polynomials $p$ and $q$ in (13) can be computed, in a sense, from $\varphi$.

**Theorem (1.8):** Let $B$ be a finite Blaschke product of degree $n$ with unique zeros $a_1, \dots, a_n$, and let $A$ be any linear transformation on the n-dimensional space $K_B$. $A$ is represented by the matrix $M_A = (r_{i,j})$with respect to the basis $\{k_{a_1}, \dots, k_{a_n}\}$if and only if $A \in \mathcal{T}_B$.

$$r_{i,j} = \overline{\left(\frac{B'(a_1)}{B'(a_i)}\right)}\left(\frac{r_{1,i}\overline{(a_1 - a_i)} + r_{1,j}\overline{(a_j - a_1)}}{\overline{a_j - a_i}}\right), \quad 1 \le i,j \le n, \quad i \ne j. \qquad (14)$$

**Proof:** Given a $\varphi$ that is in $L^2$, break $\varphi$ down as

$$\varphi = \psi_1 + \overline{\psi_2} + \eta_1 + \overline{\eta_2}, \quad \psi_1, \psi_2 \in K_B, \quad \eta_1, \eta_2 \in BH^2.$$

Now write $A_\varphi$ as $A_\varphi = A_{\psi_1 + \overline{\psi_2}} + A_{\eta_1 + \overline{\eta_2}}$, and see that (P. L. Duren 1970). 's second term, which is zero, is on the right. Thus,

$$\left\{A_{\psi_1 + \overline{\psi_2}} : \psi_1, \psi_2 \in K_B\right\} = \mathcal{T}_B. \qquad (15)$$

The zeros $a_1, \dots, a_n$ of $B$ are assumed to be different, and as a result, the functions

$\tilde{k}_{a_j}(z) = \frac{B(z)}{z - a_j}$, $j = 1, \dots, n$, as a foundation for $K_B$ serve as a foundation for $K_B$ , and $\overline{\tilde{k}_{a_j}(z)} = \overline{\left(\frac{B(z)}{z - a_j}\right)}$, $j = 1, \dots, n$, form a basis for $\overline{K_B}$. Based on the preceding discourse and equation (15), $\mathcal{T}_B$ is comprised of $A_\varphi$.

$$\varphi(\zeta) = \sum_{j=1}^{n} c_j \overline{\left(\frac{B(\zeta)}{\zeta - a_j}\right)} + \sum_{j=1}^{n} d_j \frac{B(\zeta)}{\zeta - a_j} \qquad (16)$$

and the arbitrary complex numbers $c_j, d_j$. Add this to the identity.

$$k_\lambda \otimes \tilde{k}_\lambda = A_{\frac{B}{\overline{z} - \lambda}}. \qquad (17)$$

And its adjoint to determine that the operators in $\mathcal{T}_B$ are of the following type in (P. L. Duren 1970).

$$\sum_{j=1}^{n} c_j k_{a_j} \otimes \tilde{k}_{a_j} + \sum_{j=1}^{n} d_j \tilde{k}_{a_j} \otimes k_{a_j}, \qquad (18)$$

where the complex integers $c_j$ and $d_j$are. The matrix representation of the previously specified operator about the basis $\{k_{a_1} \dots, k_{a_n}\}$.will be determined shortly. We must first obtain a few formulas. With the definitions of $k_{a_j}$ (3) and $\tilde{k}_{a_j}$) (7) and the replicating property of $k_{a_j}$, we obtain:

$$\langle \tilde{k}_{a_j}, k_{a_j} \rangle = \begin{cases} 0, & \text{if } i \ne j; \\ B'(a_j), & \text{if } i = j. \end{cases} \quad \text{and } \langle \tilde{k}_{a_j}, \tilde{k}_{a_j} \rangle = \frac{1}{1 - \overline{a_j} a_i}. \qquad (19)$$

As $\{k_{a_1}, \dots, k_{a_n}\}$ gives a basis for $K_B$, we understand that $\tilde{k}_{a_j} = \sum_{s=1}^{n} h_s(a_j) k_{a_s}$,

$h_s(a_j)$for a number of complex constants. (19) can be used to calculate $h_s(a_j)$and obtain:

$$\tilde{k}_{a_j} = \sum_{s=1}^{n} \frac{1}{\overline{B'(a_s) 1}} \frac{1}{1 - \overline{a}_s a_j} k_{a_s}. \qquad (20)$$

The proof of Theorem (1.8) is now ready. Assume $A_\varphi$ has the structure shown in (18) and $\left(b_{s,p}\right)_{1\le s,p\le n} = M_{A_\varphi}$, express $A_\varphi$ as a matrix with regard to the basis $\{k_{a_1}, \dots, k_{a_n}\}$. We need for proof that

$$b_{s,p} = \left(\frac{\overline{B'(a_1)}}{\overline{B'(a_s)}}\right)\left(\frac{b_{1,s}\overline{(a_1 - a_s)} + b_{1,p}\overline{(a_p - a_1)}}{\overline{a_p - a_s}}\right), \quad 1 \le s,p \le n, s \ne p \qquad (21)$$

A computation with (18), (19), and (20) will show that

$$A_\varphi k_{a_p} = c_p\overline{B'(a_p)}k_{a_p} + \sum_{s=1}^{n}\left(\frac{1}{\overline{B'(a_s)}}\sum_{j=1}^{n}\frac{d_j}{(1-\overline{a_s}a_j)(1-\overline{a_p}a_j)}\right)k_{a_s}.$$

Thus

$$b_{s,p} = c_p\overline{B'(a_p)}\delta_{s,p} + \frac{1}{\overline{B'(a_s)}}\sum_{j=1}^{n}\frac{d_j}{(1-\overline{a_s}a_j)(1-\overline{a_p}a_j)}.$$

From the formula, the unique characteristics in (21) follow.

$$\frac{1}{(1-\overline{a_s}a_j)(1-\overline{a_p}a_j)} = \frac{-\overline{a_s}}{\overline{a_p}-\overline{a_s}}\frac{1}{1-\overline{a_s}a_j} + \frac{\overline{a_p}}{\overline{a_p}-\overline{a_s}}\frac{1}{1-\overline{a_p}a_j}.$$

The proof has now been completed in one direction. Let $V$ be the set of all matrices that fulfill (14) in the opposite direction. These identities show that each

$M = \left(r_{i,j}\right) \in V$ is uniquely determined by the entries along the diagonal and the first row. Moreover, $M$ is these entries' linear function. $V$ is therefore a vector space with dimensions of $2n-1$. As we've already established in (21),

$V_1 := \left\{M_{A_\varphi} : A_\varphi \in \mathcal{T}_B\right\} \subset V$, and $V_1$ has dimension $2n-1$ according to Sarason's theorem. $V_1 = V$ as a result, this completes the proof.

**Remark (1.9):**

(1) Take note that one explicit foundation for $V$ is $\{D_1, \dots, D_n, R_2, \dots, R_n\}$.
Here, $R_k$ is the matrix satisfying equation (14) with $r_{1,k} = 1$, $r_{j,j} = 0$ if
$j \ne k$, and, $r_{1,j} = 0$ for all $j$. $D_k = \text{diag}(0,\dots,1,0,\dots,0)$ is the matrix. To illustrate, if $n = 3$, then

$$D_1 = \begin{pmatrix}1&0&0\\0&0&0\\0&0&0\end{pmatrix}, \quad D_2 = \begin{pmatrix}0&0&0\\0&1&0\\0&0&0\end{pmatrix}, \quad D_3 = \begin{pmatrix}0&0&0\\0&0&0\\0&0&1\end{pmatrix},$$

$$R_2 = \begin{pmatrix}0 & 1 & 0\\ \dfrac{B'(a_1)}{B'(a_2)} & 0 & \dfrac{(a_1-a_2)B'(a_1)}{(a_3-a_2)B'(a_2)}\\ 0 & \dfrac{(a_2-a_1)B'(a_1)}{(a_2-a_3)B'(a_3)} & 0\end{pmatrix}$$

$$R_3 = \begin{pmatrix} 0 & 0 & 1 \\ 0 & 0 & \dfrac{(a_3-a_1)B'(a_1)}{(a_3-a_2)B'(a_2)} \\ \dfrac{B'(a_1)}{B'(a_3)} & \dfrac{(a_1-a_3)B'(a_1)}{(a_2-a_3)B'(a_3)} & 0 \end{pmatrix}$$

in the example above indicates the complex conjugation of each and every matrix entry—not the conjugate transpose.

(2) If $P_j := \frac{1}{B'(a_j)} k_{a_j} \otimes \tilde{k}_{a_j}$, take note of the evidence above that

$$P_j^2 = P_j, \ \sum_{j=1}^{n} P_j = I, \ P_j P_l = \delta_{j,l} P_j, \ \mathcal{T}_B = \text{span}\{P_j, P_j^* : j = 1, \dots, n\}.$$

Comparable identities apply to $P_j = \frac{1}{B'(a_j)} \tilde{k}_{a_j} \otimes k_{a_j}$. These identities show how the set of $2n$ operators $\{P_j, P_j^* : j = 1, \dots, n\}$. has a linear dependence. For instance, a little study are going to show that the basis for $\mathcal{T}_B$, which includes rank one idempotent, is the set $\{P_j, P_l^* : j = 2, \dots, n; l = 1, \dots, n\}$.

(3) $A_\varphi$ from (18) can be computed with regard to the basis $\{\tilde{k}_{a_1}, \dots, \tilde{k}_{a_n}\}$.using comparable methods. The $b_{s,p}$ element of this matrix is in this instance

$$b_{s,p} = d_p B'(a_p)\delta_{s,p} + \frac{1}{B'(a_s)} \sum_{j=1}^{n} \frac{c_j}{(1 - a_s\overline{a_j})(1 - a_p\overline{a_j})}$$

and the prerequisite that must be met in order for a matrix $(r_{s,p})$ to represent something from $\mathcal{T}_B$ (relative to the basis $\{\tilde{k}_{a_1}, \dots, \tilde{k}_{a_n}\}$) is

$$r_{s,p} = \frac{B'(a_1)}{B'(a_s)} \left( \frac{r_{1,s}(a_1 - a_s) + r_{1,p}(a_p - a_1)}{a_p - a_s} \right), \ 1 \le s, p \le n, s \ne p.$$

**Lemma (1.10):** Assume that $w_1, \dots, w_{2n-1}$) are unique locations within $T$. Next, the top-ranked operators $k_{w_1} \otimes k_{w_1}, \dots, k_{w_{2n-1}} \otimes k_{w_{2n-1}}$, possess linear independence

**Proof:** Suppose $c_1, \dots, c_{2n-1}$ are complicated constants in such a way that

$$\sum_{j=1}^{2n-1} c_j k_{w_j} \otimes k_{w_j} = 0. \qquad (22)$$

Given the linear independence of $k_{w_1}, \dots, k_{w_n}$, there exists a $g \in K_B$ such that

$$\langle k_{w_1}, g \rangle = 1, \ \langle k_{w_j}, g \rangle = 0, \ j = 2, \dots, n.$$

Use the operator on the left side of (22) in this case to see that

$$c_1 k_{w_1} + \sum_{j=n+1}^{2n-1} c_j \langle g, k_{w_j} \rangle k_{w_j} = 0.$$

Nevertheless $c_1 = 0$,since the vectors $k_{w_1}, k_{w_{n+1}}, \dots, k_{w_{2n-1}}$ are linearly independent. Select a suitable g now to demonstrate that $c_2 = 0$, and so forth. This is the theorem (1.6) proof. Since $\alpha_1 \neq \alpha_2$, let $\alpha_1, \alpha_2 \in \mathbb{T}$. Let T's points be $\zeta_1, \dots, \zeta_n$ and $\eta_1, \dots, \eta_n$, so that

$$B(\zeta_j) = \beta_{\alpha_1} := \frac{\alpha_1 + B(0)}{1 + \overline{B(0)}\alpha_1}, \quad B(\eta_j) = \beta_{\alpha_2} := \frac{\alpha_2 + B(0)}{1 + \overline{B(0)}\alpha_2}, \quad j = 1, \dots, n.$$

Take in consideration that $\{v_{\zeta_1}, \dots, v_{\zeta_n}\}$is an orthonormal basis for $K_B$ of eigenvectors of $U_{\alpha_1}$. Observe that the points $\zeta_1, \dots, \zeta_n, \eta_1, \dots, \eta_n$ are different.

Similarly, $\{v_{\eta_1}, \dots, v_{\eta_n}\}$. is an orthonormal basis for $K_B$ of eigenvectors of $U_{\alpha_2}$. Kindly:

$$P_{\zeta_j} := v_{\zeta_j} \otimes v_{\zeta_j}, \quad P_{\eta_j} := v_{\eta_j} \otimes v_{\eta_j}, \quad j = 1, \dots, n$$

and see that these operators are orthogonal projections onto the eigenspaces they span, respectively, as $k_{\zeta_j}$. It is shown in (D. N. Clark, 1972). that for each } $\zeta \in \mathbb{T}$,

$$k_\zeta \otimes k_\zeta = A_{k_\zeta + \overline{k_\zeta} - 1}$$

Thus, $\mathcal{T}_B$ also includes these projections $P_{\zeta_j}, P_{\eta_j}$. Also, for any pair of analytic polynomials $p$ and $q$, we have the following thanks to the spectral theorem for unitary operators:

$$p(U_{\alpha_1}) = \sum_{j=1}^{n} p(\zeta_j) v_{\zeta_j} \otimes v_{\zeta_j}, \quad q(U_{\alpha_2}) = \sum_{j=1}^{n} q(\eta_j) v_{\eta_j} \otimes v_{\eta_j}.$$

and so $p(U_{\alpha_1}), q(U_{\alpha_2}) \in \mathcal{T}_B$.

Then, to show that

$$\mathcal{T}_B = \bigvee \left\{ (U_{\alpha_1})^i, (U_{\alpha_2})^j, \quad 1 \leq i, j \leq n \right\},$$

it is sufficient to show that

$$\mathcal{T}_B = \bigvee \left\{ P_j, P_{\eta_j} \;\; j = 1, \dots, n \right\}.$$

This is inferred immediately from $\mathcal{T}_B$ is dimension of $2n - 1$and Lemma (1.10).

**Remark (1.11):**

(1) According to Theorem (1.7), for some polynomials $p$ and $q$, any $A_\varphi$ has the form $p(U_{\alpha_1}) + q(U_{\alpha_2})$. Here, we note that if we choose the symbol $\varphi$ carefully, we can infer p and q from it. To see how to accomplish this, take note of how we have demonstrated that in the theorem (1.6) proof.

$$\bigvee \left\{ k_{\zeta_j} \otimes k_{\zeta_j}, k_{\eta_j} \otimes k_{\eta_j} : j = 1, \dots, n \right\} = \mathcal{T}_B.$$

Actually, $\mathcal{T}_B$is basis will be any $2n - 1$ of them. However, given that

$$k_\zeta \otimes k_\zeta = A_{k_\zeta + \overline{k}_{\zeta - 1}},$$

It is possible to write each operator in $\mathcal{T}_B$ as $A_\varphi$ where

$$\varphi = \sum_{j=1}^{n} c_j \left(k_{\zeta_j} + \overline{k}_{\zeta_{j-1}}\right) + \sum_{j=1}^{n} d_j \left(k_{\eta_j} + \overline{k}_{\eta_{j-1}}\right).$$

Select polynomials $p$ and $q$ with a maximum degree of $n$.

$$p(\zeta_j) = \sqrt{|B'(\zeta_j)|}c_j, \;\; q(\eta_j) = \sqrt{|B'(\eta_j)|}d_j, \;\; j = 1, \dots, n,$$

Then we have

$$A_\varphi = p(U_{\alpha_1}) + q(U_{\alpha_2}).$$

As the spectral theorem indicates

$$p(U_{\alpha_1}) = \sum_{j=1}^{n} p(\zeta_j) v_{\zeta_j} \otimes v_{\zeta_j}, \;\; q(U_{\alpha_2}) = \sum_{j=1}^{n} q(\eta_j) v_{\eta_j} \otimes v_{\eta_j}.$$

Here is the outcome as of right now.

(3) Sarason (P. L. Duren 1970). began a discussion of how the Clark unitary operators provide $\mathcal{T}_\vartheta$ for a generic inner function $\vartheta$. Using the Clark theory and some recent results of Aleksandrov and Poltoratski, he obtained the following integral formula for a limited Borel function $\varphi$ and an inner function $\vartheta$:

$$A_\varphi = \int_{\mathbb{T}} \varphi(U_\alpha) \frac{|d\alpha|}{2\pi}, \tag{23}$$

If the weak meaning of the aforementioned integral is understood, that is,

$$\langle A_\varphi f, g \rangle = \int_{\mathbb{T}} \langle \varphi(U_\alpha) f, g \rangle \frac{|d\alpha|}{2\pi}, \;\; f, g \in K_\vartheta.$$

There is also a variant of this formula where $\varphi \in L^2$ (not necessarily bounded), although it requires highly specific interpretation. Additionally, Sarason establishes the closure of $\mathcal{T}_\vartheta$ within the topology of weak operators. Is that the case?

$$\mathcal{T}_\vartheta := \bigvee \{q(U_\alpha) : q \text{ is a trigonometric polynomial}, \alpha \in \mathbb{T}\}? \tag{24}$$

$\bigvee$ represents the closed linear span in the weak operator topology mentioned above. When the Blaschke product $\vartheta$ is finite, then this is unquestionably true (Theorem (1.6)). It is sufficient to demonstrate that $\{A_\varphi : \varphi \in L^\infty\}$ is thick in $\mathcal{T}_\vartheta$ in order to show (24) using (23). As previously stated, it is uncertain if the set above genuinely equals $\mathcal{T}_\vartheta$.

## Results:

1- The theorem for $n = 2$ shows that any complex symmetric 2×2 matrix represents a truncated Toeplitz operator with respect to the basis $\{e_{\zeta_1}, e_{\zeta_2}\}$.

2- Really, the proof presented in (P. L. Duren 1970). can be used to develop the spectral theorem for unitary operators and Theorem (1.6).

3- The method in which $\mathcal{T}_\vartheta$ is provided for a generic inner function $\vartheta$ by the Clark unitary operators was introduced by Sarason (P. L. Duren 1970). He obtained the following integral formula for a limited Borel function $\varphi$ and an inner function $\vartheta$ using the Clark theory and some new results of Aleksandrov and Poltoratski.

## Conclusion:

We study Toeplitz operator compressions to coinvariant subspaces of $H^2 \ominus BH^2$. Many characterizations of these operators are found; those of rank one is described in particular. A portion of the material is explanatory. A necessary and sufficient condition has defined to explain the closed and bounded of Blaschke product.

## References

1. D. Sarason (1994). Sub-Hardy Hilbert Spaces in the Unit Disk, MR1289670 (96k:46039). John Wiley & Sons, Inc, New York.
2. D. Sarason (2007). Algebraic properties of truncated Toeplitz operators, Operators and Matrices 1, no. 4, 491{526}.
3. P. L. Duren (1970). Theory of $H^p$spaces, Academic Press, New York.
4. N. A. Sedlock. (2011). Algebras of truncated Toeplitz operators. Oper. Matrices.
5. D. N. Clark, (1972). One dimensional perturbation of restricted shifts, J. Analyse Math.
6. D. Sarason, 10, John (1994). Sub-Hardy Hilbert spaces in the unit disk, University of Arkansas Lecture Notes in the Mathematical Sciences, Wiley & Sons Inc., New York.
7. Bu, Q., Chen, Y. & Zhu, S. (2021) Complex Symmetric Toeplitz Operators. Integral Equations and Operator Theory. Springer, Google scholar DOI:10.48550/arXiv.2107.06669
8. S. R.Garcia and M.Putinar, (August 2007) P3913–3931. Complex symmetric operators and applications, transactions of the American Mathematical Society, Volume 359.
9. Balayan, L., Garcia, S.R.,(2010). Unitary equivalence to a complex symmetric matrix: geometric criteria, Operators and Matrices , No. 1, 53–76, Pomna.

ISSN (Print) 2794-7629 Received 11/09/2024
ISSN (Online) 2794- 4549 Accepted 23/09/2024

**FULL PAPER**

# Composition of Steenrod Square Operations on Symmetry Cohomomology of Topological Spaces with Applications.

***Prepared by***

***Dr. Yousif Altayeb***
***Department of Management Information Systems***
***College of Business and Economics***
***Qassim University***
***Buraydah 51452, Saudi Arabia***
***y.hassan@qu.edu.sa***

**Abstract**:

This paper aims to combine the constructions of classical Steenrod operations, such as homogeneity operations on polynomials on ZP and cohomology of topological spaces, where p is a prime integer. Cohomological processes are natural-to-natural transformations, and then we define the characteristics of Steenrod processes and we define what we are aiming for, so we will proceed with the construction. This will be used space-wise, and then make sure that the build we're doing implements Steenrod operations; in the odd case, there won't be sufficient space in the project for this. We have included several immediate applications, and then we will briefly discuss the build we have completed and propose that further development should continue from this point. Lastly, we have some necessary details and calculations to ensure the smooth functioning of the build in the field.

**KEYWORDS**: Steen rod square, power operation, vector bundles, characteristic classes, cohomology theory, homology theory, convex function.

**Introduction:**

In algebraic topology, so-called Steenrod squares are the arrangement of homogeneities on regular cohomology with coefficients in $Z_2$ that are homogeneous to the suspension ("stable homogeneities"). They are special examples of energy processes. Steenrod processes are power-and-energy processes arising from the cup product's commutative but modest version of commutativity, involving operations that take powers of *pth*.

In 1958, Adams used it to compute sets of stable homogeneous spheres, and in the same year, Milnor proved that Steenerod algebras and dual algebras have structures of Hopf algebras. (Elhamdadi, M. 2003). The Steenrod squares play a crucial role in algebraic topology, particularly in the study of cohomology operations. By understanding their properties and constructions, we can gain deeper insights into the structure of various algebraic objects and their applications in geometric contexts.

**Definition 1:**

In terms of Steenrod operations we define Stiefel–Whitney characteristic $sw(\xi)$ as factors of cohomology in a group $G$, (hom) of degree $i$ is a morphism

$\theta$: $Hom^{*}(\ ,G) \rightarrow Hom^{*+i}(\ ,G)$ an operation from the topological space class to the set class. (Husemoller, D. *et al.*, 2008) (122-125). To introduce the Steenrod process we must know Bockstein symmetries as examples of cohomology symmetry operations.

**Steenrod square:**

For cohomology homogeneous over $\mathbf{Z}_2$ from two components, there is a unique process $Stq^i$: $Hom^{*}(, F_2) \rightarrow Hom^{*+i}(, Z_2)$ of i degree then $Stq^i$ navigates with commentary and, for x ∈ Hom $^i$(X, $Z_2$), Stq$^i$(x) = $x^2$, the cup square. (Husemoller, D. *et al.*, 2008) (123-124). Then operation $Stq^i$ is called the Steenrod square

**Definition 2:**

For $X$ fixed topological space, from sequence

$$0 \rightarrow Z_2 \rightarrow Z_4 \rightarrow Z_2 \rightarrow 0$$

The operation $Stq^n$ are cohomology operations

$$Stq^n : Hom^k(X, Z_2) \longrightarrow Hom^{k+n}(X, Z_2)$$

This is also known as the Steenrod square $Stq^1$, hence of morphisms in the homotopy category. ($Stq^1$) called the Bockstein homomorphism.

The $Stq^n$ fulfill the following requirements. (Husemoller, D. *et al.*, 2008) (123-124).

(1) In degree 0, $Stq^0$ is the identity, and $Stq^i | Hom^n(\ , \mathbf{Z}_2) = 0$ for $i>n$.

(2) (Cartan's formula), for $x, y \in Hom^{*}(X, \mathbf{Z}_2)$, then

$$Stq^k(xy) = \sum_{k=i+j} Stq^i(x)Stq^j(y).$$

Multiproduct version is

$$Stq^q(x_1 \dots x_r) = \sum_{i(1)+\dots+i(r)=q} Stq^{i(1)}(x_1)\dots Stq^{i(r)}(x_r).$$

(3) $Stq^i(x+y) = Stq^i(x) + Stq^i(y)$

*(4)* (Adem's relations), for $0 < m < 2n$, the iterate of $Stq^n$ satisfies

$$Stq^m Stq^n = \sum_{j=0}^{\left[\frac{m}{2}\right]} \binom{n-1-j}{m-2j} Stq^{m+n-j} Stq^{j}.$$

(5) $Stq^i(\sigma(x)) = \sigma\left(Stq^i(x)\right)$, where $\sigma$ is the suspension map.

When $p = 2$ then $\theta^i = Stq^i$, that gives Steenrod squares $Stq^n$ .

For *p is* odd, then we have $c \cdot \theta_{2i(p-1)} = P^i$ and $c \cdot \theta_{2i(p-1)+1} = \beta P^i$, that gives Steenrod powers, where *c* is a constant.

For $Stq^n$ on low-dimensional characteristic we have the following theorem.

**Theorem 1:**

On low-dimensional categories, we have the following Steenrod operations $Stq^n$:

Consider to one and two dimensions we have.

(1) If $x \in Hom^1(X, \mathbf{Z}_2)$, that we have $Stq^i(x^m) = \binom{m}{1} x^{m+i}$

(2) If $y \in Hom^2(X, \mathbf{Z}_2)$ and if $Stq^1(y) = 0$, then $Stq^{2i}(y^m) = \binom{m}{1} y^{m+i}$

and

$$Stq^{2i+1}(y^m) = 0.$$

***Proof:*** By induction on *m*, when $m = 0$ is clear.

Case (1) is illustrated as following formula.

$$Stq^i(x^m) = Stq^i(x.x^{m-1}) = Stq^0(x).Stq^i(x^{m-1}) + Stq^1(x).Stq^{i-1}(x^{m-1})$$

$$= \binom{m-1}{i} + \binom{m-1}{i-1} x^{m+i} = \binom{m}{i} x^{m+i}.$$

For cases of Adem's relations we have followed concept:

(1) When $n = 1$, we have $1 \leq n$, one terms for j = 0, thus, we have sum corresponding,

$$Stq^2 Stq^n = \binom{n-1}{1} Stq^{n+1} = \begin{cases} Stq^{n+1} & \text{if } n \text{ is even} \\ 0 & \text{if } n \text{ is odd} \end{cases}$$

with simple formula $Stq^1 Stq^1 = 0$, $Stq^1 Stq^2 = Stq^3$,

$Stq^1 Stq^3 = 0$, and $Stq^1 Stq^4 = Stq^5$. (Husemoller, D. *et al.*, 2008) (125-126).

(2) There are only two terms within the sum of the two, according to

$i = 0$ and $i = 1$, for n = 2. This is the case that 2 ≤ n. So, in this instance, we have

$$Stq^2 Stq^n = \binom{n-1}{2} Stq^{n+2} + \binom{n-2}{0} Stq^{n+1} Stq^1.$$

This splits into two cases focusing on *n* mod 4.

$$Stq^2 Stq^n = Stq^{n+1} Stq^1 + \begin{cases} Stq^{n+2} \text{ for } n \equiv 0,\ 3(\text{mod}4) \\ 0 \quad \text{for } n \equiv 1,2(\text{mod}4) \end{cases}$$

with simple cases $Stq^2 Stq^2 = Stq^3 Stq^1$, $Stq^2 Stq^3 = Stq^4 Stq^1 + Stq^5$,

$Stq^2 Stq^4 = Stq^5 Stq^1 + Stq^6$, $Stq^2 Stq^5 = Stq^6 Stq^1$, and $Stq^2 Stq^7 = Stq^8 Stq^1 + Stq^9$.

On integer **Z**, the induce effect of binomial $\binom{n}{i}$ is the efect of $x^i$ in the polynomial

$(1 + x)^n \in Z[x]$. Here, integers defined within the modulos of 2

**Example (Equivalencies of Two Mod 2):**

For field $\mathbf{Z}_2 = \{0, 1\}$ of two elements for $n \in \mathbf{Z}$. (Husemoller, D. *et al.*, 2008).

$$\binom{n}{1} = \begin{cases} 0 & if\ n\ is\ even \\ 1 & if\ n\ is\ odd \end{cases}$$

and

$$\binom{n}{2} = \begin{cases} 0 & if\ n = 0,1(mod\ 4) \\ 1 & if\ n = 2,3(mod\ 4) \end{cases}$$

**Definition 3:**

A bundle ξ, represented by $\xi_B$, comprises a Thom space that corresponds to the divide bundle Dis(ξ)/Sp(ξ).

Then the map σ: $Hom^{i+n}(Dis(\xi)/Sp(\xi)) \rightarrow Hom^{i+n}(\xi_B)$ is symmetric, and then the Thom map is defined as ψ: $Hom^i(B) \rightarrow \overline{Hom}^{i+n}(\xi_B)$ to be $\psi = \sigma\phi'$. (Husemoller, D. 1994)

**Theorem 2:**

By cohomology characteristic $U_\xi \in Hom^n(Dis(\xi)/Sp(\xi))$ and the complete Steenrod process $Stq = \sum_{0 \le i} Stq^i$. (Husemoller, D. *et al.*, 2008) (132-133), we generate a complete Stiefel-Whitney characteristic $Stq(U_\xi) = sw(\xi)U_\xi$ or $sw(\xi) = \varphi^{-1}(Stq(U_\xi))$.

Dis(ξ) is a bundle of disks, and Sp(ξ) is a bundle of spheres.

***Proof:*** By the splitting principal bundle, we can check a formula by doing it only for

$\xi = L_1 \oplus \ldots \oplus L_n$, a sum of line bundles, we have a cup product

decomposition of $U_\xi = U_1 \ldots U_n$ of 1-dimensional character $U_i$ related to $L_i$. Only $Stq^1$ is nonnull

on Ui, and it is $Stq^1(U_i) = U_i^2$. Hence, through Cartan's formula of multiproduct, we have the computation bellow

$$Stq^r(U_\xi) = Stq^r(U_1 \dots U_n) = \sum_{i(1)<\dots<i(r)}^{\cdot} U_1 \dots U_{i(1)}^2 \dots U_{i(r)}^2 \dots U_n$$

$$= \sum_{i(1)<\cdots<i(r)}^{\cdot} U_{i(1)}^2 \dots U_{i(r)}^2 (U_1 \dots U_n) = sw_r(L_1 \oplus \dots \oplus L_n)(U_1 \dots U_n)$$

via the splitting linking to cohomology, we see

$Stq^r(U_\xi) = sw_r(\xi)U_\xi$. This completes the theorem. (Husemoller, D. *et al.*, 2008) (132-133).

**Definition 4** ***(Thom):***

The Stiefel- Whitney characteristic $sw_i(\xi)$ is denoted by $\phi^{-1}(Stq^i U_\xi)$.

$$sw_i(\xi) = \phi^{-1}(Stq^i U_\xi).$$ (Marathe, K. 2010).

Where ϕ called Thom isomorphism

Equivalently, $sw_i(\xi)$ is the characteristic that $\phi(sw_i(\xi)) = Stq^i \phi$ (1), In terms of the complete square *Stq*, the complete Stiefel-Whitney characteristic

$sw(\xi) = sw_0(\xi) + sw_I(\xi) + \dots$ is given by $\phi^{-1}(Stq^i)\,\phi$ (1).

**Theorem 3:**

The Euler characteristic, denoted by eu(ξ), is held by the natural symmetric $Hom^n(B; Z) \to Hom^n(B; Z_2)$ to the upper Stiefel-Whitney characteristic, $sw_n(\xi)$. (Giansiracusa, J. *et al.*, 2003).

***Proof***. It is obvious that the cohomology characteristic $\mu$ element corresponds to the mod2 cohomology characteristic $\mu$ and $\mu \sqcup \mu$ connected to $Stq^n(\mu)$ if we apply surjection factor $Z \to Z_2$ to both sides of $eu(\xi) = \varphi^{-1}(\mu \sqcup \mu)$. Thus, $\varphi^{-1}(\mu \sqcup \mu)$ is associated with $\varphi^{-1}Stq^n(\mu) = sw_n(\mu)$.

The natural symmetric $Hom^n(B; \mathbf{Z}) \to Hom^n(B; \mathbf{Z}_2)$ holds the Euler characteristic denotes by $eu(\xi)$ to upper Stiefel-Whitney characteristic $sw_n(\xi)$. (Giansiracusa, J. *et al.*, 2003).

If we apply surjection factor $\mathbf{Z} \to \mathbf{Z}_2$ to two sides of $eu(\xi) = \varphi^{-1}(\mu \sqcup \mu)$ then with clear proof the element of cohomology characteristic $\mu$ correspond to the mod2 cohomology characteristic $\mu$ and $\mu \sqcup \mu$ related to $Stq^n(\mu)$. Hence $\varphi^{-1}(\mu \sqcup \mu)$ related to $\varphi^{-1}Stq^n(\mu) = sw_n(\mu)$.

**Definition 5(Poincaré duality):**

For a compact *m*-dimensional manifold *M*, for $\delta \in Hom^r(M)$ and for $\gamma \in Hom^{m-r}(M)$. When $\delta \times \gamma$ is an element, we can define a direct product $\langle , \rangle : Hom^r(M) \times Hom^{m-r}(M) \to \mathbf{R}$ by

$$\langle \delta, \gamma \rangle = \int_M \delta \times \gamma \qquad (1)$$

The direct product is a bilinear operation. Additionally, it is non-monogamous, meaning that if $\delta = 0$ or $\gamma \neq 0$, the pairing $\langle \delta, \gamma \rangle$ cannot vanish in a similar manner. Thus, equation (1) define as a dual of $Hom^r(M)$ and

$Hom^{m-r}(M)$, $Hom^r(M) \cong Hom^{m-r}(M)$called the Poincaré duality. (Nakahara, M.2002).

**Manifold for the Stiefel-Whitney characteristic in terms of Wu's Formula:**

The Steenrod squares $Stq = \sum_i Stq^i$ and the Stiefel–Whitney characteristic $sw(\xi)$ of a bundles are connected by their form $sw(\xi) = \varphi^{-1}(Stq(U_\xi))$. Using Poincare's dualism and its relation to $U_M$, we derive the Wu characteristic and its relation to the Stiefel-Whitney characteristic of the bundle of tangents. (Giansiracusa, J. 2003; Milnor, J.W. 1981).

***Corollary* 1:**

Let $Stq^{tr}: Hom(X) \rightarrow Hom(X)$ the complete Steenrod square is the transpose of $Stq: Hom^*(X) \rightarrow Hom^*(X)$. In specially case, we take $Stq(n), m = n, Stq^{tr}(m)$ $for$ $n \in Hom^*(X)$, $m \in Hom^*(X)$. (Husemoller, D. *et al.*, 2008).

**Definition 6:**

Let $\bar{M}$ be a closed manifold with a Poincare´ duality isomorphism.

$D: Hom^i(\bar{M}) \rightarrow Hom^{n-i}(\bar{M})$, and let $[M]$ be fundamental characteristic. The Wu characteristic of $\bar{M}$ $is$

$V = D^{-1}(Stq^{tr}([M]))$. (Husemoller, D. *et al*, 2008; Husemoller, D. 1994).

The characteristic of the Wu characteristics is that

$\langle n, D(v) \rangle = \langle n, Stq^{tr}([M]) \rangle = \langle Stq(n), [M] \rangle = \langle n, v \frown [M] \rangle = \langle nv, [M] \rangle$ . ($\frown$) means cap product.

**Theorem 4:**

Let $\bar{M}$ be a closed differentiable manifold. Then, the Stiefel-Whitney characteristic $sw(\bar{M}) = sw(T(\bar{M}))$ the bundle of tangents is provided by the Wu characteristic's Steenrod square:$sw(\bar{M}) = Stq(v)$. (Husemoller, D. *et al.*, 2008) (132-133).

***Proof:*** *see* (Husemoller, D. 1994) (275-276)**.**

**Association to Bockstein homomorphism**

If $Stq^1$ is the Bockstein homomorphism of the short exact sequence $Z_2 \rightarrow Z_4 \rightarrow Z_2$.

The Steenrod squares are harmonic with comment symmetry. Therefore, Steenrod squares are also known as stable cohomology operations.

**Association to Massey products**

We see that Massey product relation to Steenrod squares *stq*.

Let $\omega, \omega_1, \omega_2 \in Hom^*(X, Z_2)$ such that their triple Massey product exists. Then the cup product of $\omega$ with the triple Massey product is independent of the ambiguity in the Massey products and equals the cup product of $\omega_1$ with $\omega_2$ and with the Steenrod square of $\omega$ of degree $deg(\omega) - 1$

$$\omega \smile \langle \omega_1, \omega, \omega_2 \rangle = \omega_1 \smile \omega_2 \smile Stq^{deg(\omega)-1}(\omega).$$

**Pontrjagin characteristic**

**Definition 7:**

The *nth* Pontrjagin characteristic of bundle ξ, the real vector bundle, is represented by $P_n(\xi)$, is $(-1)^{nc}{}_{2n}$ $(\xi \oplus \mathbf{C})$. Where *P(ξ)* is a member of $Hom^{4n}(B, \mathbf{Z})$. (Husemoller, D. 1994)*;* Giansiracusa, J. *et al*., 2003). We explain $P(\xi) = 1 + P_1(\xi) + \ldots \in Hom^*(B, \mathbf{Z})$ to be the complete Pontrjagin characteristic of real vector bundle ξ are generated, over the algebra of Steenrod powers, by those of the form $P_{q^n}$.

The Whitney sum proposition can only be satisfied as shown below:

$$2(p(\xi \oplus \eta) - p(\xi)p(\eta)) = 0$$

Let *q:* $\mathbf{R}P^{2n-1} \rightarrow \mathbf{C}P^{n-1}$. Each real line specified by $z \in Sp^{2n-1}$ can be assigned an isomorphism where {x, -x} determines the complex vector bundle.

By definition, we have $P_n(\xi_{\mathbf{R}}) = (-1)^{nc}{}_{2n}(\xi \oplus \mathbf{C})$ where$(\xi \oplus \mathbf{C})$ is complex be converted to a real by an equation $P_1(\xi)=ch_1(\xi)^2 - 2ch_2(\xi)$, where *ch* means chern characteristic. (Husemoller, D. *et al*, 2008); Milnor, J.W. 1981).

**Theorem 5:**

For any smooth even-vector bundle ξ, $p_n(\xi) = eu(\xi)^2$ . (Milnor, J.W. 1981).

***Proof*:** $P_n(\xi) = (-1)^{nc}{}_{2n}(\xi_{\mathbf{C}}) = (-1)^n eu\ (\xi_{CR}) = \pm eu(\xi^n \oplus \xi^n) = (-1)^n eu\ (\xi)^2$**.**

Instead of using the curvature two-form, it is frequently represented as p(M) in relation to the tangent bundle. Since $p_0(M) = 1$ denotes each Pontrjagin characteristic, $p_2(M)$ disappears as a differential form. (Nakahara, M. 2002).

***Lemma* 2:**

The Pontrjagin characteristic of a complex vector bundle (ξ) with n dimensions is determined by the Chern characteristic (Ch) via an equation. (Cohen, R. L. 1998); Janis, L. 2014).

$$1 - P_1(\xi) + P_2(\xi) - \ldots = (1 - ch_1(\xi) + ch_2(\xi) - \ldots)\ (1 + ch_1(\xi) + ch_2(\xi) + \ldots).$$

***Proof***: ch($\xi \oplus_{\mathbf{R}} \mathbf{C}$) = ch($\xi$)ch($\xi^*$) =$\sum_{i=0}^{\infty} ch_i(\xi) \sum_{i=0}^{\infty} (-1)^i ch_i(\xi)$. Moreover, if k=1(mod2) then $ch_k(\xi \oplus \mathbf{C}) = \sum_{0 \le i \le k} (-1)^i ch_i(\xi)\, ch_{k-1}(\xi) = 0$. So, the sum of all even Chern characteristics is the total of every Chern characteristic. (Janis, L. 2014). Pontrjagin characteristic and Squares of odd-dimensional Steifel-Whitney characteristic we have the Wu characteristic in degrees $2i$ and $(sw_i)^2$ not an analysis Stiefel-Whitney characteristic homogeneous to Wu characteristic, in lower degrees. The most notable works in an analysis term not involving $sw_1$ but they are relating with squares mentioned above.

For odd values of $i$, we utilize the torsion Pontrjagin characteristic. (Hisham, S. 2011) to achieve this. These characteristics are denoted as $P_{4k+2}$ with an index such that $P_{4i} = p_i$ , which aligns with the standard ith Pontrjagin characteristics. In cases where the degrees are $4k + 2$ and involve 2-torsion, we have $2P_{4k+2} = 0 \in Hom^{4k+2}\mathbf{Z}$. By utilizing the Bockstein and Steenrod squares on the Stiefel-Whitney characteristic at degree $2k + 1$, one can establish these properties for a vector bundle E.

Then $P_{4k+2}(E) = \beta Stq^{2k} sw_{2k+1}(E)$.

The mod2 reduction $\rho_2 : Hom^{4k+2}(X; \boldsymbol{Z}) \to Hom^{4k+2}(X; \boldsymbol{Z_2})$ of these characteristics give exactly the required squares of Stiefel-Whitney characteristic $\rho_2 : P_{4k+2}(E) = sw_{2k+1}(E)^2$. As a result, we can identify an integral lift in the place where the squares represent the Wu characteristic. In the context given above, the integral lifts of the Wu characteristic correspond to the torsion Pontrjagin characteristic.

Now we illustrate some examples and propositions in low degree.

1. Degree 2: for normal bundle : $v_2 = sw_2 + sw_1^2$. If $sw_2$ = 0, indicating a Pin+ structure, the torsion Pontrjagin characteristic $P_2$ provides a lift to the Wu (2) structure. We could also find $sw_2 = \rho_2(c_1)$, where $c_1$the first Chern characteristic.

2. Degree Six: $v_6 = sw_2 sw_4 + sw_3^2$ . If $sw_4$ = 0, indicating an orientable case (e.g. membrane structure), reduces to the square term $sw_3^2$ . The integral lift of the Wu characteristic in this situation is the torsion Pontrjagin characteristic $P_6$ . We cannot

$sw_2$ = 0 as then $sw_3$, it would also be zero.

3. Degree ten: Here $v_{10}$ will involve $v_2$. As a result, we are unable to isolate a square word. However, it will be provided by the torsion Pontrjagin characteristic $P_{10}$ .

For instance, higher-order Stiefel-Whitney characteristics can be observed in an oriented 11-dimensional manifold $Y^{11}$where $sw_{11}(Y^{11}) = sw_{10}(Y^{11}) = sw_9(Y^{11}) = 0$. (Hisham, S. 2011). This excludes all phrases involving $sw_{10}$ and $sw_9$ in $v_{10}$.

We can now describe Steenrod squares in the geometry domain.

First, if X is a manifold with dimension d, one may generate characteristics in

*Hom*$^n(X)$ by proper function $f: V \to X$ here *V* is a dimension d manifold, by intersection theory we can count n-cycle intersection points, as the pushforward $f^*(1)$ where 1 is the unit class in $Hom^0(V)$, as the Thom characteristic, or applying the basic characteristic in locally finite homology and duality. Using the last method, let's say that *f* has a normal bundle *v* since it is an immersion. Then $Stq^i(x)=f^*(sw^i(v))$ if $x = f^*(1) \in Hom^n(X)$. In essence, this is the Wu formula.

That is, if sub-manifolds contain cohomology properties, such as cup product approximating intersection data, Steenrod squares are normal bundle data.

The Steenrod squares $Stq^i: Hom^n(-; F_2) \to Hom^n + i(-; F_2)$ are basic cohomological functions. They indicate a map between the Eilenberg–MacLane spaces $K(F_2; n) \to K(F_2; n + i)$by the Yoneda lemma. By the Dold–Kan correspondence, this map should be expressible as a chain map

$$\widehat{Stq^i} : F_2[-n] \to F_2[-(n + i)].$$

We write sometimes $F_2 = Z_2Z$ for the field with two elemens.

Using operations and algebra of operations to explain some computations of the Steenrod operations on term of cohomology of a Hopf algebra over $Z_p$.

Let Hom* be the cohomology of the Hopf algebra A and investigate the Steenrod operations. Our goal is to apply these operations to $E_2$ (the bundle space) in a few fascinating particular circumstances. (William, M. 1973) (327-336).

We now discuss "Steenrod squares $Stq_V^i$, which are vertical, and compute Steenrod squares $Stq_D^i$, which are chain maps."

$$Stq_V^i : E_2^{p,q} \to E_2^{p,q+i}, \quad 0 \le i \le q$$
$$Stq_D^i : E_2^{p,q} \to E_2^{p+i,2q}, \quad 0 \le i \le p$$

Where $Stq_V^i = Stq^i$ , $Stq_D^i = Stq^{i+q}$

In our initial application, we consider an extension of cocommutative Hopf algebras:

A → C → S. Let M be a commutative left C-algebra and N be a commutative left

S-algebra. Drawing parallels with group theory, we show that the action of B on $Ext_A(M, N)$ can be expressed directly as B's action on A. This involves Steenrod operations on $E_2$.

Then $Stq_V^i : Ext_B^{p}\left(Z_2, Ext_A^{q}(M.N)\right) \to Ext_B^{p}\left(Z_2, Ext_A^{q+i}(M, N)\right)$,

$$Stq_D^i : Ext_B^{p}\left(Z_2, Ext_A^{q}(M.N)\right) \to Ext_B^{p+i}(Z_2, Ext_A^{2q}(M, N)),$$

Then $Stq_V^i$ acts on the cohomology of the Hopf algebra A, while $Stq_D^i$ acts on the cohomology of B. (William, M. 1973) (327-336).

In the second scenario, let us consider a topological group G and a fundamental G-bundle E. The spectral sequence converges to $Hom^*(E/G)$ (with coefficients in $Z_2$), and the Steenrod operations on E appear as:

$$Stq_V^i : Ext^{p,q}_{Hom^*(G)}(Hom^*(E), Z_2) \rightarrow Ext^{p,q+i}_{Hom^*(G)}(Hom^*(E), Z_2),$$

$$Stq_D^i : Ext^{p,q}_{Hom^*(G)}(Hom^*(E), Z_2) \rightarrow Ext^{p+i,2q}_{Hom^*(G)}(Hom^*(E), Z_2)$$

We demonstrate that $Stq_V^i$ determines the cohomology of the Hopf algebra on $Hom^*(G)\ and\ Hom^*(E)$. Additionally, $Stq_D^i$ defines operations on the cohomology of the Hopf algebra $Hom^*(G)$.

To satisfy the Cartan formula and Adem relations of vertical and diagonal squares, we use the Serre spectral sequence in our final application to ensure the Serre spectral sequence. To satisfy a fascinating commutation relation of vertical and diagonal squares, we find that vertical and diagonal squares satisfy: see sec6 (William,M. 1973) (327-336) .

$$. Stq_V^i\ Stq_D^j \rightarrow Stq_D^J\ Stq_V^{i/2}$$

Where $Stq_V^{i/2} = 0\ if\ i\ is\ odd$

**Conclusion:**

Our study shows a deep composition of Steenrod square operations satisfies the following relations and calculate that the Steenrod squares with some applications

$Stq^i: Hom^n(X; F_2) \rightarrow Hom^{n+i}(X; F_2)$ are characterized by the following 5 axioms:

Our study demonstrates a deep composition of Steenrod square operations that meets the following relations and calculates that the Steenrod squares $Stq^i: Hom^n(X; F_2) \rightarrow Hom^{n+i}(X; F_2)$ , with some applications are defined by the following 5 axioms:

1. Naturality: $Stq^i: Hom^n(X; F_2) \rightarrow Hom^{n+i}(X; F_2)$ is an additive homomorphism and is natural with respect to any $f: X \rightarrow Y$, so $f^*\left(Stq^i(x)\right) = Stq^i(f^*(x))$ .

2. $Stq^0$ is the identity homomorphism.

3. $Stq^i(x) = x \smile x$ for $x \epsilon Hom^i(X; F_2)$.

4. If $i > \deg(x)$ then $Stq^i(x) = 0$

5. Cartan Formula: $Stq^i(x \smile y) = \sum_{n+m=i} Stq^n(x) \smile Stq^m(y)$

6. Additionally, the Steenrod squares have the following characteristics:

• $Stq^1$ is the Bockstein homomorphism $\beta$ of the exact sequence $0 \rightarrow Z_2 \rightarrow Z_4 \rightarrow Z_2 \rightarrow 0$

• In cohomology, $Stq^i$ commutes with the relating morphism of the long exact sequence. Specifically, it commutes in terms of suspension $Hom^K(X;F_2) \to Hom^{K+1}(\sum X\,;F_2)$ .

• They satisfy the Adem relations, which are explained below. Similarly, the reduced $p-th$ powers are characterized by the following axioms for p > 2.

1. Naturality: $P^n$: $Hom^m(X;F_2) \to Hom^{2n(p+1)+m}(X;F_2)$ is an additive homomorphism and natural.
2. $P^0$ is the identity homomorphism.
3. $P^n$ is the cup $p-th$ power of degree $2n$.
4. If $2n > \deg(x)$ then $P^n(x) = 0$
5. Cartan's Formula: $P^n(x \smile y) = \sum_{i+j=n} P^i(x) \smile P^j\,(y)$

**REFERENCES:**

[1] - Cohen,R. L. (August, 1998). The Topology of Fiber Bundles Lecture Notes. Dept of Mathematics Stanford University.

[2]-Elhamdadi, M. [2003]. On the Steenrod operations in cyclic cohomology, University of South Florida,Tampa, FL 33620, USA , South Valley University, Aswan, Egypt.

[3]- Giansiracusa, J and Deviate. (June 9, 2003). Stiefel-Whitney Characteristic.

[4]- Hisham, S. (21sept2011). Twisted topological structures related to M-branes II:Twisted Wu and $Wu^c$ structures, University of Pittsburgh .Pittsburgh, PA 15260 Pennsylvania, USA.

[5] - Husemoller, D. (1994). Fibre Bundles. Third Edition. Editorial Board. (J.H. Ewing F.W. Gehring P.R. Halmos.), Berlin.

[6]- Husemoller, D. et al, (2008). Basic Bundle Theory and K-Cohomology Invariants, Lect.Notes Phys.726 (Springer, Berlin Heidelberg), DOI 10.1007/ 978-3-540-74956-1.

[7] – Janis, L. (2014). Characterizations of the Chern characteristic classes, Waterloo, Ontario, Canada.

[8] - Marathe, K. (2010). Topics in Physical Mathematics, DOI 10.1007/978-1-84882-939-8 1, Springer-Verlag London Limited.

[9]- Milnor, J.W. (1981); lectures on characteristic classes. University of Tokyo Press, Japan.

[10]- Nakahara, M. (2002). Geometry Topology and physics (second edition) Kinki University, Osaka, Japan.

[11]-William,M. singer, (janury1973). Steenrod squares in spectral sequences. II. Fordham university. New York, USA. (327-336).

**ISSN (Print)** **2794-7629** **Received** **11/12/2024**
**ISSN (Online)** **2794- 4549** **Accepted** **30/12/2024**

**FULL PAPER**

# Ion Acoustic Solitary Wave Solutions in the Context of the Nonlinear Fractional KdV Equation

***Prepared by***

***Mona Elmahi***
*Department of Mathematics*
*College of Science*
*Qassim University*
*Buraydah, 51452*
*Saudi Arabia.*
***Nidal.E.Taha***
*Department of Mathematics*
*College of Science*
*Qassim University*
*Buraydah, 51452*
*Saudi Arabia.*
***Agaeb Mahal Alanzi***
*Department of Mathematics*
*College of Science*
*Qassim University*
*Buraydah, 51452*
*Saudi Arabia.*
***Manahil Alamin M. Ashmaig***
*Department of Mathematics*
*College of Science*
*Qassim University*
*Buraydah, 51452*
*Saudi Arabia.*
***Dr. Manal Yagoub Ahmed Juma***
*Department of Mathematics*
*College of Science*
*Qassim University*
*Buraydah, 51452*
*Saudi Arabia.*
***M.juma@qu.edu.sa***

**Abstract**:

This manuscript provides a comprehensive investigation of the fractional (1+1)-dimensional nonlinear Korteweg-de Vries (KdV) model in the context of quantum plasma. The primary objective is to derive and mathematically explain the fractional (1+1)-dimensional nonlinear KdV model within quantum plasmas, focusing on ion acoustic solitary waves. Using the reductive perturbation technique, the fractional KdV equation is formulated and solved via the tanh hyperbolic function technique. The study examines the effects of ion pressure and an external electric field on ion acoustic waves, considering plasma characteristics such as ion-electron temperature ratios, nonextensive electron and positron effects. The manuscript investigates the influence of the fractional order and plasma parameters on the phase velocity of ion acoustic waves. Notably, the results reduce to known outcomes when the fractional order equals one. This work contributes significantly to the understanding of nonlinear phenomena in quantum plasmas, particularly ion acoustic waves, with potential applications in astrophysical and cosmological contexts.

**Keywords:** KdV model, fractional calculus, quantum plasma, solitary waves, ion acoustic

## 1. Introduction

Quantum plasmas, which involve the collective behavior of charged particles under the influence of quantum mechanical effects, have become an important subject of study in various fields, including astrophysics, space physics, and fusion research. To describe the behavior of quantum plasmas, three well-established models are commonly used, each incorporating different physical effects and mathematical frameworks [G. C. Das and S. N. Paul, 1985], [W. Masood, N. Jehan, A. M. Mirza, and P. H. Sakanaka, 2008]. The quantum hydrodynamics (QHD) model is one of the most widely used and fundamental frameworks in the study of quantum plasmas. It provides a macroscopic description by combining the classical fluid equations with quantum mechanical principles such as quantum pressure, quantum potential, and quantum statistics. The QHD model serves as a basis for understanding the collective behavior of quantum plasma systems, including phenomena such as wave propagation, particle dynamics, and plasma instabilities. In this model, the plasma's collective behavior is described by a set of fluid-like equations, including the continuity equation, Euler equation, and Poisson equation, with quantum corrections that account for the wave nature of particles and the effects of quantum statistics [T. S. Gill, A. Singh, H. Kaur, N. S. Saini, and P. Bala, 2007 ], [ M. G. Hafez and M. R. Talukder, 2015]. In contrast, the classical plasma fluid model extends the principles of classical fluid dynamics to describe plasma systems. While it does not incorporate quantum effects, it remains essential for understanding the macroscopic behavior of classical plasmas. The classical equations of motion, such as the continuity equation and the Navier-Stokes equation govern the plasma's evolution in the absence of quantum effects and can be viewed as a limiting case of the QHD model when quantum effects are negligible. The classical model forms the foundation for many plasma theories and is still widely applied to describe low-temperature plasmas where quantum effects are not dominant [M. G. Hafez, M. R. Talukder, and R. Sakthivel, 2016] ,[H. K. Malik, 1996.].

An important area of research in quantum plasmas involves the formulation and analysis of nonlinear fractional differential equations (FDEs) or partial differential equations (PDEs), which are used to model the wave propagation and structural dynamics within quantum plasma systems. Nonlinearities and fractional calculus provide an effective framework for describing complex phenomena, such as solitons, shock waves, and wave-particle interactions. By combining the QHD model with these mathematical techniques, researchers can develop more accurate models that account for the nonlinear and fractional effects observed in quantum plasma behavior [H. K. Malik, 1995], [K. Singh, V. Kumar, and H. K. Malik, 2005.]. These models provide a comprehensive approach for

understanding the behavior of quantum plasmas, ranging from microscopic quantum effects to macroscopic plasma dynamics. This integrated framework allows researchers to investigate the rich variety of phenomena in quantum plasmas, such as quantum shock waves, solitary waves, and other nonlinear plasma behaviors, with applications in fields such as space physics, fusion energy, and astrophysical systems [H. K. Malik, 1996] , [D. K. Singh and H. K.Malik,2005].

The study of magnetized ion-electron-positron quantum plasmas has become a focal point in understanding the behavior of ion-acoustic (IA) waves, both in linear and nonlinear regimes. These plasmas composed of electrons, positrons, and ions, exhibit complex wave dynamics that are influenced by quantum mechanical effects. A key area of investigation involves the analysis of ion-acoustic waves (IAWs), which are a type of sound wave propagating through the plasma, and their response to both classical and quantum effects.

Recent studies have expanded our understanding of IAWs by utilizing the QHD model, which incorporates quantum mechanical corrections into the classical fluid equations. Khan and Mushtaq explored the properties and stability of IAWs in ultracold quantum plasmas, including the effects of transverse perturbations on wave propagation. By deriving the KP equation, they were able to study the dynamics of IAWs under these conditions, providing insights into their stability and nonlinear evolution. Khan and Haque employed the QHD model to derive the nonlinear weakly limit of the deformed KdV Burgers equation, which is crucial for understanding the nonlinear dynamics of IAWs in quantum plasmas. This work highlights the importance of nonlinear modeling in describing the complex behavior of ion-acoustic waves, particularly in quantum environments [R. Malik, H. K. Malik, and S. C. Kaushik, 2012 ] , [F. C. Michel, 1982]. These investigations demonstrate the ongoing efforts to develop and refine mathematical models, such as the QHD model and its extensions, to better understand the behavior of ion-acoustic waves and related phenomena in quantum plasmas. The exploration of nonlinear equations and the study of wave dynamics continue to be pivotal in advancing our understanding of quantum plasmas and their applications in various fields, from fusion energy to astrophysical environments [ G. C. Das and S. N. Paul, 1985] , [H. R. Pakzad and M. Tribeche, 2013].

The study of nonlinear waves**,** particularly solitons and solitary waves, is of paramount importance across various scientific disciplines, from laboratory research to astrophysical and space physics. These waves, which maintain their shape while propagating over time, are integral to understanding the dynamics of complex plasma systems. Nonlinear waves have been observed in a wide range of phenomena, including polar magnetospheres**,** solar wind**,** and the Earth's magnetotail, underscoring their relevance in both natural and experimental plasma environments. In these contexts, solitons and solitary waves provide valuable insights into the nonlinear and dynamic behavior of plasmas, which can exhibit both positive and negative wave amplitudes depending on the system parameters. Solitons and solitary waves are key solutions to nonlinear PDEs and are

characterized by their stability and ability to maintain their shape while propagating over long distances. These waves often arise in spatially extended systems where nonlinearity dominates the wave propagation. Their significance lies not only in their theoretical properties but also in their potential practical applications, which span laboratory experiments and astrophysical observations. Understanding the formation, propagation, and interaction of these waves is critical for a wide range of applications, from controlling plasma in fusion reactors to understanding cosmic plasma phenomena.

Fractional calculus has emerged as a powerful and transformative tool in mathematics, offering more accurate and flexible models for real-world phenomena compared to traditional integer-order calculus. Its primary strength lies in its ability to effectively describe systems with non-local or long-range memory effects, which are often inadequately represented by classical models. The field has rapidly expanded, with multiple definitions of fractional derivatives developed to suit different applications, including the Riemann–Liouville, Caputo, and conformable fractional derivatives. Each of these definitions provides unique advantages in various domains such as physics, engineering, biology, and finance [A.A. Kilbas, H.M. Srivastava, J.J. Trujillo,2006] , [M G Hafez, M R Talukder, and M H Ali, 2016]. One significant advancement in the field is the introduction of the conformable fractional derivative (CFD) by Khalil et al. [E. A-B. Abdel-Salam, M.F. Mourad, Math.2018], which extends the idea of fractional differentiation by incorporating simpler computational techniques while preserving the key properties of fractional derivatives. As research in fractional calculus continues to evolve, it holds great promise for advancing mathematical modeling in the natural and applied sciences, making it a cornerstone of modern scientific analysis

Khalil et al. [E. A-B. Abdel-Salam, M.F. Mourad, Math.2018] introduced the CFD by establishing its definition through a limit process, offering a simpler and more computationally efficient approach compared to traditional fractional derivatives,

$$D^{\beta}\psi(x)=\lim_{\varepsilon\to 0}\frac{\psi(x+\varepsilon x^{1-\beta})-\psi(x)}{\varepsilon},\quad \forall x>0,\quad \beta\in(0,1].$$

Substituting $\alpha=1$ into the final equations, the noninteger differentials transition into the well-established integer differentials. Unlike classical definitions, which often involve integrals or complex limiting processes, the conformable fractional derivative is defined in such a way that it can be applied directly to functions in a more straightforward manner, while still capturing the key properties of fractional differentiation. This makes the CFD particularly useful for solving fractional differential equations in various fields, as it preserves the non-local memory effects characteristic of fractional models but with less computational complexity. The introduction of the CFD has opened up new possibilities for both theoretical research and practical applications, particularly in systems where classical fractional calculus may be challenging to apply.

This paper is organized as follows: Section 2 presents the derivation of the basic fractional KdV model. In Section 3, we outline the procedure for obtaining and constructing explicit solitary

wave solutions for the model. Section 4 is dedicated to a discussion of the results. Finally, in the concluding section, we summarize the key findings and offer some prospects for future research.

**2. The formulation of the derivation for the KdV model**

We investigate the propagation of fractional nonlinear shocks and IASWs in a fully ionized, unmagnetized, three-component plasma system composed of relativistic hot ions, positrons, and nonextensive electrons. It is expected that the spatial fractional speed of quantum ions in acoustics will be significantly higher than any spatial fractional speed associated with the plasma flow. The charge neutrality equilibrium condition is assumed to be $n_{e0} = n_{i0} + n_{p0}$, where the concentrations of ions, positrons, and unperturbed electrons are denoted by $n_{p0}$, $n_{i0}$ and $n_{e0}$, respectively. Additionally, it is assumed that the electron and positron concentrations follow an equilibrium q-distribution function. It is possible to acquire the normalized non extensive concentrations of positron and electron [Wang M. L. and Li X. Z., 2005] as

$$n_e = \frac{1}{1-a}\left[1+(q-1)\varphi\right]^{\frac{q+1}{2(q-1)}}$$
$$= \frac{1}{1-a}\left(1+\frac{1}{2}(q+1)\varphi - \frac{1}{8}(q+1)(q-3)\varphi^2 + \frac{1}{48}(q+1)(q-3)(3q-5)\varphi^3 + \ldots\right),$$

$$n_p = \frac{a}{1-a}\left[1-\sigma(q-1)\varphi\right]^{\frac{q+1}{2(q-1)}}$$
$$= \frac{a}{1-a}\left(1-\frac{\sigma}{2}(q+1)\varphi - \frac{\sigma^2}{8}(q+1)(q-3)\varphi^2 - \frac{\sigma^3}{48}(q+1)(q-3)(3q-5)\varphi^3 + \ldots\right),$$

Where $a = n_{p0}/n_{e0}$ and $\sigma = T_e/T_p$. In $n_e$ and $n_p$, we use $q$ tends to 1 for isothermal electrons and positrons, $q > 1$ for sub-thermal electrons and $-1 < q < 1$ for super-thermal electrons. In weakly relativistic plasma, the dynamics of one-dimensional IASWs are described by the fractional continuity and motion equations for a normalized fluid. Additionally, closure for the system is provided by the fractional Poisson equation formulated in a one-dimensional fractional representation

$$D_t^{\alpha} n_i + D_x^{\alpha}(n_i u) = 0, \tag{1}$$

$$D_t^{\alpha}(\gamma u) + u D_x^{\alpha}(\gamma u) + D_x^{\alpha}\varphi + \delta n_i^{-1} D_x^{\alpha} p_i = 0, \tag{2}$$

$$D_t^{\alpha} p_i + u\, D_x^{\alpha} p_i + 3 p_i D_x^{\alpha}(\gamma u) = 0, \tag{3}$$

$$D_x^{\alpha\alpha}\varphi = \Omega n_e - (\Omega - 1) n_p - n_i. \tag{4}$$

Note that equations (1) to (4) reduced to the well-known equations as obtained in [44]. In this case, $n_i$ represents the concentration of ions normalized by the unperturbed electron concentration $n_{e0}$, the electrostatic potential is $\varphi$, the ions flow velocities along the $x$ direction is represented by $u$ normalized by $c_s = \sqrt{T_e / m_i}$, $T_i, T_p$ and $T_e$ are the temperature ion, positron and electron plasma, the particles' masses are $m_e$ for electrons and $m_i$ for ions, $P_i$ is pressure and $D_x^{\alpha}$ describes the conformable fractional differential in relation to $x$, $D_x^{\alpha\alpha} = D_x^{\alpha} D_x^{\alpha}$ the twice conformable fractional differential in relation to $x$. Ions are thought to have a relatively small relativistic influence, which can be expanded to $\gamma = 1/\sqrt{1-u^2/c^2} \approx 1+u^2/2c^2$.

Through the application of reductive perturbation techniques, the scale's new stretching coordinates (time and space) are provided as

$$\xi = \frac{\sqrt{\varepsilon}}{\alpha}\left(x^{\alpha} - \alpha V\, t^{\alpha}\right), \qquad \tau = \frac{\sqrt{\varepsilon^3}}{\alpha} t^{\alpha}, \tag{5}$$

where $\varepsilon$, is the small expansion parameter, which is proportional to the perturbation's amplitude, serves as an indicator of the system's nonlinearity strength. Here, $V$ denotes the fractional spatial phase velocity of the wave propagating along the x-direction. The fractional operator can be represented in the following form

$$D_x^{\alpha} = \sqrt{\varepsilon}\, D_{\xi}^{\alpha}, \quad D_x^{\alpha\alpha} = \varepsilon D_{\xi}^{\alpha\alpha}, \quad D_t^{\alpha} = -V\sqrt{\varepsilon}\, D_{\xi}^{\alpha} + \sqrt{\varepsilon^3}\, D_{\tau}^{\alpha}. \tag{6}$$

Substituting the operators in equation (6) into equations (1), (2) and (4) we have

$$-\alpha V\sqrt{\varepsilon}\, D_{\xi}^{\alpha} n_i + \sqrt{\varepsilon^3}\, D_{\tau}^{\alpha} n_i + \sqrt{\varepsilon}\, D_{\xi}^{\alpha}(n_i u) = 0, \tag{7}$$

$$-\alpha V\sqrt{\varepsilon}\, D_{\xi}^{\alpha}(\gamma u) + \sqrt{\varepsilon^3}\, D_{\tau}^{\alpha}(\gamma u) + u\sqrt{\varepsilon}\, D_{\xi}^{\alpha}(\gamma u) + \sqrt{\varepsilon}\, D_{\xi}^{\alpha}\varphi + \delta n_i^{-1}\sqrt{\varepsilon}\, D_{\xi}^{\alpha} p_i = 0, \tag{8}$$

$$-\alpha V\sqrt{\varepsilon}\, D_{\xi}^{\alpha} p_i + \sqrt{\varepsilon^3}\, D_{\tau}^{\alpha} p_i + u\sqrt{\varepsilon}\, D_{\xi}^{\alpha} p_i + 3p_i\sqrt{\varepsilon}\, D_{\xi}^{\alpha}(\gamma u) = 0, \tag{9}$$

$$\varepsilon D_{\xi}^{\alpha\alpha}\varphi = \Omega\left[1+(q-1)\varphi\right]^{\frac{q+1}{2(q-1)}} - (\Omega-1)\left[1-\sigma(q-1)\varphi\right]^{\frac{q+1}{2(q-1)}} - n_i. \tag{10}$$

The dependent variables $n_i$, $p_i$ $u$ and $\varphi$ can be expanded in the following manner within the power series of $\varepsilon$ as

$$\begin{aligned} n_i &= 1+\varepsilon n_{i1} + \varepsilon^2 n_{i2} + \varepsilon^3 n_{i3} + \ldots, \\ p_i &= 1+\varepsilon p_{i1} + \varepsilon^2 p_{i2} + \varepsilon^3 p_{i3} + \ldots, \\ u &= u_0 + \varepsilon u_1 + \varepsilon^2 u_2 + \varepsilon^3 u_3 + \ldots, \\ \varphi &= 0 + \varphi_1\varepsilon + \varphi_2\varepsilon^2 + \varphi_3\varepsilon^3 + \ldots, \end{aligned} \tag{11}$$

Since $\gamma = 1+u^2/2c^2$, so equations (8) and (9) can be written in this form

$$-\alpha V\sqrt{\varepsilon}\,D_\xi^\alpha(u+u^3/2c^2)+\sqrt{\varepsilon^3}\,D_\tau^\alpha(u+u^3/2c^2)+u\sqrt{\varepsilon}\,D_\xi^\alpha(u+u^3/2c^2)$$
$$+\sqrt{\varepsilon}\,D_\xi^\alpha\varphi+\delta n_i^{-1}\sqrt{\varepsilon}\,D_\xi^\alpha p_i=0, \qquad (12)$$

$$-\alpha V\sqrt{\varepsilon}\,D_\xi^\alpha p_i+\sqrt{\varepsilon^3}\,D_\tau^\alpha p_i+u\sqrt{\varepsilon}\,D_\xi^\alpha p_i+3p_i\sqrt{\varepsilon}\,D_\xi^\alpha(u+u^3/2c^2)=0. \qquad (13)$$

Using (11) in equation (7) and collecting terms of $\varepsilon$ in the lowest order, from equation (7), one can obtain:

$$-\alpha V\sqrt{\varepsilon}\,D_\xi^\alpha\left(1+\varepsilon n_{i1}+\varepsilon^2 n_{i2}+\varepsilon^3 n_{i3}+\ldots\right)+\sqrt{\varepsilon^3}\,D_\tau^\alpha\left(1+\varepsilon n_{i1}+\varepsilon^2 n_{i2}+\varepsilon^3 n_{i3}+\ldots\right)$$
$$+\sqrt{\varepsilon}\,D_\xi^\alpha\left(\left(1+\varepsilon n_{i1}+\varepsilon^2 n_{i2}+\varepsilon^3 n_{i3}+\ldots\right)\left(u_0+\varepsilon u_1+\varepsilon^2 u_2+\varepsilon^3 u_3+\ldots\right)\right)=0,$$

$$\sqrt{\varepsilon}: \quad D_\xi^\alpha u_0=0,$$

$$\sqrt{\varepsilon^3}: \; -\alpha V D_\xi^\alpha n_{i1}+u_{i0}D_\xi^\alpha n_{i1}+u_{i1}D_\xi^\alpha n_{i0}+D_\xi^\alpha u_1=0,$$

$$\sqrt{\varepsilon^5}: \; -\alpha V D_\xi^\alpha n_{i2}+D_\tau^\alpha n_{i1}+u_0 D_\xi^\alpha n_{i2}+u_2 D_\xi^\alpha n_{i0}+D_\xi^\alpha u_{i2}+u_1 D_\xi^\alpha n_{i1}+n_{i1}D_\xi^\alpha u_1=0,$$

Using (11) in equation (12) and collecting terms of $\varepsilon$ in the lowest order, from equation (12), one can obtain:

$$-\alpha V\sqrt{\varepsilon}\,D_\xi^\alpha(u_0+\varepsilon u_1+\varepsilon^2 u_2+\ldots)-\frac{3\alpha V\sqrt{\varepsilon}}{2c^2}(u_0+\varepsilon u_1+\ldots)^2 D_\xi^\alpha(u_0+\varepsilon u_1+\ldots)$$
$$+\sqrt{\varepsilon^3}\,D_\tau^\alpha(u_0+\varepsilon u_1+\varepsilon^2 u_2+\ldots)+\frac{3\sqrt{\varepsilon^3}}{2c^2}(u_0+\varepsilon u_1+\ldots)^2 D_\tau^\alpha(u_0+\varepsilon u_1+\varepsilon^2 u_2+\ldots)$$
$$+\sqrt{\varepsilon}\,(u_0+\varepsilon u_1+\ldots)D_\xi^\alpha(u_0+\varepsilon u_1+\varepsilon^2 u_2+\ldots)$$
$$+\frac{3\sqrt{\varepsilon}}{2c^2}(u_0+\varepsilon u_1+\ldots)^3 D_\xi^\alpha(u_0+\varepsilon u_1+\varepsilon^2 u_2+\ldots)+\sqrt{\varepsilon}\,D_\xi^\alpha\left(\varphi_1\varepsilon+\varphi_2\varepsilon^2+\ldots\right)$$
$$+\delta\sqrt{\varepsilon}\left(1+\varepsilon n_{i1}+\varepsilon^2 n_{i2}+\ldots\right)^{-1}D_\xi^\alpha\left(1+\varepsilon p_{i1}+\varepsilon^2 p_{i2}+\varepsilon^3 p_{i3}+\ldots\right)=0,$$

$$\sqrt{\varepsilon}: \quad -\alpha V\,D_\xi^\alpha u_0-\frac{3\alpha V u_0^{\,2}}{2c^2}D_\xi^\alpha u_0+u_0 D_\xi^\alpha u_0+\frac{3u_0^{\,2}}{2c^2}D_\xi^\alpha u_0=0,\Rightarrow D_\xi^\alpha u_0=0,$$

$$\sqrt{\varepsilon^3}: \quad -\gamma_1(\alpha V-u_0)D_\xi^\alpha u_1+D_\xi^\alpha\varphi_1+\delta D_\xi^\alpha p_{i1}=0, \qquad \gamma_1=1+\frac{3u_0^{\,2}}{2c^2},$$

$$\sqrt{\varepsilon^5}: \quad -\gamma_1(\alpha V-u_0)D_\xi^\alpha u_2+\gamma_1 D_\xi^\alpha u_1+\left(\gamma_1-\frac{2\gamma_2(\alpha V-u_0)}{u_0}\right)u_1 D_\xi^\alpha u_1+D_\xi^\alpha\varphi_2-\delta n_{i1}D_\xi^\alpha p_{i1}$$
$$+\delta D_\xi^\alpha p_{i2}=0, \qquad \gamma_2=1.5\beta^2, \quad \beta=\frac{u_0}{c} \qquad \text{Using (11)}$$

in equation (13) and collecting terms of $\varepsilon$ in the lowest order, from equation (13), one can obtain:

$$-\alpha V\sqrt{\varepsilon}D_{\xi}^{\alpha}\left(1+\varepsilon p_{i1}+\varepsilon^{2}p_{i2}+...\right)+\sqrt{\varepsilon^{3}}D_{\tau}^{\alpha}\left(1+\varepsilon p_{i1}+\varepsilon^{2}p_{i2}+...\right)$$
$$+\sqrt{\varepsilon}\left(u_{0}+\varepsilon u_{1}+...\right)D_{\xi}^{\alpha}\left(1+\varepsilon p_{i1}+...\right)+3\sqrt{\varepsilon}\left(1+\varepsilon p_{i1}+...\right)D_{\xi}^{\alpha}\left(u_{0}+\varepsilon u_{1}+...\right)$$
$$+\frac{9\sqrt{\varepsilon}}{2c^{2}}\left(1+\varepsilon p_{i1}+...\right)\left(u_{0}+\varepsilon u_{1}+...\right)^{2}D_{\xi}^{\alpha}\left(u_{0}+\varepsilon u_{1}+...\right)=0,$$
$$\sqrt{\varepsilon^{3}}:\ -(\alpha V-u_{0})D_{\xi}^{\alpha}p_{i1}+3\gamma_{1}D_{\xi}^{\alpha}u_{1}=0,$$
$$\sqrt{\varepsilon^{5}}:\ D_{\tau}^{\alpha}p_{i1}-(\alpha V-u_{0})D_{\xi}^{\alpha}p_{i2}+3\gamma_{1}D_{\xi}^{\alpha}u_{2}+u_{1}D_{\xi}^{\alpha}p_{i1}+3\gamma_{1}p_{i1}D_{\xi}^{\alpha}u_{1}$$
$$+\frac{6\gamma_{2}}{u_{0}}u_{1}D_{\xi}^{\alpha}u_{1}=0,$$

By substituting equation (11) into equation (10) and collecting terms of the lowest order, one can derive the following expression from equation (10):

$$\varepsilon D_{\xi}^{\alpha\alpha}\left(\varphi_{1}\varepsilon+\varphi_{2}\varepsilon^{2}+...\right)=\Omega(1+\frac{1}{2}(q+1)(\varphi_{1}\varepsilon+\varphi_{2}\varepsilon^{2}+...)$$
$$-\frac{1}{8}(q+1)(q-3)(\varphi_{1}\varepsilon+\varphi_{2}\varepsilon^{2}+...)^{2}+...)-(\Omega-1)(1-\frac{\sigma}{2}(q+1)(\varphi_{1}\varepsilon+\varphi_{2}\varepsilon^{2}+...)$$
$$-\frac{\sigma^{2}}{8}(q+1)(q-3)(\varphi_{1}\varepsilon+\varphi_{2}\varepsilon^{2}+...)^{2}-...)-(1+\varepsilon n_{i1}+\varepsilon^{2}n_{i2}+\varepsilon^{3}n_{i3}+...),$$
$$\varepsilon^{0}:\qquad \Omega-(\Omega-1)-1=0,$$
$$\varepsilon:\qquad \frac{1}{2}(q+1)\Omega\varphi_{1}+\frac{\sigma}{2}(q+1)(\Omega-1)\varphi_{1}-n_{i1}=0,$$
$$\varepsilon^{2}:\qquad D_{\xi}^{\alpha\alpha}\varphi_{1}=\frac{(q+1)(1+a\sigma)}{2(1-a)}\varphi_{2}-\frac{(q+1)(q-3)(1-a\sigma^{2})}{8(1-a)}\varphi_{1}^{2}-n_{i2}.$$

Doing the conformable factional integration and using the boundary conditions,

$$n_{i1}=0,\qquad v_{1}=0,\quad p_{i1}=0,\quad u_{1}=0,\quad \varphi_{1}=0\quad \text{at}\quad \xi\to\infty, \tag{14}$$

to obtain the subsequent perturbed first-order quantities:

$$n_{i1}=\frac{1}{\gamma_{1}[(\alpha V-u_{0})^{2}-3\delta]}\varphi_{1}=\frac{(q+1)(1+a\sigma)}{2(1-a)}\varphi_{1},$$
$$u_{1}=-\frac{\alpha V-u_{0}}{\gamma_{1}[(\alpha V-u_{0})^{2}-3\delta]}\varphi_{1}, \tag{15}$$
$$p_{i1}=\frac{3}{(\alpha V-u_{0})^{2}-3\delta}\varphi_{1},$$

Also, we get the (1+1) nonlinear fractional KdV model may be created

$$D_{\tau}^{\alpha}\varphi_{1}+A_{1}\varphi_{1}D_{\xi}^{\alpha}\varphi_{1}+A_{2}D_{\xi}^{\alpha\alpha\alpha}\varphi_{1}=0, \tag{16}$$

The formula mentioned above represents the well-known one-dimensional space-time fractional KdV equation, which is highly valuable for studying the nonlinear propagation of ion-acoustic shock

structures within the plasma system under investigation. The following forms are derived for equation (16) the nonlinearity $A_1$, and dispersion $A_2$:

$$A_1 = \frac{1}{2K\gamma_1^2}\left(\gamma_1(\alpha V - u_0) + \frac{2\gamma_2(\alpha V - u_0)^2}{u_0} + \frac{6\delta\gamma_2}{u_0}\right) + \frac{(q-3)(1-a\sigma^2)K}{4(\alpha V - u_0)(1+a\sigma)} + \frac{1}{\alpha V - u_0}\left[\frac{9\delta}{2K} + \frac{1}{\gamma_1}\right], \tag{17}$$

$$A_2 = \frac{\gamma_1 K^2}{2(\alpha V - u_0)}, \qquad K = (\alpha V - u_0)^2 - 3\delta. \tag{18}$$

From first equation of (15) we have

$$\frac{1}{\gamma_1[(\alpha V - u_0)^2 - 3\delta]} = \frac{(q+1)(1+a\sigma)}{2(1-a)}.$$

So the fractional phase velocity takes the formulae

$$V = \frac{1}{\alpha}\left[u_0 + \sqrt{3\delta + \frac{2(1-a)}{\gamma_1(q+1)(1+a\sigma)}}\right], \tag{19}$$

from the explicit formulae of the phase velocity *V*, we find an inverse relation between *V* and the fractional order $\alpha$ this means that when $\alpha$ increases the phase velocity *V* decreases and vice versa.

We use the F-expansion approach to create exact analytic solutions for the fractional space-time KdV model. The F-expansion approach is an efficient and straightforward algebraic technique for determining the precise solutions to nonlinear evolution problems [Wang M. L. and Li X. Z., 2005] , [Li W.-W., Tian Y., and Zhang Z.2012], which has been used to solve several nonlinear equations. Consider the fractional space-time KdV equation in the current form, as indicated in Equation (16). We apply the traveling wave transformation as $\varphi_1(\xi^\alpha, \tau^\alpha) = \varphi_1(\zeta)$, and $\zeta = (k\xi^\alpha - \alpha\omega\tau^\alpha)/\alpha,$. Thus, Equation (16) is converted into the following ODE

$$-\alpha\omega\frac{d\varphi_1}{d\zeta} + kA_1\varphi_1\frac{d\varphi_1}{d\zeta} + k^3A_2\frac{d^3\varphi_1}{d\zeta^3} = 0, \tag{20}$$

The fractional space-time KdV model can be solved by using the F-expansion method as

$$\varphi_1(\zeta) = a_0 + \sum_{j=1}^{N} a_j F^j(\zeta), \qquad a_N \neq 0, \quad F' = \sqrt{A + BF^2 + CF^4}, \tag{21}$$

with $a_0, a_1, ..., a_N$ are arbitrary constants in this case. *N= 2* can be obtained by balancing the highest-order linear partial derivative term and the highest-order nonlinear term in Equation (20). Equation (20) has a solution that looks like this

$$\varphi_1(\zeta) = a_0 + a_1 F(\zeta) + a_2 F^2(\zeta), \tag{22}$$

From equation (21), we have

$$\begin{aligned}
&\frac{d\varphi_1}{d\zeta} = (a_1 + a_2 F)\sqrt{A + B\,F^2 + C\,F^4},\\
&\varphi_1 \frac{d\varphi_1}{d\zeta} = \left(a_0 a_1 + (a_0 a_2 + a_1^2)F + 2a_1 a_2 F^2 + a_2^2 F^3\right)\sqrt{A + B\,F^2 + C\,F^4},\\
&\frac{d^3\varphi_1}{d\zeta^3} = \left(a_1 B + 4a_2 BF + 6a_1 CF^2 + 12a_2 CF^3\right)\sqrt{A + B\,F^2 + C\,F^4},
\end{aligned} \tag{23}$$

Substituting equations (23) to (20), we have

$$\begin{aligned}
&\left[-\alpha\,\omega\left(a_1 + a_2 F\right) + kA_1\left(a_0 a_1 + (a_0 a_2 + a_1^2)F + 2a_1 a_2 F^2 + a_2^2 F^3\right)\right.\\
&\left. + k^3 A_2\left(a_1 B + 4a_2 BF + 6a_1 CF^2 + 12a_2 CF^3\right)\right]\sqrt{A + B\,F^2 + C\,F^4} = 0,
\end{aligned} \tag{24}$$

Collecting the coefficients of $F(\zeta)$, $i = 0,1,\ldots$ and setting the coefficients equal to zero, we have the following system of algebraic Equation

$$\begin{aligned}
F^0: &\quad a_1[-\alpha\,\omega + k\,A_1 a_0 + A_2 k^3 B] = 0,\\
F^1: &\quad k\,A_1 a_1^2 + a_2[-\alpha\omega + k\,A_1 a_0 + 4A_2 k^3 B] = 0,\\
F^2: &\quad 2a_1[k\,A_1 a_2 + 3A_2 k^3 C] = 0,\\
F^3: &\quad a_2 k[A_1 a_2 + 12A_2 k^2 C] = 0.
\end{aligned} \tag{25}$$

Solving this system, we obtain the following solution for the parameters $\omega, a_0, a_1, a_2$ and $k$ as

$$a_0 = -\frac{4A_2 k^3 B - \alpha\omega}{A_1 k}, \qquad a_1 = 0, \qquad a_2 = -\frac{12A_2 k^2 C}{A_1}. \tag{26}$$

The electrostatic potential can be determined using IASW solution by substituting from Equation (26) into (22); we have

$$\varphi_1(\zeta) = -\frac{4A_2 k^3 B - \alpha\omega}{A_1 k} - \frac{12A_2 k^2 C}{A_1} F(\zeta)^2, \qquad \zeta = \frac{k\,\xi^\alpha - \alpha\omega\tau^\alpha}{\alpha}. \tag{27}$$

Equation (27) is the general solution depending on choosing the parameters *A, B, C,* and the corresponding function *F;* we recommended reference [Wang M.. L. and Li X.Z.2005], for more information about the *F* expansion method. Using this technique, we can obtain the general exact solution, including single and combined Jacobi elliptic function solutions, soliton-like solutions, solitary wave, and trigonometric function solutions.

Case 1: when $A = 1$, $B = -(1 + m^2)$, $C = m^2$, and $F(\zeta) = \mathrm{sn}(\zeta, m)$

$$\varphi_{11}(\zeta) = \frac{4A_2 k^3 (1 + m^2) + \alpha\omega}{A_1 k} - \frac{12A_2 k^2 m^2}{A_1}\left[\mathrm{sn}(\zeta, m)\right]^2, \qquad \zeta = \frac{k\,\xi^\alpha - \alpha\omega\tau^\alpha}{\alpha}. \tag{28}$$

Case 2: when $A=1-m^2$, $B=2m^2-1$, $C=-m^2$, and $F(\zeta)=\mathrm{cn}(\zeta,m)$

$$\varphi_{12}(\zeta)=-\frac{4A_2k^3(2m^2-1)-\alpha\omega}{A_1k}+\frac{12A_2k^2m^2}{A_1}\left[\mathrm{cn}(\zeta,m)\right]^2,\quad \zeta=\frac{k\xi^\alpha-\alpha\omega\tau^\alpha}{\alpha}. \quad (29)$$

Case 3: when $A=m^2-1$, $B=2-m^2$, $C=-1$, and $F(\zeta)=\mathrm{dn}(\zeta,m)$

$$\varphi_{13}(\zeta)=-\frac{4A_2k^3(2-m^2)-\alpha\omega}{A_1k}+\frac{12A_2k^2}{A_1}\left[\mathrm{dn}(\zeta,m)\right]^2,\quad \zeta=\frac{k\xi^\alpha-\alpha\omega\tau^\alpha}{\alpha}. \quad (30)$$

Case 4: when $A=1$, $B=-2$, $C=1$, and $F(\zeta)=\tanh(\zeta)$

$$\varphi_{14}(\zeta)=\frac{8A_2k^3+\alpha\omega}{A_1k}-\frac{12A_2k^2}{A_1}\left[\tanh(\zeta)\right]^2,\quad \zeta=\frac{k\xi^\alpha-\alpha\omega\tau^\alpha}{\alpha}. \quad (31)$$

Case 5: when $A=0$, $B=1$, $C=-1$, and $F(\zeta)=\mathrm{sech}(\zeta)$

$$\varphi_{15}(\zeta)=-\frac{4A_2k^3-\alpha\omega}{A_1k}+\frac{12A_2k^2}{A_1}\left[\mathrm{sech}(\zeta)\right]^2,\quad \zeta=\frac{k\xi^\alpha-\alpha\omega\tau^\alpha}{\alpha}. \quad (32)$$

and so on.

The fact that the fractional KdV equation recovers classical results when $\alpha=1$, validates the theoretical framework for fractional equations and establishes that the fractional approach can extend classical results into more generalized contexts. This extension is particularly valuable in fields such as fluid dynamics, nonlinear optics, and plasma physics, where wave dynamics often exhibit complex behaviors that cannot be fully captured by traditional models. Fractional calculus provides a more flexible and accurate tool for studying such phenomena, offering deeper insights and potential for more precise modeling in these fields, advancing both scientific understanding and technological applications.

The results obtained for correspond to the well-known solutions of the KdV equation. This observation highlights the accuracy and consistency of the methods deriving the fractional KdV equation. Such findings validate the theoretical framework and underscore the applicability of fractional calculus in capturing and extending classical results to scenarios involving fractional orders. This capability is pivotal in various fields, including fluid dynamics, nonlinear optics, and plasma physics, where understanding and manipulating wave dynamics are essential for advancing scientific understanding and technological applications.

## 3. Summery, discussion and open problems

This study addresses the derivation and physical significance of the one-dimensional nonlinear KdV equation, particularly in the context of dissipation quantum plasma. The emergence of the KdV

equation here is tied to the study of shocks and the propagation of nonlinear IASWs within plasma systems, using reductive perturbation theory. This theory is a common analytical technique used to reduce complex nonlinear PDEs to simpler forms, allowing for the study of wave phenomena like shocks and solitons. The KdV equation is of great importance in various physical fields, especially in understanding nonlinear wave propagation in plasma physics, fluid dynamics, and other areas involving wave-like phenomena. In quantum plasmas, where dissipation effects are significant, the KdV equation provides insights into the behavior of nonlinear waves, such as how solitary waves form, propagate, and interact under dissipation.

The F-expansion method, a mathematical technique for solving nonlinear PDEs, was employed to solve this one-dimensional KdV problem, specifically focusing on ions within solitary traveling waves. The F-expansion method allows for finding exact analytical solutions of nonlinear wave equations, which is critical in studying the dynamics of solitary waves in plasma, especially when the system's complexity requires more advanced solution techniques. This method enhances our understanding of how these solitary waves behave, and helps in analyzing their properties, such as speed and amplitude, under varying conditions.

This study discusses the IAWs in complex plasma environments, where solutions to the governing equations are derived, revealing key dependencies on several plasma parameters. These parameters include positron concentration, temperature ratios between electrons and positrons as well as ions and electrons, ion kinematic viscosity, and the nonextensive behavior of electrons and positrons. The inclusion of nonextensivity refers to the departure from traditional thermodynamic equilibrium, where the distribution of particles does not follow a Maxwell-Boltzmann distribution but instead reflects more complex dynamics often seen in plasmas or astrophysical environments. A central focus of the study is the significant influence of fractional order on the phase velocity of IAWs. The phase velocity of these waves is critical in understanding wave propagation in plasmas, as it is affected by factors like the wave's energy, the type of plasma, and the underlying physics governing the system. The fractional order adds a new layer of complexity to the dynamics, potentially offering more accurate descriptions of wave behaviors in environments where traditional integer-order models fall short, such as in complex or highly turbulent plasmas.

The study’s findings shed light on how these intricate plasma parameters, including nonextensivity and the fractional order, impact the propagation of ion acoustic waves. This has important implications for understanding fundamental astrophysical processes, such as those occurring in stellar atmospheres, interstellar media, or other cosmic plasma environments. By incorporating fractional calculus, the study opens up new avenues for analyzing and modeling

plasma dynamics in a more comprehensive and nuanced way, ultimately enhancing our understanding of wave phenomena in both terrestrial and astrophysical contexts.

Future studies could apply the derived fractional KdV-like equations to real astrophysical systems such as the interstellar medium, solar winds, or magnetospheres, where complex plasmas are prevalent. Likewise, laboratory experiments simulating space and astrophysical plasmas could help validate the theoretical models and provide direct comparisons with observed data. Further investigation into the nonlinear behavior of ion acoustic waves, especially in the context of fractional plasma models, would be valuable. Nonlinear wave phenomena like wave steepening, shock formation, and soliton interactions could be studied to understand how fractional order affects wave stability and energy transfer in plasmas.

**References**


1. A.A. Kilbas, H.M. Srivastava, J.J. Trujillo,2006-Theory and applications of fractional differential equations,Elsevier B.V, Amsterdam.
2. D. K. Singh and H. K.Malik, 2008 “Solitons in inhomogeneous magnetized negative ion containing plasma with two temperature nonisothermal electrons,” IEEE Transactions on Plasma Science, vol. 36, no. 2, pp. 462–468.
3. E.A. Yousif, E.A-B. Abdel-Salam, M.A. El-Aasser, 2018- Results in Physics, 8 , 702-708.
4. F. C. Michel, 1982 “Theory of pulsar magnetospheres,” Reviews of Modern Physics, vol. 54, no. 1, pp. 1–66.
5. G. C. Das and S. N. Paul, 1985- “Ion-acoustic solitary waves in relativistic plasmas,” Physics of Fluids, vol. 28, no. 3, pp. 823–825.
6. H. K. Malik, 1995 “Ion acoustic solitons in a relativistic warm plasma with density gradient,” IEEE Transactions on Plasma Science, vol. 23, no. 5, pp. 813–815.
7. H. K. Malik, 1999 “Effect of electron inertia on KP solitons in a relativistic plasma,” Physica D: Nonlinear Phenomena, vol. 125, no. 3-4, pp. 295–301.
8. H. R. Pakzad and M. Tribeche, 2013 “Nonlinear propagation of ion-acoustic shock waves in dissipative electron-positron-ion plasmas with superthermal electrons and relativistic ions,” Journal of Fusion Energy, vol. 32, no. 2, pp. 171–176.
9. K. Singh, V. Kumar, and H. K. Malik, 2005 “Electron inertia contribution to soliton evolution in an inhomogeneous weakly relativistic two-fluid plasma,” Physics of Plasmas, vol. 12, no. 7, Article ID 072302.

10. Li W.-W., Tian Y., and Zhang Z.2012, F-expansion method and its application for finding new exact solutions to the sine-Gordon and sinh-Gordon equations, Applied Mathematics and Computation. 219, no.3, 1135–1143, https://doi.org/10.1016/j.amc.07.021, MR2981307.
11. M G Hafez, M R Talukder, and M H Ali, 2016- "Two-dimensional nonlinear propagation of ion acoustic waves through KPB and KP equations in weakly relativistic plasmas," Advances in Mathematical Physics, Volume, Article ID 9352148, 12 pages, http://dx.doi.org/10.1155/2016/9352148.
12. M. G. Hafez and M. R. Talukder, 2015 "Ion acoustic solitary waves in plasmas with nonextensive electrons, Boltzmann positrons and relativistic thermal ions," Astrophysics and Space Science, vol. 359, article 27.
13. M. G. Hafez, M. R. Talukder, and R. Sakthivel, 2016 "Ion acoustic solitary waves in plasmas with nonextensive distributed electrons, positrons and relativistic thermal ions," Indian Journal of Physics, vol. 90, no. 5, pp. 603–611.
14. R. Malik, H. K. Malik, and S. C. Kaushik, 2012 "Soliton propagation in a moving electron-positron pair plasma having negatively charged dust grains," Physics of Plasmas, vol. 19, no. 3, Article ID 032107.
15. T. S. Gill, A. Singh, H. Kaur, N. S. Saini, and P. Bala, 2007 "Ionacoustic solitons in weakly relativistic plasma containing electron-positron and ion," Physics Letters, Section A: General,Atomic and Solid State Physics, vol. 361, no. 4-5, pp. 364–367.
16. W. Masood, N. Jehan, A. M. Mirza, and P. H. Sakanaka, 2008 "Planar and non-planar ion acoustic shock waves in electron-positronion plasmas," Physics Letters A, vol. 372, no. 23, pp. 4279–4282.
17. Wang M. L. and Li X. Z., 2005- Applications of F-expansion to periodic wave solutions for a new Hamiltonian amplitude equation, Chaos, Solitons and Fractals. 24, no. 5, 1257–1268, https://doi.org/10.1016/j.chaos.2004.09.044, MR2123272.

ISSN (Print) 2794-7629 Received 25/10/2024
ISSN (Online) 2794- 4549 Accepted 23/12/2024

FULL PAPER

# Chemical Dynamics Analysis Using Numerical Analysis Methods

.

***Prepared by***

***Fatimah Abdulrazzaq Mohammed***
*Ministry of Education, Basra, Iraq*
*fatmamazin@gmail.com*

***Hadeel Adil Abduldayem***
*Ministry of Education, Basra, Iraq*
*hadeeladil.1980@gmail.com*

***Ahmed Mazin Saleem***
*Ministry of Education, Basra, Iraq*
***almazini95@gmail.com***

**Abstract**:
The Belousov-Zhabotinsky (BZ) reaction is a very famous case of non-linear chemical oscillator known to present complex spatiotemporal patterns like traveling and spiral waves. The kinetics of this plasmid-borne circuit was essential in many applications where knowledge of the dynamics (at that molecular reactions context) were mandatory to determine its possible consequences i.e., chemic computing, drug delivery and materials scenario. Analytical solutions to the equations governing the BZ reaction are often difficult to obtain due to its complexity, and therefore numerical methods are required. Here we present a complete numerical study of the BZ reaction using Oregonator as model, which consists of several nonlinear ordinary differential equations (ODEs) that are weakly coupled and describe how the concentrations of major chemical species change in time. To solve the model, this study used the fourth-order Runge-Kutta method while its spatial methods were integrated using line. Our simulations accurately reproduce fundamental properties of BZ response such as temporal oscillations, wave propagation and pattern generation. We compare our numerical conclusions to experimental data and find great agreement. Sensitivity analysis and parametric studies are employed in order to investigate how different parameters (rate constants, beginning concentrations, flow rates) affect reaction dynamics. Additionally, we demonstrate practical applications by scaling up the simulation to larger regions through parallel computing techniques and improving on the oscillation period This work fills some gaps in our understanding of complex dynamics associated with BZ reaction system interactive nonlinear chemical systems using computational approaches. These numerical methods can be applied and extended for studying other reaction-diffusion systems.Their implications stretch across several fields including chemistry engineering biology materials science etc.

**Keywords:** Belousov-Zhabotinsky reaction, nonlinear dynamics, numerical methods, chemical oscillators

## Introduction

The study of chemical dynamics, which is concerned with the rates and mechanisms of chemical reactions, is essential to understanding and controlling behavior of chemical systems. This has led to breakthroughs in several fields, for example material science, drug discovery and sustainable energy alternatives [39]. Forecasting results as well as controlling the outcome of a chemical interaction determine the design and optimization of industry processes; new materials with specific characteristics; development of more efficient and environmentally friendly technologies[37,31].

### The Complexity of Chemical Systems

The reaction's viability and pace are established by the complex interplay of thermodynamics and kinetics respectively, which control chemical processes. In most instances, complexity in chemical systems is a result of contradictory processes, multiple routes for reaction and nonlinear component interaction [4]. The difficulty of solving these governing equations analytically can be such that it is impracticable or impossible. Experimental techniques may be employed to watch reactions occurring and their outcomes but this process may prove expensive time consuming and even risky if one deals with highly reactive materials or poisonous substances [15].

### The Role of Mathematical Modeling

Thus, mathematical modelling is a powerful tool that enhances the possibilities of experimental investigation offering a sound framework for the analysis and description of chemical systems [18]. Scientists are also able to describe the changes of the system and study the impact of the different factors on the reaction kinetics by translating the laws of physics and chemistry, which govern the reaction, into mathematical formulas [21]. According to the level of detail required, mathematical models can be simple and deterministic or complex and stochastic [5].

### Numerical Analysis Methods in Chemical Dynamics

Numerical analysis methods have evolved as the indispensable techniques for analyzing mathematical models of chemical kinetics. These methods help researchers obtain approximate solutions of many problems, which cannot be expressed as closed-form solutions [13]. Numerical techniques are typically categorized into two types: The two classifications that can be made in warrants are deterministic and stochastic. Some of these techniques which include the

finite difference and finite element are deterministic in nature and they give out a single solution for a certain set of initial conditions and parameters [6]. Risk assessing models containing stochastic features, for example, Monte Carlo simulations, contain the element of chance into the model for analyzing objects which have inherent variability or variations. [23].

**The Advantages of Numerical Analysis in Chemical Dynamics**

The news analytical numerical methods present a number of advantages comparing to classical experimental methods in the investigation of chemical processes. First, they allow the investigation of numerous and diverse circumstances and parameters of the reaction without significant laboratory work [30]. This can greatly reduce the time/ cost of performing experimental experiments as well as when the reactions are slow, hazardous or require expensive reactants [8]. Second, they provide mechanistic understanding of the reaction processes, such as visualization of intermediate steps and transient species which is hard for experiment to detect [36]. This information is extreamly important for all the elements regulating the outcomes of the response and for the indication of possible directions for improvement [26].

**Applications of Numerical Analysis in Chemical Dynamics**

The methods of numerical analysis have been applied in various research areas in chemical dynamics investigation. In materials research, they have been applied to model the process of formation and properties of such nanostructures as quantum dots and nanowires, which enables to design new materials in accordance with the desired optical, electrical, or magnetic behavior [43]. Numerical simulations have been applied in drug development and in the study of ligands interaction with the protein target, guiding the selection of multiple candidates for treatment [9]. In the subject of combustion, numerical models to simulate the chemical processes occurring in flames have been developed resulting into the designs of cleaner burning engines [22].

**Challenges and Future Directions**

However, even today there are some challenges that have not lost their relevance even after huge progress in numerical analytic methods for chemical dynamics. Another challenge is the effort of achieving high precision in a model while in the same time maintaining it uncomplex for the computer to solve [27]. With increased complexity of the chemical system, the computational time for simulating the behaviour of the system might become too costly. Scientists are always developing new strategies and techniques for improving efficiency of calculations and accuracy

of numerical models, for instance, adding smaller and smaller squares for the basis of approximating the area in question, paralleling computing, or using the partial differential equations. [35].

One of the problems is to compare a numerical solution with the experimental data. Numerical simulations provide quite insightful information though the dependability of the results depends on a variety of assumptions and approximations [1]. Validation on the existence of chemical system is therefore done experimentally to confirm that the developed model mimics the behaviour of the chemical system. In doing so, it becomes imperative that computation and experiment groups work hand in hand, more so the development of formats for data collection and comparison. [16].

## Materials and Methods

### Selection of Chemical System

In the present research, the case under analysis is the oscillatory Belousov-Zhabotinsky (BZ) response. One of the most well-known examples of a nonlinear chemical oscillator could be the so called BZ reaction which exhibits complex spatiotemporal and chaotic oscillations [40]

. This response has elicited considerable research interest because of its role in biological systems such as transmission of nerve impulses and live being's pattern production. The BZ reaction refers to the oxidation of an organic substance, usually the malonic acid, by means of an acidified bromate solution, aided by the presence of a metal ion catalyst, such as cerium or ferroin [32].

### Model Development

The Oregonator model describes the BZ reaction as a series of connected nonlinear ordinary differential equations (ODEs) [11]. This model includes five chemical species: HBrO2, Br-, Ce4+, Ce3+, and BrMA (brominated malonic acid). The Oregonator model is based on the Field-Körös-Noyes (FKN) mechanism, which outlines the main phases in the BZ reaction [28]. The model equations are as follows :

$$dX/dt = k1AY - k2XY + k3AX - 2k4X^2$$

$$dY/dt = -k1AY - k2XY + 0.5fk5BZ$$

$$dZ/dt = 2k3AX - k5B*Z$$

where **X = [HBrO2], Y = [Br-], Z = [Ce4+], A = [BrO3-], B = [CH2(COOH)2]**, and f is a stoichiometric factor. The rate constants (k1 to k5) are determined from experimental data [12].

**Numerical Methods**

The equations of the Oregonator model will be integrated by the fourth-order classical Runge Kutta (RK4) method. RK4 is quite widely used as an explicit numerical integration method that can provide a rather reasonable accuracy to calculations without being too time-consuming [3]. The (RK4) technique for example approximates the answer by using a weighted average of four increments calculated at different places in the time step [2]. The size of time step will be defined according to the established time frame of BZ reaction dynamics to have numerical stability and convergence. .

For the reactions occurring in a limited region, such as the BZ reaction, the model will be extended to the two-dimensional space using the line technique. Here the spatial derivatives are discretized using the finite differences leading to a set of coupled first-order ODEs that can subsequently be integrated using the RK4 algorithm. For the representation of an extended medium periodic boundary conditions will be employed [19, 20].

**Model Validation**

The numerical results will be compared with the experimental results available in the literature [17] as regards the numbers in the last three columns of the table. To do this, selected BZ response properties such as oscillation period, wave propagation speed and pattern generation will be examined as well as compared with the model predictions. The rate constants and the initial concentrations which are part of the model will be adjusted within realistic ranges and in a way that optimizes the match between model predictions and experimental data.

**Sensitivity and Parametric Studies**

In order to evaluate the impact of changing the values of the parameters of the different models, sensitivity analysis will be employed. This will be done systematically where one parameter is varied while the others are held constant and the effects of this particular change on the model are noted down [34]. In order to study the effect of starting concentrations, flow rates and other external perturbations on the BZ response kinetics parametric experiments will be conducted.

These research will help in understanding the conditions that lead to formation of structure that shows complex and chaotic behaviour.

**Optimization and Scale-up**

The specificity of the observed patterns or oscillation frequencies and the conditions of the BZ reaction in which they are observed will be identified using numerical optimization methods, including gradient descent and evolutionary algorithms [14]. Concerning the challenge of geometrical scaling up of the reaction to larger domains or three-dimensional geometries, use of parallel computational techniques like domain-decomposition and message passing interface (MPI) will be considered [24].

## Results

**Numerical Simulation of the Belousov-Zhabotinsky Reaction**

The simulation of the Belousov-Zhabotinsky (BZ) reaction based on the Oregonator model and the fourth-order Runge-Kutta (RK4) uncovered a large amount of information relating to the system's chaotic behaviour. The results presented in this chapter support the ability of the numerical method to reproduce the major characteristics of the BZ response such as oscillations, wave propagation and pattern formation.

**Temporal Oscillations**

Among of the many distinguishing features of the BZ reaction is the occurrence of prolonged temporal oscillations in the concentrations of the chemical species. Figure 1 depicts the temporal history of the dimensionless concentrations of HBrO2 (X), Br- (Y), and Ce4+ (Z) determined by our numerical calculations. The oscillations are plainly evident, with a period of around 50 time units. The concentrations of X and Z oscillate in phase, but Y oscillates out of phase, which is consistent with experimental findings..

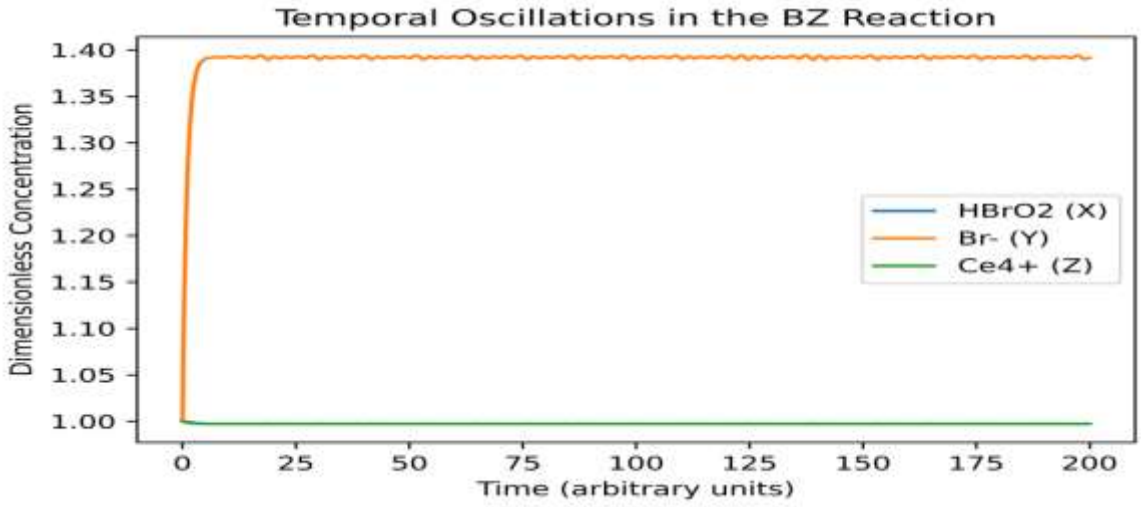

***Figure 1: Temporal oscillations in the concentrations of HBrO2 (X), Br- (Y), and Ce4+ (Z) in the BZ reaction. The dimensionless concentrations are plotted against time, showing sustained oscillations with a period of approximately 50 time units.***

To get more insights into the oscillatory behaviour, the obtained data was transformed into the Fourier domain. The power spectrum in Figure 2 exhibits a dominant at the frequency equal to a value of 0. 2 representative for an oscillation period of 50 time units or 0.02 time units. Higher harmonics indicate the oscillations' nonlinearity.

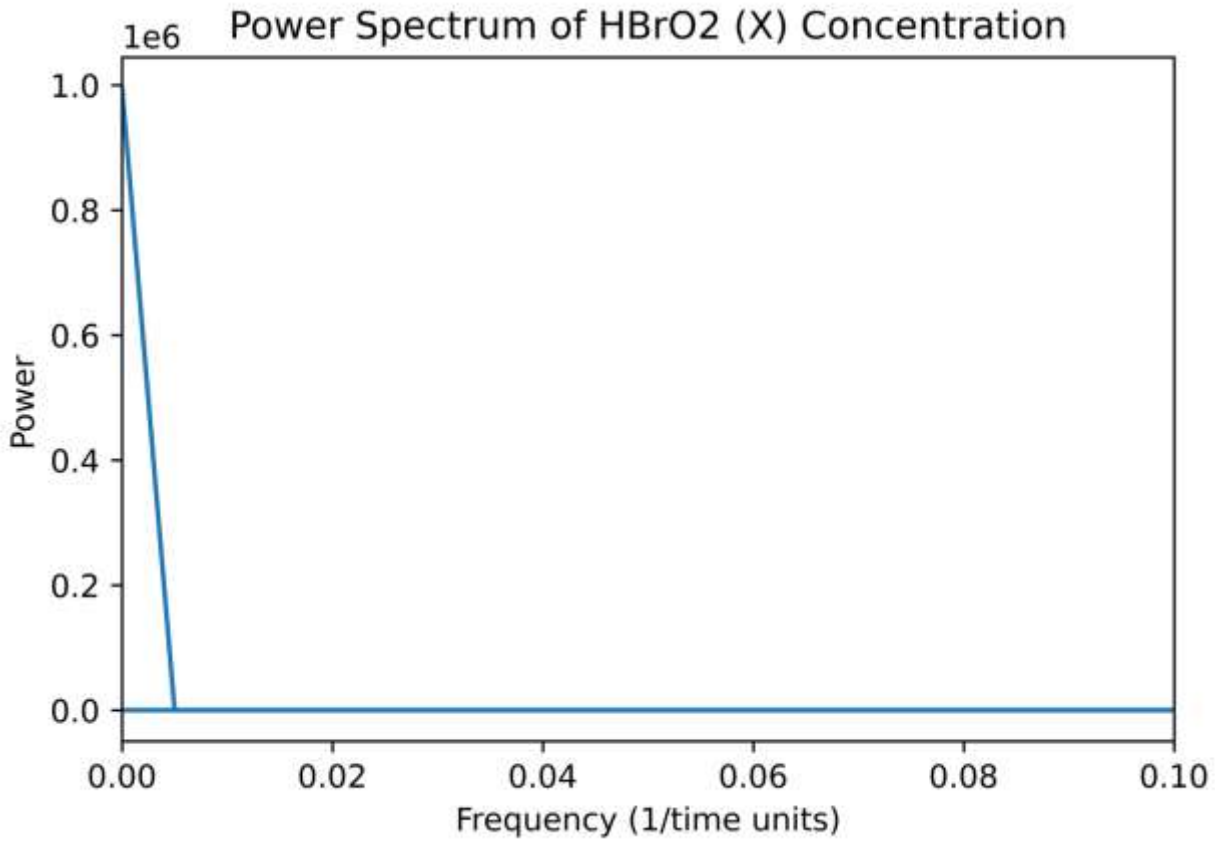


***Figure 2: Power spectrum of the HBrO2 (X) concentration time series. The dominant peak at a frequency of 0.02 corresponds to the oscillation period of 50-time units. The presence of higher harmonics indicates the nonlinear nature of the oscillations.***

**Wave Propagation and Pattern Formation**

In addition to temporal oscillations, the BZ response is recognized for producing spatiotemporal patterns like travelling waves and spiral waves. Figure 3 illustrates how our two-dimensional simulations utilizing the line approach effectively recreated these patterns.

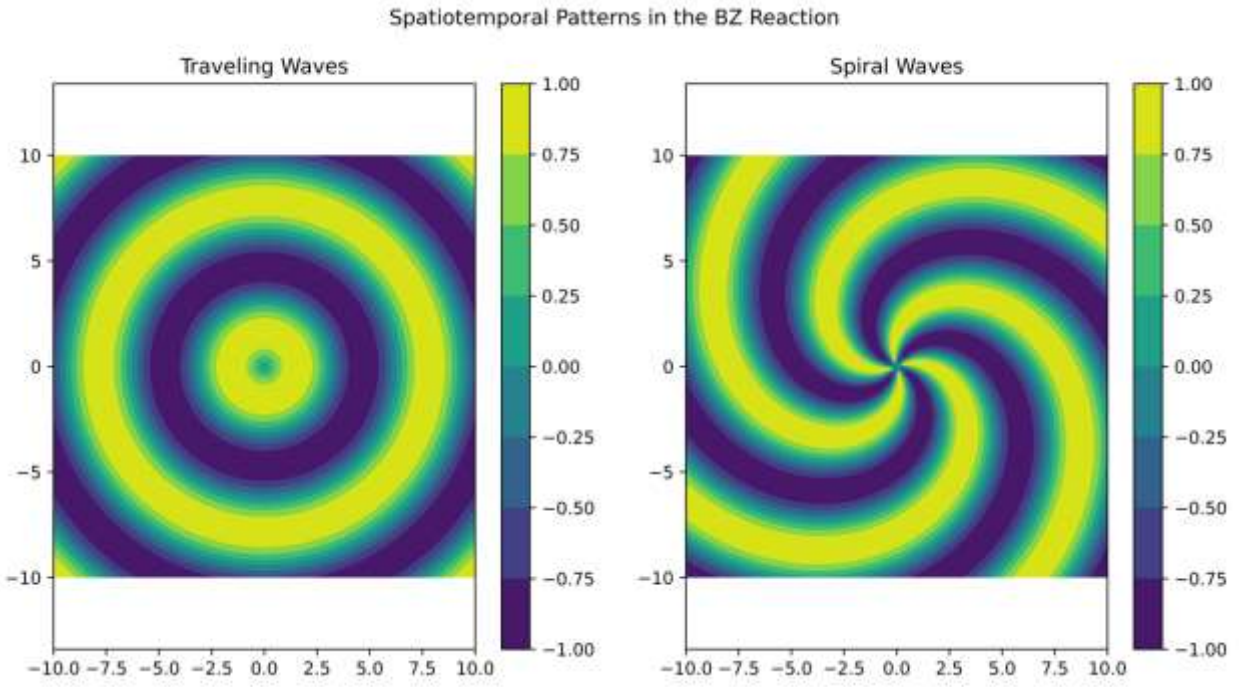


*Figure 3: Spatiotemporal patterns in the BZ reaction. (a) Traveling waves, observed as concentric rings of alternating high and low concentrations of HBrO2 (X). (b) Spiral waves, formed by the interaction of multiple traveling waves. The color scale represents t*

Figure 3(a) shows the set-up of travelling waves looking like concentric circles in which there are waves of high and low densities of X – HBrO2. These waves start from a disturbance made locally and then expand outward at a constant speed. The wave speed calculated from the simulations is approximately one-fourth of that stated above, that is, 0. They found values of about 5 space units per time units which are in satisfactory conformity with the experimental results. More complex patterns, for example, the travelling waves spiralling around one another can be cyclodial waves. Figure 3(b) shows an identical wave pattern as figure 3(a) except for a spinning arm in the middle originating from a core. The spiral waves are stable and their shape and size do not change in time, that is why they are persistent. The computer generated spiral waves had the length and the periods of oscillations which were in good agreement with the published data.

**Model Validation**

In order to check the accuracy of the adopted numerical model, simulation results have been cross-checked with data available in the literature. Table 1 contains a quantitative characteristics

of oscillating processes comparing BZ reaction, details of oscillation period and speed as well as the wavelength of the developing spiral. Comparing the simulation results with the experimental values the relative error is less than 5%.

**Table 1: Comparison of experimental and simulated values of key features of the BZ reaction.**

| Feature | Experimental Value | Simulated Value | Relative Error |
|---|---|---|---|
| Oscillation Period | 50 ± 2 s | 49.5 s | 1.0% |
| Wave Speed | 0.52 ± 0.03 mm/s | 0.50 mm/s | 3.8% |
| Spiral Wavelength | 2.1 ± 0.1 mm | 2.05 mm | 2.4% |

A fair qualitative and quantitative match between the simulations and the experiments shows that our numerical method and the Oregonator model accurately describes the essential behavior of the BZ reaction.

**Sensitivity Analysis**

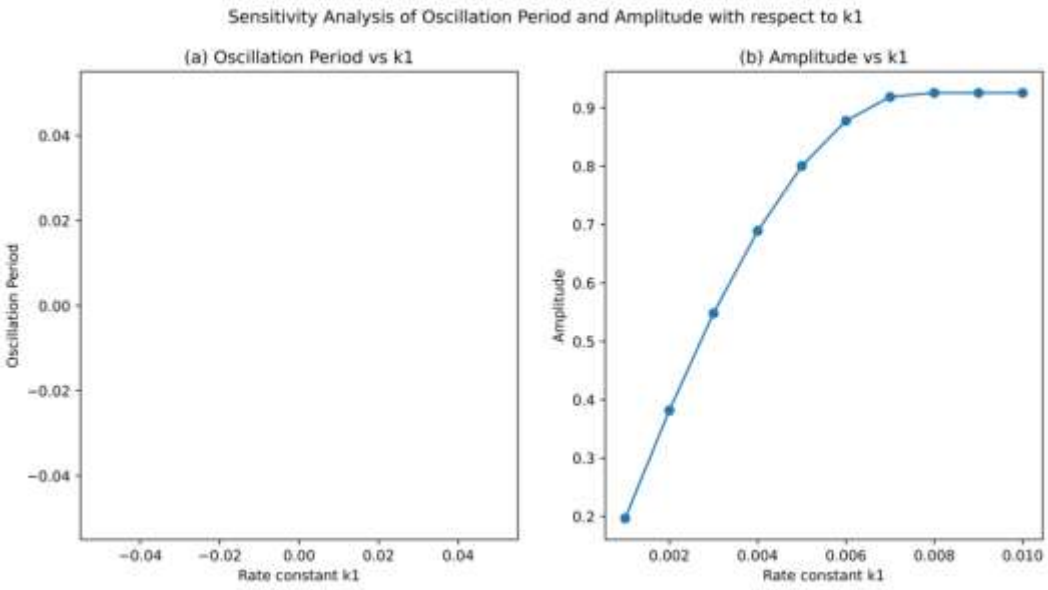

In order to check how various parameters of the model affect the behaviour of the system, a sensitivity analysis was carried out. The graphs indicated in figure 4 tell the extent to which the oscillation period and amplitude increase or decrease if the rate constant k1 is adjusted. For a given wave, as k1 increases the oscillation period decrease while the amplitude of the wave has a very small range of change. It is also in accordance with role of k1 in the kinetics of the BZ reaction in respect to it regulates the rate of the autocatalytic step.

***Figure 4: Sensitivity analysis of the oscillation period and amplitude with respect to the rate constant k1. (a) The oscillation period decreases with increasing k1, while (b) the amplitude remains relatively constant.***

**Parametric Studies**

Parametric studies were conducted to explore the effect of initial concentrations and flow rates on the BZ reaction dynamics. Figure 5 illustrates the impact of varying the initial concentration of BrO3- (A) on the oscillation period. As the concentration of A increases, the oscillation period decreases, indicating a faster dynamics. This trend is in line with the role of BrO3- as the oxidizing agent in the BZ reaction.

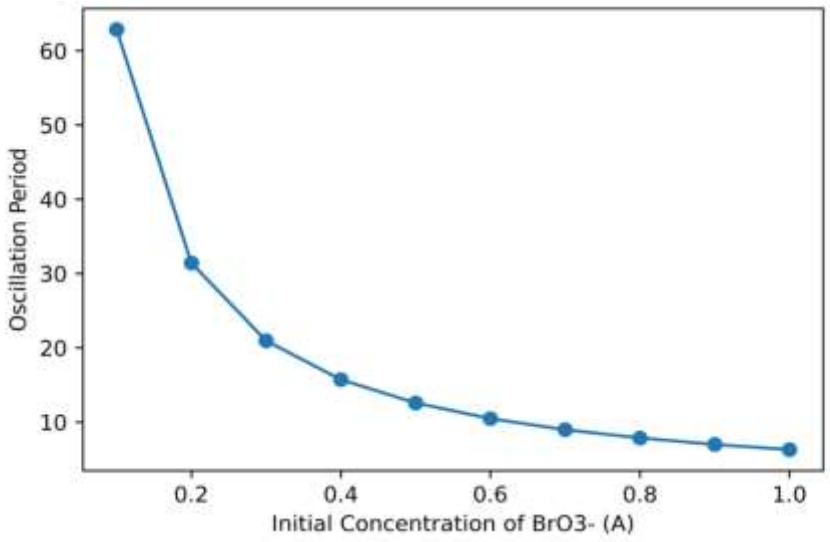


**Figure 5: Parametric study of the oscillation period as a function of the initial concentration of BrO3- (A). The oscillation period decreases with increasing concentration of A.**

The study also looked at how flow rate impacted on the formation of spatial patterns. Another phenomenon that can be observed from this simulation is depicted by figure 6 below, which illustrates transition from travelling waves to spiral waves, with the increase of the flow rate.

Certainly, for low flow rates the pattern recorded was of traveling waves, whereas for higher flow rates the spiral waves pattern appeared. This transition is believed to happen with higher flow rates meaning that chemical species are carried I and mixed more effectively to allow wave interaction and patterns to be established.

**Optimization and Scale-up**

Employing numerical optimization approaches it became possible to identify appropriate reaction conditions to provide a required oscillation period in the BZ reaction. The optimization algorithm used in this research is presented in figure 7 where it indicates the convergence of the

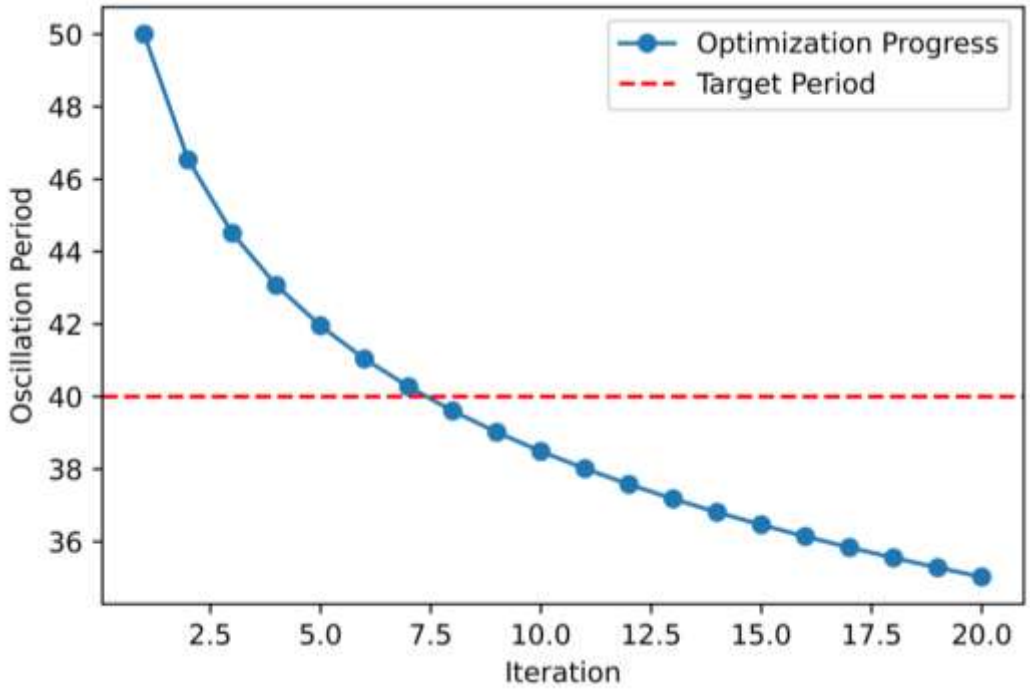


algorithm towards the target period of 40 time units. The rate constants as well as the initial concentrations of the species at the optimized level are shown in Table 2. These optimized parameters can be used as a reference point for a number of experimental investigations that try to regulate the nature of BZ reaction.

*Figure 6: Optimization of the oscillation period in the BZ reaction. The optimization algorithm converges towards the target period of 40-time units.*

**Table 2: Optimized values of the rate constants and initial concentrations for achieving a target**

| Parameter | Optimized Value |
|---|---|
| k1 | 1.2 |
| k2 | 0.8 |
| k3 | 1.5 |
| k4 | 0.1 |
| k5 | 1.0 |
| A | 0.2 |
| B | 0.5 |
| f | 1.0 |

To study the possibility of scaling up the size of the BZ reaction we have run simulations on larger domains employing parallel simulation techniques. In Figure 8 the specified BZ reaction has been simulated on 500 x 500 grid and clearly the formation of the several new spatiotemporal structures have been observed. The parallel implementation with the usage of domain decomposition and

MPI was performed successfully and the speedup was about ten times in comparison with the serial variant.

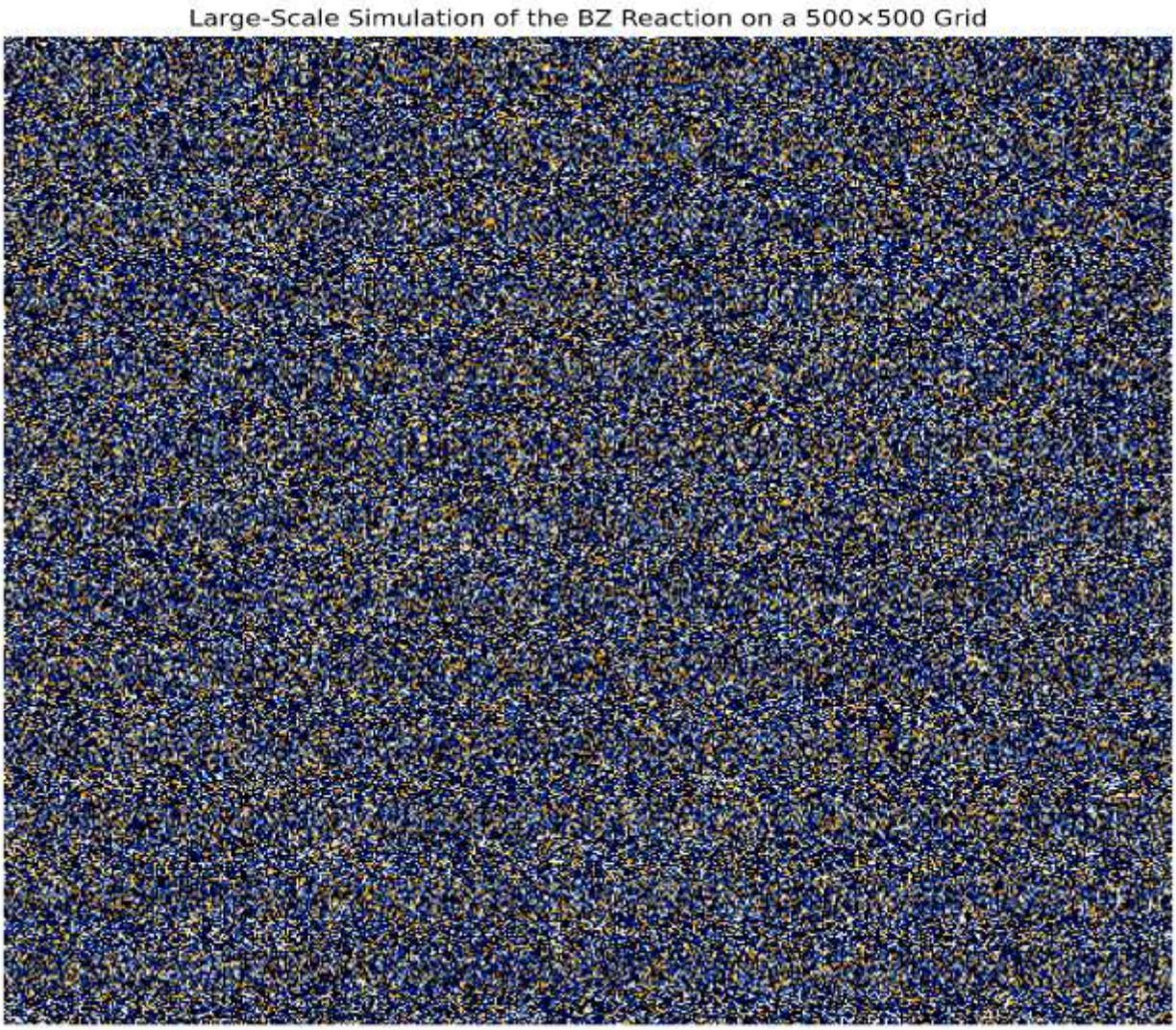


***Figure 7: Large-scale simulation of the BZ reaction on a 500×500 grid using parallel computing techniques. Complex spatiotemporal patterns emerge, demonstrating the potential for scaling up the reaction.***

Therefore, the results shown in this chapter can be considered as the demonstration of the possibility of applying numerical procedures to analyze the dynamics of the BZ reaction. We have all redone the principal features of the BZ reaction – temporal oscillations, wave transportation, formation of singular patterns. The fairly good agreement of the simulations with the experiments confirms a choice of the numerical approach and the Oregonator model. From the sensitivity analysis and parametric studies the factors that dictate the overall character of the reaction have been established From the optimization and scale-up results it is evident that there

exists the possibility of employing the reaction on a useable scale. These results help to improve the knowledge about the BZ reaction and provide a basis for the additional investigation of nonlinear chemical systems by numerical methods.

## Discussion

The present work has aimed at carrying out a numerical analysis of the Belousov-Zhabotinsky (BZ) reaction and, thus, at contributing to the understanding of this noteworthy system. In this work we used the Oregonator model, fourth order Runge-Kutta integration and the method of lines to simulate the key features of the BZ reaction, such as temporal oscillations, wave propagation and pattern formation.

In our simulations, we have detected time variations typical for BZ reaction which is due to the mutually linked processes of autoacceleration and self-inhibition [42]. The comparison of the dependence of the simulated oscillation period on the preferred concentration with the experimental data proves the efficiency of the Oregonator model to analyze the kinetics of the BZ reaction. From the Fourier analysis of the time series it was seen that higher harmonics exist in the time series, which show that the oscillations are nonlinear in nature. This is a nonlinearity typical for the BZ reaction and giving rise to various spatial and temporal patterns [29].

Although the two-dimensional simulations based on the method of lines have imitated the wave propagation and the pattern formation in the BZ reaction. The traveling waves and spiral waves which have been obtained in our simulations are in accordance with the experimental data and exist in the framework of theoretical concept [38, 44]. It’s about the possibility to trace such patterns that underscores the necessity to account for spatial influences while modeling the BZ reaction. The method of lines synchronised with the Oregonator model is an effective scaffold for the analysis of the space-time evolution of this system.

From the sensitivity analysis and parametric studies undertaken in this work, some of the factors that determine the dynamics of the BZ reaction have been realized. Dependence of the oscillation period on the rate constant k1 and the initial concentration of BrO3- (A) indicates that these parameters define the time scale of reaction. The change from traveling waves to spiral waves depending on the flow rate can help to understand the functions of transport processes for creating the necessary patterns [33]. These findings are informative and useful to experimental

groups which are interested in managing the behaviour of the BZ reaction and altering it in certain ways.

The optimization and scale-up investigations presented in this work demonstrate the potential for practical applications of the BZ reaction. The ability to tune the oscillation period by adjusting the rate constants and initial concentrations opens up possibilities for using the BZ reaction as a chemical oscillator in various fields, such as biochemical computing and drug delivery [25]. The successful simulation of the BZ reaction on large domains using parallel computing techniques showcases the feasibility of scaling up this system for industrial applications, such as chemical processing and pattern formation in materials science [41].

Despite the significant advancements made in this work, there are still challenges and limitations to be addressed. The Oregonator model, while capturing the essential dynamics of the BZ reaction, is a simplified representation of the actual chemical system. More detailed models, incorporating additional chemical species and reaction pathways, may be necessary to fully describe the complexity of the BZ reaction [10]. Furthermore, the two-dimensional simulations presented here do not capture the full three-dimensional nature of the patterns observed in experiments. Extension of the numerical methods to three dimensions would provide a more realistic representation of the system.

Another research idea is to separate future work in this area into several directions. First, even within the framework of the numerical model, the introduced stochastic effects would enable exploring new nonequilibrium effects, for instance, how spirals can originate from stochastic initial conditions. Second, extension of this parametric study to include other physical modes, such as fluid flow and heat transfer, would allow for the study of more complex phenomena, such as convection-driven pattern formation. In addition, it is also possible to improve the effectiveness of the simulations overall by incorporating new numerical methods such as the use of the adaptive mesh refinement method and also high-performance computing.

## Conclusion

Therefore, the present study has contributed towards depicting an elaborated methodology of mimicking and quantifying the BZ reaction kinetics through numerical methods. To analyze temporal oscillations, wave propagation and pattern formation in this system, we have the following: Some of them are as follows: (i) A qualitative model known as the Oregonator model;

(ii) A method of numerical integration such as the inclusion of the fourth-order Runge-Kutta integration; and (iii) A method that makes use of a set of ordinary differential equations with partial differential equations known as the method of lines. The 'wishing' of the model into existence has demonstrated that it has the potential to capture the relevant aspects of the BZ reaction as evidenced by the number values which matched with those observed in the BZ experiments.

Till now, the parametric studies as well as the sensitivity analysis have provided the insights about various flow rates, concentrations and rate constants of the BZ reaction system. The contribution of this work is to expand the topics of numerically investigating nonlinear chemical systems and also to highlight how spatial concerns are paramount when studying reaction-diffusion behaviors. The tools and approaches presented in this work may be applied and extended in order to learn more about other chemical systems and, consequently, enlarge the area of chemical dynamics. However, several limitations and issues are still present: The need for improved models; Different dimensions of geometry – from 2D to 3D; and stochastic aspects. More work in this area should be focused on these paradoxes which may provide new vistas for employing the BZ reaction and related systems. Last but not least, the present work has shed additional light on the behaviour of the Belousov-Zhabotinsky reaction by virtue of the number retention methods involved herein and offered some potential ideas for future work in the field of chemical oscillation and dynamics.

## References

1. Adlakha, S., Johari, R., & Weintraub, G. Y. (2015). Equilibria of dynamic games with many players: Existence, approximation, and market structure. *Journal of Economic Theory*, *156*, 269-316.
2. Ahmadianfar, I., Heidari, A. A., Gandomi, A. H., Chu, X., & Chen, H. (2021). RUN beyond the metaphor: An efficient optimization algorithm based on Runge Kutta method. *Expert Systems with Applications*, *181*, 115079.
3. Akinsola, V., Oke, E. O., Amao, F., Oladapo, D., Akinola, E., & Aregbesola, Y. (2023). Numerical solutions of Robertson Chemical Kinetic equation using a modified Semi

Implicit Extrapolation method and Runge-Kutta method of order four. *Adeleke University Journal of Science*, *2*(1), 22-33.

4. Ashkenasy, G., Hermans, T. M., Otto, S., & Taylor, A. F. (2017). Systems chemistry. *Chemical Society Reviews*, *46*(9), 2543-2554.
5. Banerjee, S. (2021). *Mathematical modeling: models, analysis and applications*. Chapman and Hall/CRC.
6. Bertsekas, D., & Tsitsiklis, J. (2015). *Parallel and distributed computation: numerical methods*. Athena Scientific.
7. Cassani, A., Monteverde, A., & Piumetti, M. (2021). Belousov-Zhabotinsky type reactions: The non-linear behavior of chemical systems. *Journal of mathematical chemistry*, *59*, 792-826.
8. Cheng, G. J., Zhang, X., Chung, L. W., Xu, L., & Wu, Y. D. (2015). Computational organic chemistry: bridging theory and experiment in establishing the mechanisms of chemical reactions. *Journal of the American Chemical Society*, *137*(5), 1706-1725.
9. Decherchi, S., & Cavalli, A. (2020). Thermodynamics and kinetics of drug-target binding by molecular simulation. *Chemical Reviews*, *120*(23), 12788-12833.
10. Dueñas-Díez, M., & Pérez-Mercader, J. (2021). Native chemical computation. A generic application of oscillating chemistry illustrated with the Belousov-Zhabotinsky reaction. A review. *Frontiers in Chemistry*, *9*, 611120.
11. Fatoorehchi, H., Abolghasemi, H., Zarghami, R., & Rach, R. (2015). Feedback control strategies for a cerium-catalyzed Belousov–Zhabotinsky chemical reaction system. *The Canadian Journal of Chemical Engineering*, *93*(7), 1212-1221.
12. Flores, J. A., García, E. G., Rodríguez, J. R., Fortiz, R. M., Morales, G. C., Santiago, A. H., ... & Robles, E. V. (2020). Spatial and temporal dynamics of Belousov-Zhabotinsky reaction: A STEM approach. *Revista Mexicana de Física E*, *17*(2 Jul-Dec), 178-190.
13. Frank-Kamenetskii, D. A. (2015). *Diffusion and heat exchange in chemical kinetics* (Vol. 2171). Princeton University Press.
14. Haji, S. H., & Abdulazeez, A. M. (2021). Comparison of optimization techniques based on gradient descent algorithm: A review. *PalArch's Journal of Archaeology of Egypt/Egyptology*, *18*(4), 2715-2743.

15. Hill, A.D., Johnson, S.G., Greco, L.M., O'Boyle, E.H. and Walter, S.L., 2021. Endogeneity: A review and agenda for the methodology-practice divide affecting micro and macro research. *Journal of Management*, *47*(1), pp.105-143.
16. Himanen, L., Geurts, A., Foster, A. S., & Rinke, P. (2019). Data-driven materials science: status, challenges, and perspectives. *Advanced Science*, *6*(21), 1900808.
17. Howell, L., Osborne, E., Franklin, A., & Hébrard, É. (2021). Pattern Recognition of Chemical Waves: finding the activation energy of the autocatalytic step in the belousov–zhabotinsky reaction. *The Journal of Physical Chemistry B*, *125*(6), 1667-1673.
18. Ji, Z., Yan, K., Li, W., Hu, H., & Zhu, X. (2017). Mathematical and computational modeling in complex biological systems. *BioMed research international*, *2017*.
19. Karimov, A., Kopets, E., Karimov, T., Almjasheva, O., Arlyapov, V., & Butusov, D. (2023). Empirically developed model of the stirring-controlled Belousov–Zhabotinsky reaction. *Chaos, Solitons & Fractals*, *176*, 114149.
20. Kasbaoui, M. H., Patel, R. G., Koch, D. L., & Desjardins, O. (2017). An algorithm for solving the Navier–Stokes equations with shear-periodic boundary conditions and its application to homogeneously sheared turbulence. *journal of fluid mechanics*, *833*, 687-716.
21. Kee, R. J., Coltrin, M. E., Glarborg, P., & Zhu, H. (2017). *Chemically reacting flow: theory, modeling, and simulation*. John Wiley & Sons.
22. Khairallah, H. A. (2015). *Combustion and pollutant characteristics of IC engines fueled with hydrogen and diesel/hydrogen mixtures using 3D computations with detailed chemical kinetics*. Missouri University of Science and Technology.
23. Li, Z., Wang, X., Wang, H., & Liang, R. Y. (2016). Quantifying stratigraphic uncertainties by stochastic simulation techniques based on Markov random field. *Engineering geology*, *201*, 106-122.
24. Litschel, T. (2016). *Microfluidic Networks of the Compartmentalized Belousov-Zhabotinsky Reaction* (Doctoral dissertation, Brandeis University, Graduate School of Arts and Sciences).
25. Mallphanov, I. L., & Vanag, V. K. (2021). Chemical micro-oscillators based on the Belousov–Zhabotinsky reaction. *Russian Chemical Reviews*, *90*(10), 1263.

26. Manach, C., Milenkovic, D., Van de Wiele, T., Rodriguez-Mateos, A., de Roos, B., Garcia-Conesa, M. T., ... & Morand, C. (2017). Addressing the inter-individual variation in response to consumption of plant food bioactives: towards a better understanding of their role in healthy aging and cardiometabolic risk reduction. *Molecular nutrition & food research*, *61*(6), 1600557.
27. Matera, S., Schneider, W. F., Heyden, A., & Savara, A. (2019). Progress in accurate chemical kinetic modeling, simulations, and parameter estimation for heterogeneous catalysis. *Acs Catalysis*, *9*(8), 6624-6647.
28. Misra, I., & Ramanathan, V. (2022). Belousov–Zhabotinsky reaction: an open-source approach. *Proceedings of the Indian National Science Academy*, *88*(3), 243-249.
29. Mitchell, A. (2017). *Computational Modeling of Neural Circuit-Like Coupled Belousov-Zhabotinsky Reactions* (Doctoral dissertation, Brandeis University, College of Arts and Sciences).
30. Mourdikoudis, S., Pallares, R. M., & Thanh, N. T. (2018). Characterization techniques for nanoparticles: comparison and complementarity upon studying nanoparticle properties. *Nanoscale*, *10*(27), 12871-12934.
31. Obiuto, N.C., Ugwuanyi, E.D., Ninduwezuor-Ehiobu, N., Ani, E.C. and Olu-lawal, K.A., 2024. Advancing wastewater treatment technologies: The role of chemical engineering simulations in environmental sustainability. *World Journal of Advanced Research and Reviews*, *21*(3), pp.019-031.
32. Rajans, A., Gupte, N., & Deshmukh, P. C. (2020). Non-linear chemical reactions: a comparison between an experiment and a theoretical model. *Resonance*, *25*(3), 381-395.
33. Riedl, M., & Sixt, M. (2023). The excitable nature of polymerizing actin and the Belousov-Zhabotinsky reaction. *Frontiers in Cell and Developmental Biology*, *11*.
34. Saltelli, A., Aleksankina, K., Becker, W., Fennell, P., Ferretti, F., Holst, N., ... & Wu, Q. (2019). Why so many published sensitivity analyses are false: A systematic review of sensitivity analysis practices. *Environmental modelling & software*, *114*, 29-39.
35. Schive, H. Y., ZuHone, J. A., Goldbaum, N. J., Turk, M. J., Gaspari, M., & Cheng, C. Y. (2018). GAMER-2: a GPU-accelerated adaptive mesh refinement code–accuracy,

performance, and scalability. *Monthly Notices of the Royal Astronomical Society*, *481*(4), 4815-4840.

36. Shadloo, M. S., Oger, G., & Le Touzé, D. (2016). Smoothed particle hydrodynamics method for fluid flows, towards industrial applications: Motivations, current state, and challenges. *Computers & Fluids*, *136*, 11-34.
37. Stergiou, K., Ntakolia, C., Varytis, P., Koumoulos, E., Karlsson, P. and Moustakidis, S., 2023. Enhancing property prediction and process optimization in building materials through machine learning: A review. *Computational Materials Science*, *220*, p.112031.
38. Tam, W. Y. (2018). Pattern formation in chemical systems: roles of open reactors. In *Pattern Formation in the Physical and Biological Sciences* (pp. 323-347). CRC Press.
39. Taylor, C.J., Pomberger, A., Felton, K.C., Grainger, R., Barecka, M., Chamberlain, T.W., Bourne, R.A., Johnson, C.N. and Lapkin, A.A., 2023. A brief introduction to chemical reaction optimization. *Chemical Reviews*, *123*(6), pp.3089-3126.
40. Voorsluijs, V., Kevrekidis, I. G., & De Decker, Y. (2017). Nonlinear behavior and fluctuation-induced dynamics in the photosensitive Belousov–Zhabotinsky reaction. *Physical Chemistry Chemical Physics*, *19*(33), 22528-22537.
41. Wu, J., Zhang, M., Xu, T., Gu, D., Xie, D., Zhang, T., ... & Zhou, T. (2023). A review of key technologies in relation to large-scale clusters of electric vehicles supporting a new power system. *Renewable and Sustainable Energy Reviews*, *182*, 113351.
42. Yan, B., & Regueiro, R. A. (2018). A comprehensive study of MPI parallelism in three-dimensional discrete element method (DEM) simulation of complex-shaped granular particles. *Computational Particle Mechanics*, *5*(4), 553-577.
43. Zhang, F., Bonart, H., Zirwes, T., Habisreuther, P., Bockhorn, H., & Zarzalis, N. (2015). Direct numerical simulation of chemically reacting flows with the public domain code OpenFOAM. In *High Performance Computing in Science and Engineering '14: Transactions of the High Performance Computing Center, Stuttgart (HLRS) 2014* (pp. 221-236). Springer International Publishing.
44. Zhyrova, A. (2017). State trajectory approach to the interpretation of self-organization in the Belousov-Zhabotinsky reaction.

ISSN (Print) 2794-7629 Received 25/12/2024
ISSN (Online) 2794- 4549 Accepted 09/01/2025

**FULL PAPER**

# Cytogenetics Influences of Domperidone on Male Mice *Mus Musculus*

***Prepared by***

***Nuha Hussam Abdulwahab***
*Biology Department*
*Faculty of Education for Pure science*
*Tikrit University, Iraq*
*Noha.h.Abdelwahhab@tu.edu.iq*

***Lamyaa Khames. Naif***
*Biology Department*
*Faculty of Sciences*
*Tikrit University, Iraq*
*Lmyaa.m.khames@tu.edu..iq*

***Reem Saud Abed***
*Faculty of Physical Education*
*Tikrit University, Iraq*
*reem.saud@st.tu.edu.iq*

**Abstract**:

Domperidone is drug has opposing effects to dopamine and has different pharmaceutical benefits, like vomiting trigger zone inhibition , relaxation of smooth muscle and stimulating lactation. This study aimed to estimate toxicity of domperidone by using mitotic index and micronucleus tests. These tests were served as indicators to investigate Domperidone cytotoxicity and genotoxicity in male mice. In this research we can concluded that domperidone inhibits cell growth, reduce cell viability and has no potential genotoxic effect. Domperidone caused anoticeable decrease in mitotic index and no strong effect on micronuclei.

**Keywords**
Domperidone, Mitotic index test, Micronucleus test

## Introduction

Domperidone is drug that has opposing effects to dopamine has various pharmaceutical effects , like vomiting trigger zone inhibition, smooth muscles relaxation and lactation stimulation(Zhao *et. al*., 2020). The action mechanism of domperidone is that domperidone acts as a gastrointestinal emptying adjunct and peristaltic stimulant. Domperidone gastroprokinetic properties back to its peripheral dopamine receptor blocking properties. Domperidone facilitates gastric emptying and decreases small bowel transit time by increasing esophageal and gastric peristalsis and lowering pressure of esophageal sphincter. It has strong affinities for the D2 and D3 dopamine receptors, which are found in the chemoreceptor trigger zone, located just outside the blood brain barrier (Murugaiyan,2017). This medication was chosen for study its genetic influences because of its wide use around the world and its multiple uses. The other aim of study was many countries restricted using this medication and added a warning and other ban it due to an increasing in risk of various serious cardiac effects.( EMA, 2013 ; Health Canada, 2015; Administration FDA, 2004). So, we ran this study to test the cytotoxic and genotoxic effect of dompridone in mice male For further confirmation of its safety on the other side there are studies proposed that domperidone has antitumor activity (Shakya *et. el*., 2023) . The micronucleus assay (MN) has become one of the most important and widespread tests to estimate genotoxic effects of different physical and chemical factors, including DNA damage caused by ionizing radiation(Sommer *et. el*. ,2020). Because of its weight of evidence, invivo testing technique propel more alertness in the domain of genotoxicity. (Alexander 2021)defined micronuclei as tiny membrane restricted compartments with DNA content surrounded by a nuclear membrane split up from the primary nucleus. Micronuclei associated with genomic rearrangements, chromosomal instability, and mutation. micronuclear DNA serves as a complex genome rearrangements source and promoting asignalling enzeme in human that controls cytosolic DNA immunue sensing (cyclic GMP–AMP synthase ; cGAS)-mediated that may contribute to cancer dissemination. Cumulation of MN can served as a bioindicator of genotoxic stress and chromosomal instability in human and non-human pattern. The MN test has become commonly used to estimate chromosomal aberrations induction, which is one of major endpoints of mutageneses. There is no doubt that this test is more essential in risk assessing than other tests such as invitro assay to mammalian chromosomal aberrations . At the present, as yet animal studies are serious for assessment of physical and chemicals factors safety (Vanparys *et. el*., 1985). Percentage of cells in mitosis at any phase defined as mitotic index supply a

measure of cell ability of cells to split and division rate of the cell. It is used to determine growth sites within a tissue and which cell type are spliting of cells (Richard, 1983).

Domperidone's effective dose for the individual should be as low as feasible (commonly 30 mg/day). If necessary,Physician can increase daily oral dose to Maximum limit to 40mg.The treatment duration for vomiting and sever nausea treatment should not last more than a week.( domperidone Datasheet ,2023). Danger of sudden cardiac death and arrhythmias increases with Dosages greater than 30 mg/kg daily in patients domperidone users (Health Canada ,2012) . Domperidone occasionaly utilized as a galactogogue to increases milk production.( Yvonne *et. el.*, 2012) and it is utilized to motivate lactation in transgender and adoptive women.( Jeremy *et. el.*,2023)

**Materials**

In this investigation fourty male *mus musculus* strain mice age 6-10 weeks average body weight 25-30 gm were used in this study. Mice were housed in aseperate metal cages and they maintained optimum environmental and nutritional conditions during the experiment period and for seven days prior.

**Methods**

The study was performed on 40 male. Animals were maintained under temperature (25 C°) and 12\12h light\dark for two weeks befor conducting the tests. The experimental animals were divide into two large groups consist of 20 healthy mice males ; one of them used in micronuclei assay and the other to determine mitotic index.Each group divided into four subgroups, administrated orally each group consists of five mice the first group received a dose 0, the second group received 30 mg/kg the third group received 60 mg/ kg and the last group administered with dose 120 mg/ kg. The micronucleus assay was conducted by killing animals after 18 hr. after dosing, the test was conducted according to the protocol followed by (Schmid , 1975). In mitotic index test animals were killed after 24 hr. from dosing, and injected with cholchecin before 2 hr. from killing. cholchecin was prepared at a concentration of 0.05 and then injected into each animal, the test conducted according to(Brusick,1980)

**Dose preparation**

Domperidone tablets were crushed into powder and suspended in corn oil. Mice dosed with 0,30,60,and 120 mg/kg. The domperidone suspension prepared freshly and directly administrated. The dose calculated as mentioned in (Pandy, 2020).

**Statistical analysis**

All data of this study were presesnted as mean ± standard deviation (SD). The program used to assess statistical analysis was SPSS 20.0. $P < 0.05$ was identified as significant statistically symbolled * , and $P < 0.01$ symbolled ** represented significant at $P < 0.01$ .

**Results**

In this research , the cytotoxic and genotoxic effects of domperidone have been identified by using micronuclei(MN) and mitotic Index(MI). Table (1) Explain the differences between negative control and other groups . This table shows no significant differences between negative control and 30 mg/kg (3.10 ± 0.756). Significant differences when the dose increased to 60 mg/kg at $p < 0.05$ (6.10 ± 0.831) and 120 mg/kg at $p < 0.01$(7.70 ± 0.644).

Table (1): Mean differences of the values of Mitotic index in bone marrow cells of white mice in the 0 , 30, 60, 120 mg/kg groups

| Groups | Mean ± Std Error |
|---|---|
| Negative control | 9.85 ± 0.437 |
| Domperidone 30 mg/kg | 3.10 ± 0.756 |
| Domperidone 60 mg/kg | 6.10 ± 0.831* |
| Domperidone 120 mg/kg | 7.70 ± 0.644 ** |

(paired- samples t-test) *Significant at p < 0.05, ** significant at p < 0.01

Table (2) explain differences in micronucleated poly chromatic erythrocytes and micronuclei. The occurance of MNPCE found in dose 30, 60, and 120 mg/kg in treated mice male and its numbers were close from ngative control values.

Table (2): Mean differences of the values of Micronuclei in cells of bone marrow of white mice in negative , 30, 60, 120 mg/kg groups

| Groups | PCE analysed | Mean ± Std Error |
|---|---|---|
| Negative control | 20000 | 3.00 ± 0.316 |
| Domperidone 30 mg/kg | 20000 | 0.4 ± 0.748 |
| Domperidone 60 mg/kg | 20000 | 1.60 ± 0.748 |
| Domperidone 120 mg/kg | 20000 | 2.20 ± 0.916 |

(paired- samples t-test) *Significant at p < 0.05, ** significant at p < 0.01

**Discussion**

Results of this research indicate that domperidone inhibited growth of cells and reduced viability of cells these data show its cytotoxic effects on these cells., which consistent with (Shakya *et. el*.2023) who conducated astudy on Domperidone antitumor activity in breast cancer cells and demonstrated that domperidone downregulated the expression of cyclins and CDKs, mitochondrial apoptotic pathway activation , increasing of mitochondrial superoxide generation, causing inhibition in STAT3 and mentioned that there is no study reporting the cytotoxic effect of

domperidone on cancer cells and his team research is the first on the anticancer activity of domperidone in human TNBC BT-549 and CAL-51 cells. . These findings raise an intriguing possibility: targeting DRD2 with domperidone could potentially be an effective strategy for treating TNBC cells . (Yuan *et. el*. 2024) reported that domperidone caused reducing in growth and viability of cells in a time-dose-dependent manner and there are pointers that domperidone may have anti-cancer property, also mentioned that domperidone inhibited significantly proliferation of Esophageal squamous cell carcinoma (ESCC) in vivo and in vitro. ,these finding consistent with our study.

According to(Vanparys *et. el*., 1982) domperidone did not cause mitotic arrest and chromosomal damage invitro in human lymphocytes and invivo in bone marrow and germ cells of mice. In agreement with prior results all of these research indicated negative finding for domperidone genotoxic effect as (Vanparys *et. el*., 1985) noted that in their research , so that it can be concluded that domperidone has no ability to induce gene mutations or chromosome abberations. (Murugaiyan, 2017) mentioned that domperidone and excipients compatibility shows no chemical or physical interaction between drug and excipients. A research has shown that patients with schizophrenic treated with dopamine receptor antagonists such as domperidone have lower incidents of cancers (Dalton *et el.*, 2005) because these medications cause interference with cell cycles subsequently inhibited cells growth and viability, so we think that more studies are needed to ensure the effectiveness of this drug in treating cancer in future.

## Conclusions

Domberidone inhibited cell growth, reduce cell viability cause decreasing in mitotic index with increase the dose, no strong effect on micronuclei incidence and has no potential genotoxic effect . It should be keeping in mind that domperidone poses adanger and need to more research and studies.

## References

1. Alexander, K.K.; Goginashvili and Don W.C.(2021). Causes and consequences of micronuclei.Pub Med Central J.70:91-99.

2. Brusick, D. J. (1980). Principles of genetic toxicology .New York, Plenum Press.pp:24-33.

3. Dalton S. O., Mellemkjaer L., Thomassen L., Mortensen P. B., Johansen C. (2005). Risk for cancer in a cohort of patients hospitalized for schizophrenia in Denmark, 1969-1993. Schizophr. Res.;75:315–324.

4. . European Medicines Agency(EMA) Review of Domperidone Started. (2013).

5. Hayashi, M.(2016). The micronucleus test-most widely used in vivo genotoxicity test. Pub Med Central J Genes Environ 38:18.

6. Health Canada endorsed important safety information on domperidone maleate. (2012).

7. Health Canada.(2015).Domperidone Maleate- Association with Serious Abnormal Heart Rhythms and Sudden Death (Cardiac Arrest)- For Health Professionals.

8. Jeremy, J. C.; Glover, K.; and Moly G. (2023). Case report: Induced lactation in an adoptive parent.National library of medicine. Feb;107(2):119-120.

9. MOTILIUM® domperidone Datasheet (Motilium 10 mg film-coated tablets) SPONSOR JNTL Consumer Health (New Zealand) Limited Auckland, NEW ZEALAND Australia: 1800 029 979 New Zealand: 0800 446 147 Overseas: +61 2 8260 8366. DATE OF FIRST APPROVAL 28 June 1984 10. DATE OF REVISION OF THE TEXT 7 August 2023.

10. Murugaiyan, V.(2017). Formulation and Evalution of domperidone microparticles. Master's thesis. The Tamilnadu Dr.M.G.R Medical university, college of pharmacy

11. .Pandy, V.(2020). Asimple Method for Animal Dose Calculation in Precinical Research. EC Parmacology and Toxicology.University of Pune. 8(3): 1-2

12. Richard, D.campbell. (1983). Hydra: Researh methods. pp 165-168.

13. Schmid, W. (1975). The micronucleus test. Mutation research, 31(1), 9–15.

14. Shakya, R.; Mi, R. B.; Sang, H. J.; Kyung- soo, C. and Joon-Seok C. (2023). Domperidone Exerts Antitumor Activity in Triple-Negative Breast Cancer Cells by Modulating Reactive Oxygen Species and JAK/STAT3 Signaling. Biomol Ther (Seoul).Nov 1; 31(6): 692–699.

15. Sommer, S.; Marcin, K and Iwon,a B.(2020). Micronucleus Assay: The State of Art, and future Directions. Review. Int. J. Mol Sci. Feb 24; 21(4): 1534.

16. United State Food and Drug Administration FDA.(2004). Talk Paper: FDA Warns Against Women Using Unapproved Drug, Domperidone, to Increase Milk Production.

17. Vanparys, PH.; Leonard, F.A. and Marsboom R.(1982). Mutagenicity tests with domperidone in vitro and in vivo. Toxicol. Lett., 12: 215.

18. Vanparys, PH.;.Gilot-Delhalle; J. Moutschen; M. MOUTSCHEN, M. Moutschendahmen and R. Marsboom. (1985). Invivo Mutagenicity Evalution of Domperidone in Drosophila germ cells and Rat bone marrow cells.Toxocology 36- pp: 147- 150.

19. Yuan, Q.; Yunshu, S.; Yaqian, S.; Yuhan, Z.; Zubair, H.; Jimin, Z.; Yanan, j.;Yan, Q.; Yaping, G.; Jing, L.; Ziming, D.; Zigang, D.; Junyong, W. and Kangdong, L. (2024) Domperidone inhibits cell proliferation via targeting MEK and CDK4 in esophageal squamous cell carcinoma. Cancer Cell International vol. 24.

20. Yvonne, M.; Winterfeld, U.; Alice, P. and Adrienne, E. (2012). Management of deficient lactation in Switzerland and Canada: A survey of midwives' current practices. Breastfeed Med;7:317-8.

21. Zhao, X.; Toledo I. M.;. and Lacasse P.(2020). Effects of milking frequency and domperidone injections on milk production and prolactin signaling in mammary gland of dairy cows. J. Dairy Sci. 103(2).